# THE INFLUENCE OF SLOPE ON TURBIDITY CURRENTS AND THEIR DEPOSITS IN A PROCESS-BASED MODEL

A thesis submitted to the Delft University of Technology in partial fulfillment of the requirements for the degree of

Master of Science in Applied Earth Sciences

by

J.J.H. Blom

June 2020

J.J.H. Blom: *The Influence of Slope on Turbidity Currents and Their Deposits in a Process-based Model* (2020)


ISBN 999–99–9999–999–9

The work in this thesis was made in the:

Applied Geology
Department of Geoscience & Engineering
Civil Engineering & Geosciences
Delft University of Technology

| | |
|---|---|
| Supervisors: | Prof. dr. Joep Storms |
| | Dr. Maria Azpiroz-Zabala |
| Co-reader: | Prof. dr. Mário Franca |

# ABSTRACT

Turbidity currents transport land-derived sediment to deep sea where their deposits form large geological structures termed submarine fans. Given their large areal extent and high sand content, submarine-fan deposits form significant hydrocarbon reservoirs. Their internal architecture is often poorly resolved. With much of the three-dimensional architecture of the turbidite lobes below seismic resolution, there is commonly a significant level of uncertainty associated with respect to the reservoir geometry and quality.

At the end of submarine channels, turbidity currents lose confinement and encounter a slope break, in response, the current decelerates and forms a deposit, a turbidite. Repeated passage of turbidity currents forms a stack of deposits that are generically termed lobes.

Subsequent flow events modify the bathymetry by erosion and deposition, thereby affecting the trajectory of subsequent flow events. Due to self-formed relief, beds start stacking laterally, in *compensation*. A complex but ordered stratigraphy is created by repeated cycles of shifts in deposition, which results in variability in deposits that governs reservoir connectivity.

In this study, multiple consecutive turbidity currents flowing over self-formed relief are modeled using a process-based numerical model (Delft3D-FLOW). The response of successive turbidity currents and their deposits to variations in channel slope was tested. Models with steeper channel slope were observed to result in more vigorous flows with deposits that cover a larger surface area. Following passages of turbidity currents were observed to erode bed sediment in the channel and thereby diminish the amount of readily erodible bed sediment for following turbidity currents. With the current model set-up, the deposit relief was insufficient to observe lateral stacking of deposits.

These simulations provide insight into the depositional processes and the controls on the dimensions, geometry, and sedimentary trends of the deposits emplaced by successive turbidity currents flowing over a slope break and losing confinement.

In Nature's infinite book of secrecy,
A little I can read.

*The response of the Soothsayer when asked about his prediction capabilities in William Shakespeare's play 'Antony & Cleopatra'*

# CONTENTS

# LIST OF FIGURES

# LIST OF TABLES

# ACRONYMS

**CLTZ** channel-lobe transition-zone . . . . . 11
**RANS** Reynolds-averaged Navier-Stokes . . . . . 7
**CFL** Courant-Friedrichs-Lewy number . . . . . 17
**MORFAC** morphological acceleration factor . . . . . 72
**ADCP** Acoustic Doppler Current Profiler . . . . . 4
**CFD** Computational Fluid Dynamics . . . . . 5
**TKE** Turbulent Kinetic Energy . . . . . 22

# 1 INTRODUCTION

## 1.1 BACKGROUND INFORMATION

Submarine fan systems are sedimentary systems that typically form on the abyssal plain and receive terrigenous sediment from canyons and channels that extend across continental margins to the abyssal plain [Piper and Normark, 2001]. Submarine fans are constructed principally from the deposits of sediment gravity flows (mainly turbidity currents and debris flows), which redistribute terrigenous and shallow marine sediment into deeper water [Deptuck and Sylvester, 2017]. Sedimentation and erosion processes associated with turbidity currents are able to modify the bathymetry of the sea bottom. Many successive flow events sculpt submarine channels and distribute sediment across the ocean floor into discrete depositional bodies, often generically termed lobes [Hamilton et al., 2017]. Successive avulsions periodically relocate the fan's center of deposition. The progressive stacking of lobes and channels builds submarine fans [Piper and Normark, 2001; Jobe et al., 2017].

Over periods of the order of $10^4$ to $10^6$ years these deposits may build up into vast sediment accumulations with volumes up to millions of $km^3$ and ranging from a few km to several thousand km across [Weimer and Slatt, 2007]

Submarine fans are the final sink for large amounts of terrigenous sediments, as such the form form important — if cryptic — archives of Earth-surface processes and change, recording the interplay between climatic, eustatic and tectonic controls on the transfer of sediment from land to ocean [Prélat et al., 2009]. Additionally, submarine fans host substantial hydrocarbon resources, making them targets for hydrocarbon exploration and production [Talling et al., 2013].

### 1.1.1 Lobes

Lobes commonly accumulate at the termination of submarine channels in unconfined (i.e. non-ponded) settings, by deposition of many repeated flow events. Lobe deposits make up the greater part of the bulk volume of submarine fans [El-Gawad et al., 2014] and represent the final location of sediment in the sediment cascade from source to sink. Lobes are economically important as hydrocarbon reservoirs. Given that lobes can make for complicated reservoirs (described in Applications), better understanding of their grain size distribution and depositional architecture is required to enhance reservoir prediction capabilities [Prelat et al., 2010].

#### *Conceptual Model of Stacking in Lobes*

The dynamics of turbidity currents are highly complex owing to the non-linear feedback between turbulence and the suspended sediment [Allen, 1971; Kneller and Buckee, 2000; Parsons et al., 2007], this is elaborated upon

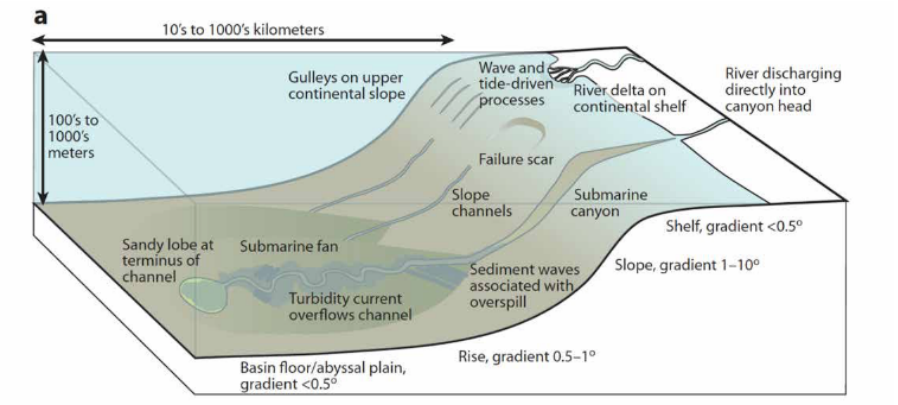


**Figure 1.1:** Schematic of the marginal environment in marine and lacustrine settings where turbidity currents arise and turbidites are deposited. From Meiburg and Kneller [2010]

.

in Section 2.1 Sediment-gravity Flows. Despite the complex mechanics that govern turbidity currents, the resulting deposit emplacement and hence stratigraphy in lobes can be remarkably ordered [Parsons et al., 2002]. This order is attributed to systematic stacking of the deposits (e.g. Mutti and Normark [1987]; Prelat et al. [2010]; Deptuck et al. [2008]; Groenenberg et al. [2010]).

The depositional sequence thought to be behind systematic stacking of lobe deposits is as follows: Each flow tends to fill topographical lows and builds a subtle depositional relief [Straub et al., 2009]. This relief affects subsequent flows, which can have implications for the spatial distribution of sediment. This topographic interaction can lead to gradual shifts in the position of successive beds. At some point, the ongoing stacking of beds redirects subsequent flows to a steeper flow path, thereby laterally migrating or "switching the lobe" to adjacent topographic lows. The next series of flow events follow this new flow path, depositing their sediment at some distance away (compensational stacking Mutti and Sonnino [1981]) and the sequence starts over. Consequently, the location where the successive lobe deposits are thickest changes over time as new beds are deposited in a different location. Similarly, successive composite bodies will see their point of thickest deposit shifting in space [Prelat and Hodgson, 2013]. This flow–deposit interaction is intrinsic to the evolution of submarine fans at a range of scales [Groenenberg et al., 2010].

A complex but ordered stratigraphy is created by repeated cycles of lobe-switching. The stratigraphy can be viewed as a record of the sediments preserved by this evolving morphology.

### 1.1.2 Applications

With large sand volumes, narrow range in grain sizes, good lateral continuity, and potentially good vertical connectivity, lobes are attractive reservoirs for hydrocarbons [Slatt, 2013]. Variation in lateral continuity, connectivity of sand volumes, and presence of fine-grained permeability baffles within lobes all impact reservoir complexity, and influence the flow behavior during hydrocarbon production.

The stratigraphic structure created by compensational stacking governs the heterogeneity and connectivity of architectural elements of submarine fan reservoirs [Cantelli et al., 2009; Hawie et al., 2019]. In this way, compensation of depositional elements has a direct bearing on the number of wells required to produce a field [Deptuck et al., 2008].

By improving understanding of the processes that control grain size trends and morphodynamics in stacked deposits, the ability to predict connectivity in the reservoir is improved [Straub and Pyles, 2012], which can lead to improvements in reservoir modelling [Groenenberg et al., 2010; Lopez-Cabrera and Manzocchi, 2017]. Better understanding of controls can also be applied to the interpretation of the stratigraphic record of submarine fans in outcrops and subsurface data-sets [Burgess et al., 2019; Hawie et al., 2019].

Additionally, the study of turbidity currents has significant application for subsea and pipeline engineering as they can cause major damage to submarine telecommunication cables, pipelines, instrumentation, and equipment [Talling et al., 2013]. Turbidity currents also play an important role in global carbon burial [Talling et al., 2015]. At last, turbidity currents are also major transport agents in artificial lakes leading to sedimentation which causes a loss of storage capacity [Commandeur, 2015].

## 1.2 MAIN RESEARCH QUESTION

A range of inter-related factors influence dimensions and architectural complexity of lobe deposits (these are discussed in more detail in Section 2.4 Controls on submarine lobe formation). The steepness of the channel (upper) and basin (lower) slope and confinement are some of the geometric controls. A broad consensus exists that slope is one of the overriding controls influencing the distribution, quality, and architecture of submarine reservoirs (e.g. Piper and Normark [2009]; Prather [2003]; Mulder and Alexander [2001]; Lomas and Joseph [2004]; El-Gawad et al. [2014]; Hamilton et al. [2017]; Parsons et al. [2002]).

Gravitational gravitational driving force for the turbidity current is a function of the slope, which affects flow velocity and bed shear stress, which increases the capacity to erode more bed sediment [Sequeiros et al., 2009] or its capacity to transport sediment without depositing (flow capacity e.g. Sequeiros [2012]; Stevenson et al. [2015]). In turn, a change in slope is expected to influence deposit geometry, thickness and grain size patterns, eventually leading to different flow–deposit interactions. Ultimately, different channel slopes are expected to produce different depositional structures and grain size trends and therefore different result in different flow–deposit interaction and stacking patterns over longer terms.

Therefore, this thesis attempts to examine the relation between channel slope and flow behavior, depositional structures and stratal patterns resulting from repeated turbidity currents in submarine fans using a process-based, numerical model.

The main research question is as follows *What is the effect of channel slope on turbidity current dynamics, flow–deposit interaction and resulting bed stacking patterns?*

To answer the main research question several sub-questions will be answered first.

1. Can flow–deposit interaction and the stratigraphic evolution of submarine fan deposits be simulated in process-based modelling suite Delft3D-FLOW?
2. How does channel slope affect turbidity current dynamics?
3. How do these altered turbidity current dynamics affect depositional patterns — where sedimentation and erosion occur?
4. If these patterns are different, how are deposit geometry, thickness and grain size trends affected and how do subsequent flows interact with these?
5. Do different depositional patterns lead differences in lobe switching (lateral stacking)?
6. Is lobe-element switching (lateral stacking) governed by inherent controls, for example once some threshold in sediment bed stacking is met?
7. If so, what is the threshold thickness of the deposits for a turbidity current trajectory to diverge, i.e. force a lobe-switch? How does this relate to channel slope?

## 1.3 APPROACH

### 1.3.1 The issue with turbidity currents

Turbidity currents can be very difficult to monitor directly, for several reasons.

First, the flows occur in a relatively inaccessible location on the deep ocean floor therefore, monitoring requires various remote-observation techniques.

Second, fan-building flows are infrequent with recurrence intervals in the order of $10^2$ to $10^6$ years [Jobe et al., 2018], so it is impossible to monitor multiple large volume turbidity currents (flows that are significant in terms of sediment transfer to the deep ocean or fan-building) .

Third, turbidity currents have a record of damaging or destroying the measuring instruments placed in their path [Talling et al., 2013].

Consequently, what is lacking for submarine fan systems that usually are available for other depositional systems are direct observations of on-going processes of erosion and deposition. Thus, there remains a 'process gap' in our understanding of the formation of submarine fan elements and their associated deposits [McHargue et al., 2011]. Therefore, the study and understanding of submarine fan systems as reservoirs has lagged behind that of the other reservoir systems [Slatt, 2013].

Our understanding of turbidity currents is based heavily on the interpretation of their deposits, together with results from small-scale laboratory experiments and numerical models. More recently, advances in technology (like Acoustic Doppler Current Profiler (ADCP)) and mooring configuration have begun to enable successful direct monitoring of sediment density currents on the ocean floor [Talling et al., 2013; Azpiroz, 2018]. Such monitoring efforts are mostly concentrated in shallow-water settings, and are biased towards frequent (sub-annual) events. However, it is the longer-runout flows which reach submarine fans that form much of the rock record, and their

character may differ significantly from shorter and more frequent events [Talling et al., 2013].

Physical experiments provide high temporal- and spatial-resolution insights into the morphodynamic processes of sediment-gravity flows and fans; however, these studies lack the long-term ($> 10 \times 10^3$ yr) perspective of stratigraphic evolution and the complexity of field-scale depositional elements [Hawie et al., 2018]. Processes that occur in scaled physical experiments may also differ significantly from those in full-scale turbidity currents, due to scaling issues and input conditions Talling et al. [2013]. Outcrop-derived information is limited in that it is often very difficult (or impossible) to unambiguously infer the character of a sediment flow from its deposit alone, as different processes can form similar deposits Talling et al. [2013]. Remote measurement techniques give valuable but incomplete information on the internal characteristics of the flow. For one, the measurement are averaged over minutes. Second, such measurements are less reliable in the near-bed region and do not give information on bedload transport [Azpiroz, 2018].

### 1.3.2 Process-Based Numerical model

A process-based numerical model simulates the flow processes and interactions between flow and sediment that form the deposits. It achieves this by numerically solving the equations that describe the governing processes in the turbidity current; fluid motion (Computational Fluid Dynamics (CFD)) and sediment transport as well as the consequences of complex relationships and non-linear feedback that result from the two. Process-based numerical models can quantitatively predict the phenomena involved in turbidity currents and their interaction with the bed on geologic timescales [Groenenberg et al., 2009]. That makes numerical models a useful tool to overcome some of the difficulties associated with field- and experimental measurements (the process-gap).

In numerical models, the conditions can be dictated, making it possible to isolate parameters and construct a large number of different setups with relative ease.

Second, parameters can be saved at predetermined times throughout the simulation. This enables high-resolution (in both time and space), quantitative observation of the development of the flow and deposits step-by-step in 3D, providing a way to gain insight into the interaction between flow and sedimentation processes associated with the formation of lobes. Direct information can be obtained on a variety of properties of the sediment bed, among them the spatially varying distribution of grain sizes. This is useful in linking flow behavior to grain size trends. Furthermore, grain size trends are extremely valuable in building hydrocarbon reservoir models [Meiburg and Kneller, 2010].

Third, numerical studies reduce the times needed to perform experiments, especially compared to (true-to-time) field studies. This way, long-term self-organized submarine fan system dynamics can be modeled, while still considering short-term processes like flow–deposit interaction and turbulence in the case of 'full-physics' process-based models.

These factors make numerical models a convenient method to understand how sedimentary and morphodynamic processes — such as flow–deposit interaction — develop. In turn, these factors enable forward stratigraphic modelling of submarine fan lobes. Forward stratigraphic modeling can

be applied to predict the location and small-scale heterogeneities of depositional systems and petroleum reservoirs, as well as the depositional response to controlling factors [Burgess et al., 2019; Hawie et al., 2019].

However, a numerical model is by definition a simplification of reality — a reasonable approximation. Not all processes can be taken into account. The governing equations are idealized and simplified and therefore require assumptions to be made, and in our case some equations (e.g. sediment transport) make us of empirically-derived relations. Moreover, discretization implies that continuous data are computed at a reduced number of points (a computational grid) and times. The solutions of the discretized equations are just an approximation of the exact solution. Nevertheless, numerical models are still a valuable tool to try to make predictions about phenomena that cannot be tested at full scale.

*Other Types of Numerical Models*

Because process-based numerical model consider the interdependence between flow and sedimentation parameters based on elementary physics [Groenenberg et al., 2010], they are able to produce more realistic models of submarine fan lobes than other types of geological modelling, such as stochastic rule-based, and diffusion-type models.

Stochastic models (e.g. object-based models Pyrcz et al. [2005]) cannot be applied to explicitly model the unpredictable behavior that results from the interaction between flow and sedimentation and therefore suffer from being geologically unrealistic [Groenenberg et al., 2010].

Diffusion type (sediment mass-balance) models are able to adequately replicate depositional patterns in submarine fans over long spatial and temporal scales. However, over shorter length and time scales, morphodynamic processes resulting from the coupling of relief, flow, and sediment transport produce behavior that is not well described by diffusion [Straub, 2019; Hawie et al., 2019].

## 1.4 PREVIOUS PROCESS–BASED MODELS OF TURBIDITES

Groenenberg et al. [2010] compared a process-based, numerical model (FanBuilder Groenenberg [2007]) constrained by parameter values based on outcrop geology (e.g. grain size & sediment volumes) to outcrops. Their numerical realizations were able to replicate some aspects of the depositional architecture noted from the outcrop geology.

Burgess et al. [2019] used Lobyte3D, a reduced-complexity model of deposition in dispersive-flow fan systems the shows emergent behavior such as lobe switching and compensational stacking of a potentially hierarchical nature due to flow over a complex, evolving seafloor topography. Their model results showed clustering of beds and, in places, ordered beds even without any external signal. However, their model does not consider a detailed fluid physical and turbulent description of the flows.

El-Gawad et al. [2014] applied a field-scale numerical model to simulate turbidity currents in deep submarine canyons located on the continental slope of the Niger Delta. They used a similar formulation to the one used in this report. They were able to simulate 'realistic' turbidity currents flowing through a channel, and demonstrated that this approach can be utilized to

calculate the inflow conditions from the core data. The simulation results allow for the prediction of the resulting sediment depositional patterns [El-Gawad et al., 2014]. Their model is not openly available.

### 1.4.1 Delft3D-FLOW

The software that was used is Delft3D-FLOW, an open-source, process-based modelling suite that incorporates hydrodynamics, sediment transport, and morphology. Delft3D-FLOW is a multi-dimensional hydrodynamic, and transport simulation program developed by Deltares.

The hydrodynamics are based on three-dimensional Navier-Stokes equations for an incompressible fluid. Delft3D-FLOW solves the Navier-Stokes equations using shallow-water assumptions with the Boussinesq approximation (small density differences compared to reference density: $\Delta\rho \ll \rho_0$) [Deltares, 2019]. The shallow-water assumptions are valid because the horizontal grid scales are much larger than the vertical grid scales [Deltares, 2019].

Three-dimensional transport of suspended sediment is calculated by solving the three-dimensional advection-diffusion (mass-balance) equation for the suspended sediment. Delft3D-FLOW includes the effect of density differences due to suspended sediment (density-driven flow) in the momentum equations. The morphology is updated at each computational time-step, ensuring that hydrodynamic flow calculations are carried out using the correct bathymetry [Deltares, 2019].

The Reynolds-averaged Navier-Stokes (RANS) equations of Delft3D-FLOW are capable of resolving turbulence. Delft3D-FLOW provides the option to use a turbulence model to account for the vertical turbulent mixing, this is discussed in more detail in Turbulence Modelling.

3D numerical models with RANS turbulence closure provide a reasonable middle ground between accurately modelling flow structures and computation time. Such models can predict Reynolds-averaged velocities and density structures on complex bathymetry using a reasonably fine grid and can be applied to a wide range of scales [El-Gawad et al., 2014]. While still computationally expensive for large-scale (tens of km) and long-term (days) simulations, the computation times are manageable.

More details on the governing equations representing the modelled processes in Delft3D-FLOW are given in Chapter 3 METHODOLOGY & MODEL SETUP. For a complete description of the governing equations, as well as the numerical methods used, the reader is referred to the Delft3D-FLOW manual which is freely available on Deltares' website [Deltares, 2019].

### 1.4.2 Delft3D-FLOW Reservoir Analogues

Delft3D-FLOW has previously been applied to construct stratigraphic forward models of fluvio-deltaic reservoirs to quantify their evolution (e.g. van der Vegt et al. [2016]; Geleynse et al. [2011]; Vacek [2018]). These models provide a three-dimensional stratigraphy and morphology, and detailed information on the temporal development of the system. This information can be used to improve building geologically realistic hydrocarbon reservoir models and quantify uncertainty [Storms et al., 2016].

By integrating these numerical analogues in the traditional reservoir modelling workflow, the geological uncertainty of important reservoir properties of reservoirs can be quantified and limited [Storms et al., 2016].

### 1.4.3 Delft3D-FLOW & turbidity currents

Delft3D-FLOW was not developed specifically for research on turbidity currents, nor stratigraphic evolution of submarine fans [Deltares, 2019; Groenenberg, 2007]. Hence, utilizing it to model the evolution of submarine fan lobes is a novel application of this software. Given that this is a novel application of Delft3D-FLOW, the feasibility of it to adequately model lobes is another sub-question of this thesis.

Modelling turbidity currents in Delft3D-FLOW has been attempted before by Commandeur [2015], who applied Delft3D-FLOW to model comparatively small volume turbidity currents in an artificial lake and demonstrated that the model was able to capture the complex behaviour of turbidity currents in artificial lakes.

Ooms [2017] performed 2D-volume models of overspill of turbidity currents in intra-slope ponded basins in Delft3D-FLOW.

,

## 1.5 OUTLINE

Chapter 2 THEORETICAL BACKGROUND gives a more detailed description of submarine fan systems, turbidity currents, submarine fan depositional elements and flow–deposit interaction.

Chapter 3 METHODOLOGY & MODEL SETUP describes the methodology and the set-up of the model, its dimensions and the selected formulations and parameters.

Chapter 5 RESULTS presents the output from the Delft3D-FLOW simulations.

In Chapter 6 INTERPRETATION the hydro- and morphodynamic evolution in a simulation is described. The output of the different scenarios are compared.

Chapter 7 DISCUSSION discusses how the model can be related to geological time and how the model compare to other models, numerical and experimental.

In Chapter 8 CONCLUSIONS, a synthesis is made of the results and interpretations of all previous chapters.

Finally, in Chapter 9 RECOMMENDATIONS & FUTURE WORK, recommendations are made for future research that can build on this work, improve the calibration of these models and improve the modelling process in general.

# 2 THEORETICAL BACKGROUND

## 2.1 SEDIMENT-GRAVITY FLOWS

Sediment-gravity flows are the main mechanism of transport, erosion, and deposition in submarine fan systems [Kuenen and Migliorini, 1950]. Sediment-gravity flows are mixtures of sediment and water that flow downslope, driven by the density difference between the particle-laden flow and the ambient water [Kuenen and Migliorini, 1950].

Submarine sediment-gravity flows can move enormous volumes of sediment and redistribute more sediment across the surface of the Earth than any other sediment flow process [Talling et al., 2015].

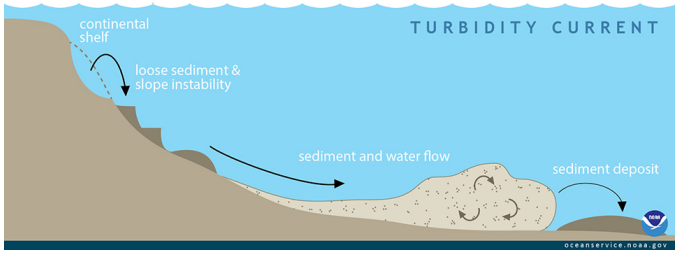


**Figure 2.1:** Diagram of turbidity current (no scale implied). From NOAA [2018]

### 2.1.1 Turbidity Currents

Turbidity currents are a type of sediment-gravity flows with dilute mass concentrations propelled by suspended sediment sustained via fluid turbulence [Parsons et al., 2007]. The turbulence in turbidity currents is typically generated by the forward motion of the current along the sea bed, the motion being in turn driven by the action of gravity on the density difference between the particle-fluid mixture and the ambient fluid [Meiburg and Kneller, 2010]. Turbidity currents are highly stratified, with sediment concentration rapidly decreasing from a maximum value close to the bottom. The grain size of suspended sediment also decreases upward, so that sand or coarser sediment is commonly restricted to the lowermost part of the submarine channel [Hiscott et al., 1997]. Another characteristic feature of turbidity currents is their velocity profile. The maximum velocity in turbidity currents is somewhere between the upper and lower boundaries of the flow, often closer to the bottom [Sequeiros, 2012; Deptuck and Sylvester, 2017].

In the transverse structure of turbidity currents (i.e. along channel from front to back), a distinction can be made between a front region (or head) and a trailing body. Regions of intense mixing most often occur at the front, here the turbidity current mixes with the ambient fluid [Parsons et al., 2007]. The flow shows a general decrease in both mean velocity and sediment

concentration upstream of the front followed by a thinning tail [Kneller and Buckee, 2000].

Turbidity currents are highly complex phenomena; they are nonuniform, unsteady, nonlinear, free boundary-flows driven by a non-conservative density difference (i.e. the density difference varies as sediment is eroded or deposited) and a combination of body and pressure forces [Kneller and Buckee, 2000].

### 2.1.2 Interaction of turbidity currents with the ocean-floor

A turbidity current interacts with the ocean-floor sediments as it accelerates down-slope. The nature of this interaction can be subdivided into three main conditions: i) **Erosive** flows that incise into the underlying substrate, and draw in sediment from the bed in a process known as entrainment. Entrainment of bed sediment increases the flow's density, potentially leading to self-acceleration of the flow. In this mode, a turbidity current accelerates via a self-reinforcing cycle of sediment entrainment, which increases the gravitational pull (i.e. negative buoyancy) on the current, and flow acceleration, which increases the capacity to entrain more bed sediment [Parker, 1982; Parker et al., 1986; Sequeiros et al., 2009]. ii) **Bypassing** flows that are able to transport all their sediment without depositing on or eroding of the ocean floor. iii) **Depositional** flows that deposit their sediment load, forming sediment accumulations on the ocean floor, these deposits are termed *turbidites*. Turbidites are formed in an incremental layer-by-layer fashion, with segregation of larger and smaller grains Kuenen and Migliorini [1950]; Talling et al. [2013]

As the flow traverses through the submarine sediment-routing system, a turbidity current can transform from one of these conditions into another [Stevenson et al., 2015]. These transformations are triggered by internal changes in the flow, such as a deceleration due to friction, but also by abrupt changes in the bathymetry over which the turbidity current flows [Pohl, 2019].

## 2.2 SUBMARINE CHANNELS

Repeated passages of turbidity currents into the deep sea are the principal processes responsible for sculpting submarine channels [Ortiz and Klompmaker, 2015]. These submarine channels range from short-lived gullies to extensive, continental-slope incising submarine canyons [Deptuck et al., 2008]. Submarine canyons are incisions into continental margins that act as conduits of sediment en route to the deep sea [Allen, 2017]. Channels within submarine fan systems (10—1000 km in length) often have levees resembling those of river channels, formed analogously by overspill from the channel onto the adjacent sea floor; deposition within the channel and on the levees often results in elevation of the channel-levee system above the surrounding surface [Normark and Damuth, 1997; Meiburg and Kneller, 2010]. Submarine channels act as conduits for turbidity currents, focusing the flow and thereby allowing for bypass of large volumes of suspended sediment down the continental slope onto the deep-marine basin floor [Stevenson et al., 2015; Pohl, 2019; Deptuck et al., 2008; Slatt, 2013].

### 2.2.1 End of submarine channels

Upon leaving the terminal channels in base-of-slope to basin floor transitions, turbidity currents usually changes in flow behavior in response to two abrupt morphological changes.

The first morphological change is a slope break — a decrease in ocean floor slope — leading to deceleration of the flow. Second, is a loss of lateral confinement, as the current is no longer channelized, it tends to spread. Upon losing confinement, turbidity currents can be prone to eroding the seafloor [Hofstra et al., 2015; Pohl, 2019]. As a result, a transitional zone characterized by erosional and bypass processes can often be found in the proximal parts of the lobe near the channel mouth [Deptuck et al., 2008]. This zone is often termed the channel-lobe transition-zone (CLTZ) [Mutti and Normark, 1987].

As the current expands radially and decelerates, the flow loses its capacity to carry sediment, and a deposit accumulates as sediment falls out of suspension. Finally, the turbidity current is depleted when it has spread out as a laterally extensive, sheet-like deposit on the ocean floor [Slatt, 2013; Kuenen and Migliorini, 1950].

## 2.3 TERMINAL LOBES

Where turbidity currents exit submarine channels, lobate sediment bodies that thin distally are deposited [Mulder and Alexander, 2001]. With repeated flow events individual depositional beds stack to form composite bodies. These composite bodies are referred to as terminal lobes. Each lobe is built by deposition of many turbidity currents characterized by different volume, concentration and velocity [Deptuck et al., 2008]. The range of flow properties reaching the distal fan is filtered as only flows with volumes on the higher end travel this far [Prelat and Hodgson, 2013; Jobe et al., 2018]. Frequent, small volume flows begin in the canyon, but often do not reach the fan. Larger and less frequent flows are responsible for building submarine fan lobes [Jobe et al., 2018].

When lobes are starved of sediment, either due to an avulsion in the feeder channel or due to lobe-switching, background sedimentation due to hemipelagic fallout can encase lobes in fine-grained mud. These form impermeable, non-reservoir bounding units that compartmentalize stratigraphically adjacent architectural elements, impeding connectivity. Therefore, they may have a significant impact on hydrocarbon production [Pyrcz et al., 2005; Parsons et al., 2007].

### 2.3.1 Compensational Stacking in Lobes

A key outcrop-derived characteristic of terminal lobe deposits is the presence of systematic vertical patterns in bed thickness [Mutti and Sonnino, 1981]. As briefly mentioned in INTRODUCTION, compensational stacking describes the tendency of deposits to preferentially fill topographic lows, smoothing out topographic relief, 'compensating' for localized deposition of discrete depositional elements [Mutti and Sonnino, 1981]. This tendency is thought to result from periodic reorganization of the sediment transport field to minimize potential energy associated with elevation gradients [Straub et al., 2009]. Compensational stacking is an extremely common fea-

ture in submarine fans, and appears to occur at both bed scale as well as at fan lobe scale and even larger scales [Groenenberg et al., 2010; Cantelli et al., 2009].

### 2.3.2 Compensation cycles

Several authors (e.g.Mutti and Sonnino [1981], Deptuck et al. [2008], Prelat et al. [2010], Straub and Pyles [2012]) suggested depositional cycles arising from compensational stacking, sometimes termed *compensation cycles*. In these models, the structure of the sediment-transport field remains fixed over geologically short time intervals. Repeated deposition by turbidity currents results in deposits with positive surface relief (aggradation). This depositional relief affects the trajectory of subsequent flows, and thus the emplacement of successive deposits [Straub et al., 2009]. Periodic avulsion redirects the sediment transport field to local topographic lows. The sediment-transport field then remains approximately fixed in space and the bed aggrades via a focusing in sediment deposition until sufficient relief develops to drive a new avulsion [Straub et al., 2009; Straub and Pyles, 2012].

Turbidite beds in terminal lobes have little-to-no lateral confinement, allowing them to spatially expand, thereby responding more easily to lateral slopes developed by depositional trends [Straub and Pyles, 2012]. Terminal lobe architecture is ultimately controlled by smaller-scale avulsions near the channel mouth that, to varying degrees, redirect sediment to different lobe settings [Deptuck and Sylvester, 2017]. These small scale avulsions, such as compensational cycles, constrain the distribution of lithofacies [Pyrcz et al., 2005].

### 2.3.3 Hierarchy

Compensational stacking occurs at a variety of scales in the lobe deposit. Hence, a number of hierarchies in lobe compensational stacking are evident [Deptuck and Sylvester, 2017]. Several authors have presented hierarchical frameworks of architectural elements to understand lobe architecture [Straub and Pyles, 2012]. While there are important differences in terminology between these schemes, all of them express a degree of organization to the architecture of submarine fans. Moreover, all schemes utilize similar descriptive aspects, including nature of bounding surfaces, external form, internal lithofacies distributions, and stacking patterns [Straub and Pyles, 2012; Groenenberg et al., 2010].

The hierarchy used in this thesis follows that proposed by Deptuck et al. [2008] and later refined by Prelat et al. [2010] and Straub and Pyles [2012]. This scheme consists of four main depositional components, with the basic principle that one or more components stack to form the next larger component of the hierarchy. Each hierarchical level is defined according to the abruptness of the shift between the thickest parts of successive bodies (lateral or proximal to distal) [Deptuck et al., 2008].

The architectural elements in the hierarchical framework from small to large are

1. **Beds** are the fundamental building block. Beds are the product of a single expanding, depositional flow event. Beds and bed-sets typically show systematic shifts in the point of the thickest deposit, caused by the subtle bathymetric influence of previous deposits on subsequent

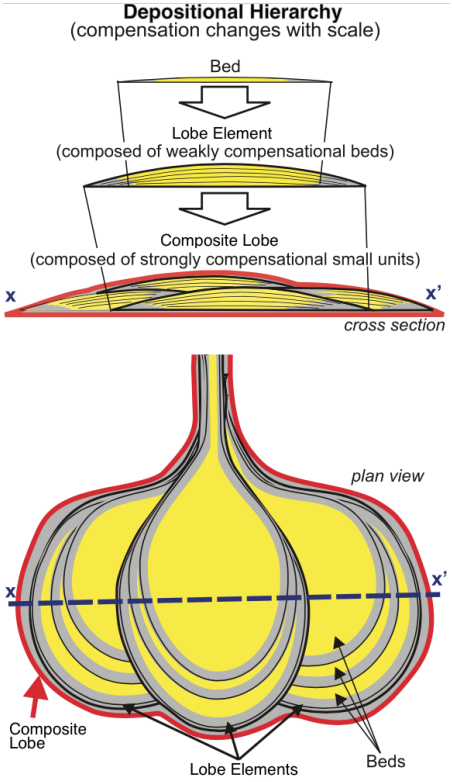


Figure 2.2: Diagram of depositional hierarchy showing scale-dependent compensation (no scale implied). Adapted from Straub and Pyles [2012]

flows [Deptuck et al., 2008]. This process is referred to here as **bed compensation**.

2. **Lobe elements** are comprised of contiguous stacks of beds. Commonly, lobe elements are radial to elongated bodies. Each lobe element probably represents the deposits from a number of flows with relatively similar properties. Autocyclic processes may prompt lobe-element switching once some threshold in bed compensation is reached, forcing a change in flow path without requiring a change in flow properties [Deptuck et al., 2008]. This process is referred to as **lobe-element compensation**.

3. **Composite lobes** consist of two or more lobe-elements separated by disconformable surfaces, such as thin (hemi-)pelagic drapes. Lobe-elements stack in an apparently arbitrary pattern within composite lobes, with shifts in position inferred to result from a change in channel-mouth position due to small-scale avulsions or channel migration.

4. **Lobe complexes** consist of stacked composite lobes that are fed by the same primary conduit.

In short; beds stack to form lobe-elements; lobe-elements stack to form composite lobes; and composite lobes stack to form lobe complexes [Deptuck et al., 2008] with different intensities of compensation occurring at each scale, large components stack more compensationally than small units [Straub and Pyles, 2012].

Beds and lobe-elements are generally below the resolvable limit of seismic but may impose significant control on the reservoir response [Slatt, 2013;

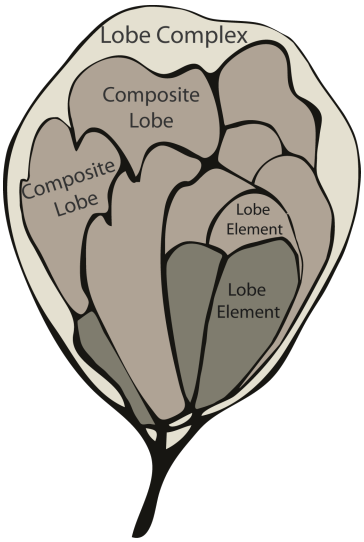


**Figure 2.3:** Plan view sketch of composite elements in depositional hierarchy (no scale implied). Adapted from Prelat et al. [2010]

Pyrcz et al., 2005]. Lobes and lobe complexes represent reservoir-scale features [Pyrcz et al., 2005]. In this study, only beds and lobe-elements are considered and modeled.

### 2.3.4 Justification for hierarchy in submarine fans

Deptuck et al. [2008] imaged lobes in small, sandy submarine fans east of Corsica using ultra-high-resolution boomer seismic profiles ( $<$ 1 m vertical resolution) and then ground truthed the sediment type using piston cores. From this, they recognized three hierarchical levels of compensational stacking. They concluded that small-scale geometries commonly mimic the large-scale geometries, so that one composite element itself is constructed of compensationally stacked smaller depositional elements.

Straub and Pyles [2012] have demonstrated that subdivision of stratigraphy into hierarchical units through field observations results in groupings with quantitatively different degrees of compensation. Their results are interpreted to document that hierarchical divisions based on compensation are justified.

## 2.4 CONTROLS ON SUBMARINE LOBE FORMATION

A range of inter-related factors control lobe formation, these factors include: i) flow properties (volume, duration, grain-size, concentration and velocity); ii) the number and frequency of flows, and their degree of variation through time; iii) sea floor morphology v) the distributary channel geometry Deptuck et al. [2008]; Hamilton et al. [2017]

### 2.4.1 Allo- vs autogenic

These controlling factors are governed by the interplay of auto- and allogenic dynamics [Groenenberg et al., 2010]. Autogenic dynamics refer to

behavior internally generated by the sedimentary system — patterns, variability, or dynamics that arise solely as a consequence of interacting components within a particular system [Hajek and Straub, 2017]. Whereas allogenic dynamics are those externally imposed on the system, such as climate, tectonic framework, and eustasy [Prelat et al., 2010]. In this study, only one autogenic control (slope) is considered.

Allogenic processes are dominant at larger spatial and longer temporal scales — at the lobe complex level. Whereas autogenic processes are dominant at smaller spatial and shorter temporal scales [Groenenberg et al., 2010] — at the bed and lobe-element scale. Allogenic control is important in the evolution and preservation of submarine fans, however, experiments on submarine fans, and other siliciclastic sedimentary landforms; deltas, and alluvial fans, indicate a high degree of autogenic behavior, on temporal and spatial scales much larger than previously thought — scales on the same level as allogenic controls. [Hajek and Straub, 2017; Hamilton et al., 2015; Wang et al., 2011; Burgess et al., 2019]. This implies that autogenic processes can produce depositional patterns similar to those associated with allogenic forcing [Hajek and Straub, 2017].

Cyclical processes like lobe-element-switching are autogenic — arising spontaneously within a sediment-transport network — and produce ordered, self-organized depositional patterns (as mentioned in Compensation cycles) [Burgess et al., 2019; Hajek and Straub, 2017]. To improve the ability to model stratigraphic architecture of submarine fans, better knowledge of what these autogenic patterns look like and what controls their underlying dynamics is needed. Better knowledge of underlying dynamics can lead to better identification of autogenic from allogenic signals, so past conditions can be better derived from deposits.

# 3 METHODOLOGY & MODEL SETUP

The principal aim of the model is to obtain a better fundamental understanding of the effect of channel slope on processes that govern the deposit geometry, flow-deposit interaction, and stacking patterns in submarine-fan systems at the level of beds over 50 successive flow events.

## 3.1 METHODOLOGY

The hydrodynamics and sedimentary processes that govern the turbidity current dynamics and are responsible for the formation of lobe deposits are modeled by simulating the governing physics. This way, a 3D representation of the simulated flow dynamics and the resulting deposits is obtained.

The model bathymetry represents a fixed, submarine distributary channel terminating into an unconfined basin plain at a base-of-slope position. A slope break coincides with the channel end, meaning the channel is steeper than the basin.

The effect of channel slope on turbidity current dynamics, deposit geometry and stacking patterns is tested by running three different scenarios in which only the channel slope is varied. All other input parameters and boundary conditions are kept constant between all simulations to isolate the effect of channel slope and to ensure the emergent dynamics are purely autogenic. So parameters given in this chapter — save for the slope — apply to all scenarios.

Flow–deposit interaction is tested by modelling the passage of repeated turbidity currents. This is achieved by running sequential simulations, in which the stratigraphic, hydrodynamic and bathymetric output of the preceding simulation are used as initial conditions for the subsequent simulations.

A number of trial models were performed before arriving at the input values of the final models reported on here. Only the results of the final models are discussed in detail in this report. A concise overview of experimental designs and their issues is given in Appendix A.

## 3.2 SIMULATED TIME

In a Delft3D-FLOW simulation, a time is determined by its number of time-steps after a reference date. A condition for the maximum admissible time-step is dictated by the Courant-Friedrichs-Lewy number (CFL) for wave propagation, a constraint that arises from the time integration scheme.

The CFL condition expresses that the distance that any information travels during the time-step length within the grid must be lower than the distance between grid elements. In other words, information from a given cell must

propagate only to its immediate neighbors in one time-step [Caminha, 2019]. The CFL is given by:

$$CFL = \frac{\Delta t \sqrt{gH}}{\Delta x} \tag{3.1}$$

where $\Delta t$ is the time step in seconds, $g$ is the acceleration of gravity, $H$ is the total water depth, and $\Delta x$ is the value of the horizontal grid spacing.

Generally, the time-step must be small enough such that the CFL does not exceed a value of 10 with $\sigma$-coordinate grid (Section 3.3.2), otherwise the simulation will produce inaccurate results [Deltares, 2019].

Each run simulates 19 hours and 48 minutes in time-steps of 0.3 min (18 sec).

For a water depth 700 m, the maximum depth in the experiments, a time-step of 0.3 min yields a satisfactory CFL of 7.46. For geological modelling in general, this a very high temporal resolution, but for modelling the detailed physics of flow-bed interaction, this is a low temporal resolution. The time-step is a compromise between these two ends. Trial simulations for this model with larger time-steps displayed numerical instabilities (see Appendix A).

| | **Model times** | |
|---|---|---|
| | Value | Units |
| **Time-step** | 0.3 | min |
| **Simulated time** | 19:48 | hh:mm |
| **Reference date** | 00:00 01/02/2020 | — |
| **Nr. of time-steps** | 3960 | — |
| **Output time-step** | 108 | min |
| **Simulation time** | 04:30* | hh:mm |
| **Reference date** | 00:00 01/02/2020 | — |

**Table 3.1**: Time values of the model.
*Simulation time varies slightly (±20 min) between scenarios and increases in 'restart' runs.

Output of hydrodynamic, morphological and sedimentary quantities is written to file every 108 minutes (1 hour and 48 minutes). Ideally, this interval would be lower, but file size constraints for storage and processing prohibit this.

## 3.3 COMPUTATIONAL GRID & GEOMETRY

Delft3D-FLOW solves the flow and transport equations on a staggered, orthogonal grid horizontally and a $\sigma$-coordinate grid vertically. A $\sigma$-coordinate grid consists of layers bounded by two $\sigma$-planes, which follow the bed level and the free water surface. The number of layers over the entire horizontal domain is constant, irrespective of the local water depth. Because the $\sigma$-coordinate grid is boundary fitted, a smooth representation of the topography is obtained [Deltares, 2019]. The $\sigma$-layer thicknesses are specified as a percentage of total depth, therefore the vertical resolution decreases automatically with depth.

### 3.3.1 Horizontal grid

The model domain is represented by a regular horizontal grid size of 132 (m-direction) by 182 (n-direction) square grid-cells of 200 m length, see Figure 3.1 for a plan view of the geometry and grid. These dimensions are a compromise between detail, numerical stability and computational time. Additionally, these dimensions are large enough for the turbidity current to spread freely in the basin without experiencing boundary reflections interfering with the flow.

An enclosure is defined to exclude inactive grid-cells from the computational domain to save on computational time and output size. The enclosure area is marked by the white line in the plan view of the domain in Figure 3.1.

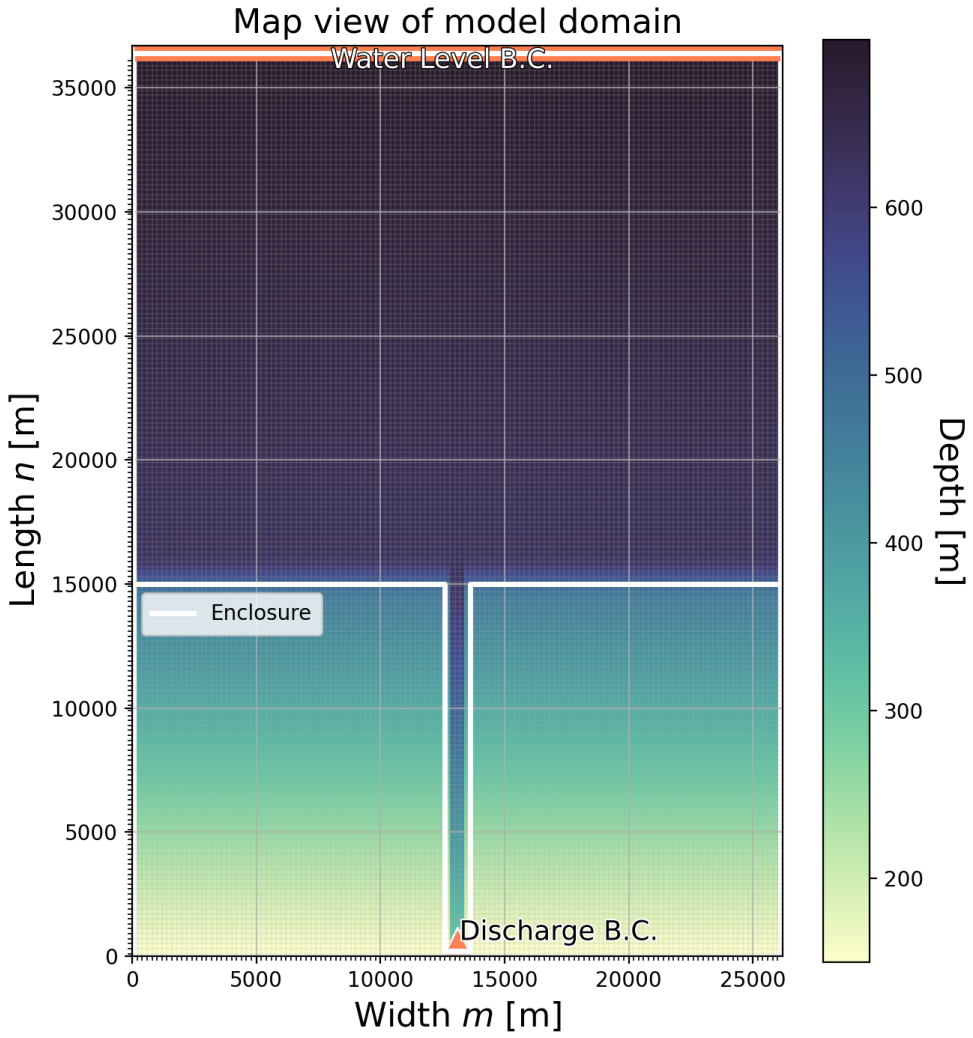


**Figure 3.1:** Plan view of model showing geometry, grid, bathymetry, enclosure and boundary conditions

### 3.3.2 Vertical grid

The vertical direction is discretized into 80 $\sigma$-layers. The thickness of $\sigma$-layers varies with depth. The $\sigma$-layers become increasingly thin towards

the bottom, decreasing from 5% of at the top, to 0.03% at the bottom layer. This translates to a 46 m top-layer and 0.2 m bottom-layer in the Slope 1.25° scenario for the deepest parts. Figure 3.2 depicts a vertical cross-section indicating the $\sigma$-grid interfaces of this scenario. In the near-bed area, the grid resolution is sufficient for practical purposes to model hydrodynamic features of the turbidity current and interaction with the bed.

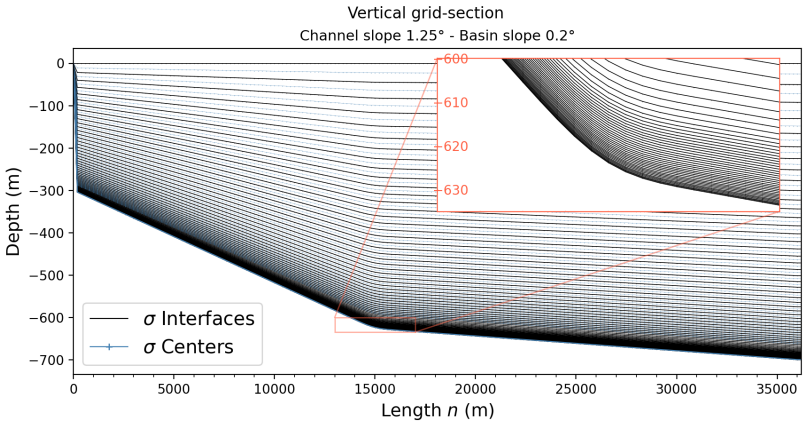


**Figure 3.2:** Vertical cross-section indicating $\sigma$-coordinate grid. Inset showing increasingly thin grid layers towards bottom. Vertical Exaggeration of 25

Only the regions disturbed by the turbidity current are of interest, so to prevent including vertical sections that are not of interest, the total water depth is set to a relatively shallow depth of at least 300 m. Another advantage of a shallower overall depth is that the $\sigma$-grid layers are thinner and therefore the vertical grid is of higher resolution.

Moreover, the CFL number depends on the radical of total water depth (see Section 3.2 and Equation 3.2), using deeper depths would lead to a higher CFL number.

### 3.3.3 Channel & Basin

A single, center-of-width 800 m-wide and 15 km long channel terminates into a basin. The length of the channel allows the turbidity current to reach developed flow conditions. The channel is bounded by steep walls of 150 m height to ensure no overspill occurs. The channel starts at a depth of 300 m and slopes down towards the basin, gradually becoming less steep near its end before terminating in to the basin.

The basin is unconfined to allow the flows to spread freely across a uniform basin floor without experiencing reflection. The basin is a sloped plane of 0.2°. This is based on values for gradient for lobe deposition areas of various ancient and modern submarine fan systems as compiled by Prelat et al. [2010].

#### *Smoothing of Slope Break*

$\sigma$-coordinate models have difficulty handling sharp topographic changes from one grid point to another, possibly giving rise to unrealistic flows [Deltares, 2019]. This was confirmed in preliminary simulations in which angular slope breaks caused numerical instabilities. To ensure stability, the slope break was smoothed by fitting a Bézier curve [Hermes, 2017] over 10

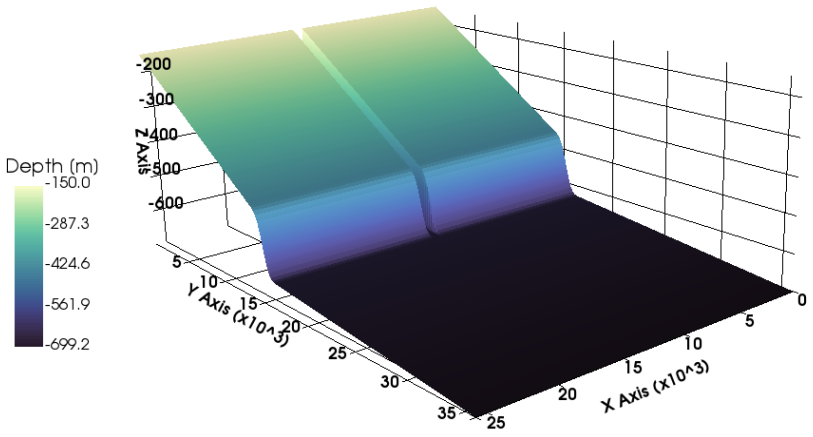


**Figure 3.3:** 3D plot of model bathymetry showing channel and basin dimension in m. Vertical exaggeration of 25

grid points centered on the slope break. Additionally, a gradual slope break is a more realistic representation of bathymetry than an angular one.

| | **Model** | |
|---|---|---|
| | Value | Units |
| **Length** $n$ | 36 | km |
| **Width** $m$ | 26 | km |
| **Grid-cell length** | 200 | m |
| **Grid-cell area** | 0.04 | $km^2$ |
| | **Channel** | |
| **Length** $n$ | 15 | km |
| **Width** $m$ | 800 | m |
| **Depth** | 150 | m |

**Table 3.2:** Dimensions of the model geometry.

## 3.4 HYDRODYNAMICS

The hydrodynamic module Delft3D-FLOW simulates three-dimensional (3D) unsteady flow and transport phenomena resulting from the effect of density differences (density-driven flow). It aims to model flow phenomena of which the horizontal length and time scales are significantly larger than the vertical scales [Deltares, 2019].

The constant water density is set to a density of 1025 $kg/m^3$, which is the average density of saline sea water at the sea surface.

| Parameter | Value | Unit |
|---|---|---|
| **Density** | 1025 | $kg/m^3$ |
| **Temperature** | 15 | °C |
| **Viscosity** | 0.001 | kg/s m |

**Table 3.3:** Constant physical parameters of seawater in model.

### 3.4.1 Turbulence Modelling

The turbulence structure affects the way in which sediment is suspended and transported and hence the way in which turbidity current behaviour and sediment deposition is modelled [Kneller and Buckee, 2000].

Turbulent flow is simulated by numerically solving the RANS equations. Here, Reynolds-averaging is used to separate turbulent fluctuations from the mean-flow. The primitive variables (e.g. velocity, viscosity, density) are averaged over the time and length scales of turbulent fluctuations. This introduces non-linear *Reynolds stresses*, which in this model are solved by the $k$-$\epsilon$ turbulence closure model based on the eddy viscosity concept [Deltares [2019] and references therein].

The $k$-$\epsilon$ model uses two transport equations (partial differential equations) to compute the transport of Turbulent Kinetic Energy (TKE) $k$, the kinetic energy of the turbulent flow per unit mass and turbulent kinetic energy dissipation rate $\epsilon$. Once $k$ and $\epsilon$ are known by means of numerical solving, the eddy viscosity and diffusivity can be determined. The output of a turbulence closure model is the eddy viscosity at each layer interface; which is used to calculate the vertical sediment mixing coefficient [Deltares, 2019].

The $k$-$\epsilon$ model is valid for highly turbulent and stratified flow like turbidity currents [Deltares, 2019]. Additionally, the $k$-$\epsilon$ model includes the effect of a vertical density gradient on damping the amount of vertical turbulent mixing, which is significant for the high-concentration, near-bed region of turbidity currents [Deltares, 2019; Ortiz and Klompmaker, 2015].

A turbulence-based model is appropriate for a situation in which there is significant vertical variation in the current properties, and hence is ideal for use with turbidity currents [Kneller and Buckee, 2000]. A drawback of the use of turbulence models is that the methods are costly in terms of computer power and time [Kneller and Buckee, 2000].

#### *Background Mixing*

Additionally, a background eddy viscosity $\nu_{back}$ is defined to account for all other forms of unresolved mixing. This is a constant amount of ambient turbulence added to the eddy viscosity $\nu_T$ computed by the $k$-$\epsilon$ model. These background values are defined as a horizontal and vertical components and are the minimum values that affect the vertical mixing of sediment [Gerritsen et al., 2008; Commandeur, 2015].

| Parameter | Symbol | Value | Units |
|---|---|---|---|
| | | **Horizontal** | |
| **Eddy viscosity** | $\nu_H$ | 1 | $m/s^2$ |
| **Eddy diffusivity** | $D_H$ | 10 | $m/s^2$ |
| | | **Vertical** | |
| **Eddy viscosity** | $\nu_V$ | $1 \times 10^{-6}$ | $m/s^2$ |
| **Eddy diffusivity** | $D_V$ | $1 \times 10^{-6}$ | $m/s^2$ |

**Table 3.4:** Uniform parameters for turbulence modelling.

## 3.5 SEDIMENTS

Processes included in sediment modelling are: i) The exchange of sediment between the bed and the flow and resulting feedback to hydrodynamics; ii) settling velocity of sediment under the action of gravity; and iii) the effect of sediment on the local mixture density and hence on turbulence damping [Deltares, 2019].

In Delft3D-FLOW, suspended sediments are represented as either 'mud' (cohesive suspended load transport) or 'sand' (non-cohesive bed- and suspended load transport) fractions [Deltares, 2019].

In this model, two sediment fractions were included. One fraction of each sediment class is defined, one cohesive and one non-cohesive fraction. The behavior of the sediments depends strongly on their parameters, which reflect their actual physical properties. Parameters for each sediment fraction are listed in Table 3.5. The specific density of both fractions is set to 2650 $\mathrm{kg\,m^{-3}}$, the density of quartz.

The morphology spin-up interval is a period of time at the start of the simulation during which no morphological changes are calculated. Here it is set to 45 min to prevent excessive morphological change close to the boundary condition shortly after the start inflow.

### 3.5.1 Critical Bed-Shear Stress

For sediment to be eroded, the force exerted by the fluid must exceed a threshold value in bed-shear stress, the so-called critical bed-shear shear stress. Conversely, for sediment to be deposited, the force exerted by the fluid must fall below a critical bed-shear shear stress. For bed-shear stresses within the range of the critical bed-shear shear stresses, fluxes between bed and water are calculated by a transport formulation [Deltares, 2019].

For the transport of non-cohesive sediment, the method of van Rijn [2007] is followed. This formulation uses several empirical relations based on grain-size classes [Deltares, 2019; van Rijn, 2007].

For cohesive sediment fractions, the fluxes between water and bed are calculated with the Partheniades-Krone formulations [Partheniades, 1965]. This formulation requires user-defined erosion parameter and critical bed-shear stresses, these are listed Table 3.5.

### 3.5.2 Settling Velocity

The settling velocity is the velocity with which particles in suspension sink to the bottom in motionless water Particle settling velocity is crucial for modelling sediment transport and deposition. The settling velocity for sand and mud fractions are strongly different in formulation. For the silt fraction, Stokes' Law can be used to calculate the settling velocity. For sand particles, a turbulent wake develops when particles settle, resulting in a departure from Stokes' Law [Sylvester, 2013] and therefore requires more complex formulations.

For silt fraction (cohesive), a settling velocity is defined in Delft3D-FLOW (see Table 3.5). For the sand (non-cohesive) fraction, Delft3D-FLOW computes the settling velocity with the method of van Rijn [2007]. The formulation used depends on the diameter of the sediment in suspension [Deltares, 2019].

The influence of salinity on flocculation of the cohesive fraction is disregarded by setting the settling velocity of saline water equal to that of fresh water [Deltares, 2019].

| | **Sand** | **Silt** | |
|---|---|---|---|
| | Value | Value | Units |
| **Name** | Medium silt | Very fine sand | — |
| **Type** | Non-cohesive | Cohesive | — |
| **Density** | 2650 | 2650 | $kg/m^3$ |
| **Dry bed density** | 1600 | 500 | $kg/m^3$ |
| **Median Grain Size ($d_{50}$)** | 100 | 25* | µm |
| **Settling velocity** | — | $3 \times 10^{-4}$ | $m/s$ |
| **Crit. bed-shear stress sed.** | — | 1000 | $N/m^2$ |
| **Crit. bed-shear stress ero.** | — | 0.1 | $N/m^2$ |
| **Erosion parameter** | — | $1 \times 10^{-3}$ | $kg/m^2 \cdot s$ |

**Table 3.5:** Parameters for sediments in model.
*$d_{50}$ converted using Stokes law

*Hindered Settling*

Settling of particles in a suspension is strongly affected by concentration. In low-concentration suspensions, particles settle freely — unhindered by other particles — on the basis of size, density, and shape according to Stokes' Law. At volume concentrations of greater than a few percent, particles no longer settle freely due to the presence of other particles and Stokes' Law breaks down. Settling of larger and denser particles displaces fluid and causes counterflow that carries smaller and lighter particles upward through the suspension, enhancing particle segregation and *hindering* settling [Major, 2003].

When a turbidity currents becomes depositional, particle concentrations near the sediment bed can become very high, which gives rise to hindered settling. Delft3D-FLOW uses the Richardson and Zaki [1954] equation to account for hindered settling. This equation calculates the reduction in particle settling velocity as a function of sediment concentration and the unhindered settling velocity [Deltares, 2019]. The reference density for hindered settling calculations is set to $1.6 \times 10^3$ kg/m$^3$.

## 3.6 BOUNDARY CONDITIONS

Boundary conditions represent the influence of the area beyond the model domain related to driving the simulation. Here, two boundary conditions are defined, a uniform water-level boundary at the end opposite to the channel, and a discharge boundary condition upstream of the channel. The boundaries along the sides (i.e.parallel to the channel) of the model are closed

The reflection parameter $\alpha$ (RPA) prescribes the reflectiveness for short-wave disturbances that propagate towards the boundary from inside the model. The RPA is set to 200 s$^2$ for the discharge and water-level boundary conditions to prevent rebound of one flow event interfering with the following one.

### 3.6.1 Side Boundaries

No flow can pass through the closed side-boundaries, the velocities normal to a closed boundary are set to zero. For large-scale simulations like this, the influence of the shear-stresses along closed boundaries can be neglected, therefore free-slip is applied for all closed side-boundaries [Deltares, 2019].

#### *Uniform Water-Level Boundary*

At the far end of the model, opposite to the discharge, an open uniform water-level boundary condition is imposed. The water-level is set to 0 m for the entire duration of the simulation. A water-level boundary acts as a nodal point for reflected disturbances [Deltares, 2019] and prevents the water-level from rising due to discharge.

### 3.6.2 Sediment Supply

Sediment supply into a Delft3D-FLOW model is specified as a mass concentration ($kg/m^3$) and water discharge ($m^3/s$) at a boundary. Initial global sediment concentrations are set to 0%. In this model, a vertical 3D-profile, discharge boundary condition is imposed upstream of the channel. This boundary condition is specified as time-series; the discharge lasts from 9 minutes to 48 minutes after the start of the simulation. A total discharge of 4500 $m^3\,s^{-1}$ is divided over the bottom 53 $\sigma$-layers one grid cell wide, this translates to an inflow height of 49.26 m.

The initial total suspended sediment concentration of the discharge is 3.0% by volume, equally divided between silt and sand (50% sand & 50% silt). This means 39.75 $kg/m^3$ of each sediment is initially in suspension.

This boundary condition can be considered the plane of origin for the flow and can be considered a finite-volume sediment release. In laboratory experiments, such a setup is often termed lock-exchange release. The flow is analogous to a surge-like turbidity current, such as one generated by slope failure.

The turbidity current is not modeled after measured values from a particular system. Values for discharge, concentration, and current inflow thickness are chosen somewhat arbitrarily. The sediment-laden flow is the only agent transporting sediment in to the model, no background sedimentation is included.

| Parameter | Value | Units |
|---|---|---|
| **Discharge** | 4500 | $m^3/s$ |
| **Duration** | 39 | min |
| **Inflow height** | 49.25 | m |
| **Inflow width** | 200 | m |
| **Concentration by mass (per sed.)** | 39.75 | $kg/m^3$ |
| **Concentration by vol.** | 3.0 | % |
| **Sediment volume*** | $3.158 \times 10^5$ | $m^3$ |
| **Morphology Spin-up Interval** | 45 | min |

**Table 3.6:** Details concerning the discharge B.C. parameters.

### 3.6.3 Bottom Roughness

Sediment transport is strongly dependent on bed roughness. Bed roughness in turn depends on the sediment transport generated by the bed forms migrating over the bed [van Rijn, 2007]. Bed roughness exists due to surface relief at the base of a flowing fluid and it exerts frictional effect on the flow. Two factors contribute to bed roughness i) grain roughness: the effects of the individual grains making up the bed and (ii) form roughness which refers to features of bedforms such as ripples and dunes Kumar [2011]. As turbidity currents are bottom hugging, the effects of bottom roughness on the flow need to be modeled.

Bottom roughness is calculated using bottom roughness length $Z_0$ (m). $Z_0$ is a function both of the bed conditions and the flow dynamics, which together create the drag.

A first estimate of the bed roughness length $Z_0$ in 3D computations can be derived from the equivalent geometrical roughness of Nikuradse, $k_s$:

$$Z_0 = \frac{k_s}{30} \tag{3.2}$$

Typical values of $k_s$ range from 0.15 m for river beds with sediment transport down to 0.01 m or less for smooth surfaces [Deltares, 2019]. A 'smooth' $k_s$ of 0.03 m is used in this model. This leads to a $Z_0$ value of $1 \times 10^{-3}$ m to include effects of grain-scale roughness and effects of bedforms and other relief that exist in a 200 m by 200 m area of sea floor [Ooms, 2017].

Other possible bottom roughness formulations, like the Chézy or Manning formulation, describe open channel flow, meaning they depend on water depth. As water depth varies strongly in this model, these formulations would lead to large differences in bottom roughness with depth, which would misrepresent the bottom roughness [Deltares, 2019; Ooms, 2017].

## 3.7 STRATIGRAPHY

The bed composition model is a layered bed stratigraphy. In this model there is one constant-thickness transport layer on the top; a number of bed composition bookkeeping to keep track of sediment deposits, and a thick base-layer that serves as a sediment reserve [Jagers, 2012].

Each half time-step the model calculates the quantity of sediment being eroded and the quantity of sediment being deposited [Deltares, 2019]. When sediments are deposited, they are initially added to the top-most *transport layer*, a homogeneously mixed bed layer. When the volume of the transport layer is exceeded, the excess sediments are pushed towards the bookkeeping layers beneath it, starting with the lowest. The bookkeeping layers are filled up to a maximum thickness, if this threshold is exceeded a new bookkeeping layer is created. If the creation of a new layer would exceed the specified maximum number of layers, layers at the bottom of the stratigraphy stack will be merged.

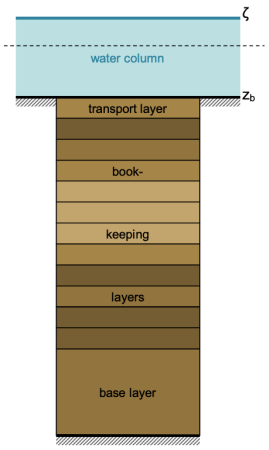


**Figure 3.5:** Diagram of layered-bed stratigraphy (underlayers). From Jagers [2012]

Only sediments in the transport layer are available for erosion, therefore the amount of sediment that can eroded or deposited per time-step is limited by the thickness of the transport layer. The erosion rate is proportional to the availability of the sediment fraction in the transport layer. After erosion, the transport layer is replenished from below [Deltares, 2019].

The transport layer is set to 50 cm thick, which is slightly more than the maximum bed erosion per run in preliminary simulations. The maximum number of bookkeeping layers is to 75, representing at most 3.75 m of stratigraphy. The initial bed sediment composition is set to match that of the flow sediment composition: 50% sand and 50% silt.

| Layer | Thickness | Units |
|---|---|---|
| **Transport layer** | 50 | cm |
| **Bookkeeping layer (max)** | 5 | cm |
| **Reserve layer** | 20 | m |

**Table 3.7:** Thicknesses for stratigraphy module layers.

## 3.8 CONSECUTIVE RUNS

The interaction between deposits and subsequent flows is tested by modelling the passage of repeated turbidity currents. This is replicated by running sequential simulations, here called runs. The preceding simulations fi-

nal (i.e.on the last time-step) stratigraphic, morpho- and hydrodynamic conditions are used as initial conditions for the subsequent simulation. So deposits emplaced during one run are left in place before commencing the next run [Azpiroz Zabala et al., 2020]. Sequential simulations enable modelling of the morphodynamic and stratigraphic evolution of lobes over longer timescales in high spatial- and temporal resolution while considering a detailed physical description.

### 3.8.1 The Issue with Passing Conditions

*Residual Hydrodynamic Conditions*

Because simulated times are not long enough for the hydrodynamics to completely return to equilibrium after a flow event, there are residual hydrodynamic conditions (e.g. velocity, suspended sediment) at the end of each run. When a subsequent run is started, Delft3D-FLOW restarts the simulation by reading all conditions on the last time-step of the previous run, including the residual hydrodynamic conditions of the previous flow event. In reality, turbidity currents do not immediately follow each other. This implies that when they exit submarine channels, the ambient water will be at rest — still and mostly devoid of suspended sediment, in contrast to our simulation (see Figure 3.6). Preferably, the next simulation should start from water-at-rest conditions, but currently restarting by reading only bed level and stratigraphy — without hydrodynamics — is not supported in Delft3D-FLOW.

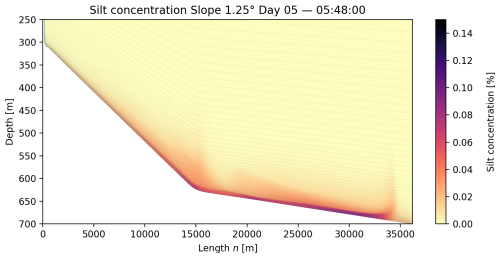


**Figure 3.6:** Vertical cross-section plot along channel showing residual suspended silt at end of 5th run. Color range decreased for emphasis.

*Transport-Layer Composition*

Trial simulations showed that the transport layer coarsens significantly in a single run, with sand volume fraction increasing to 70% within the channel and channel mouth area. After 5 runs, the bed sand volume fraction in these areas has increased to nearly 90%, as illustrated below in Figure 3.7b.

The lack of readily erodible, fine sediment in the bed reduces the volume of bed sediment that is entrained into following flows. As a result, the following flows are of lower density, and therefore do not self-accelerate like the first flow. In turn, this also means that less bed sediment in the channel is transported to- and deposited in the basin, leading to thinner deposits overall.

*Current Solution: Manually Resetting*

Passing relief and stratigraphy to the following simulation enables modelling growth of a lobe element over multiple flow events, but comes at the expense of residual hydrodynamics and quickly coarsening bed composi-

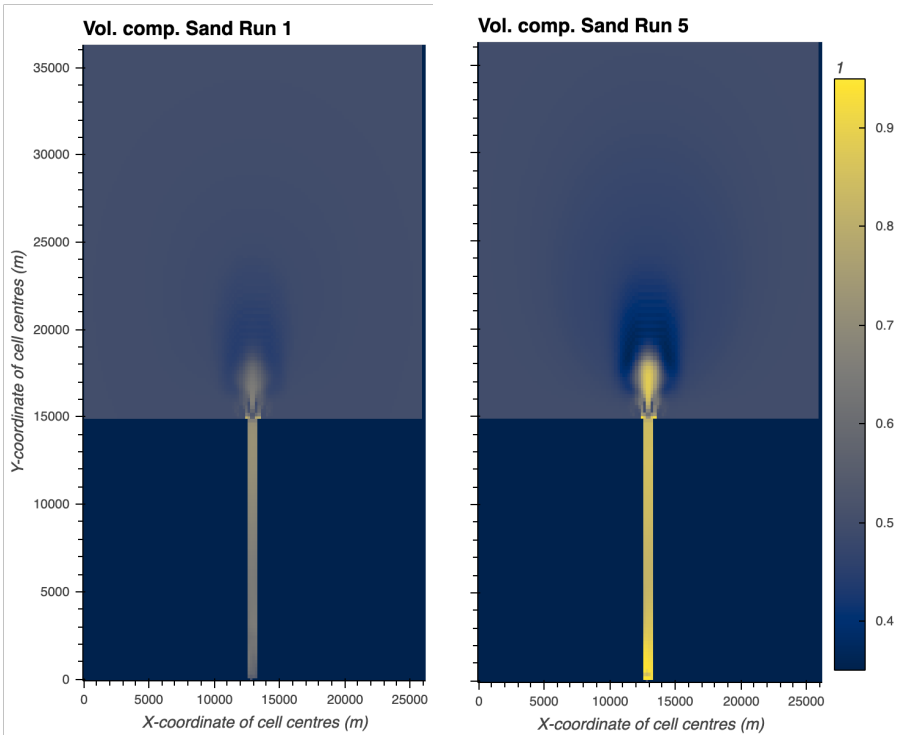


**(a)** Sand volume fraction of transport layer at end of 1st run

**(b)** Sand volume fraction of transport layer at end of 5th run

**Figure 3.7:** Example of coarsening of transport layer in channel and channel mouth over 5 runs

tion. To mitigate these issues, hydrodynamic properties are reset to resting conditions after every 5 runs. The following hydrodynamic quantities are reset to equilibrium conditions: 1) velocities; 2) density; 3) concentrations; 4) water level; 5) horizontal and vertical eddy viscosity; and 6) horizontal and vertical eddy diffusivity. The transport layer is reset to its initial 50% sand - 50% silt composition.

| Property | Delft3D Output Keywords |
|---|---|
| **Horizontal velocity** | `U1, V1` |
| **Vertical velocity** | `W, WHPY` |
| **Vertical eddy viscosity** | `VICWW` |
| **Vertical eddy diffusivity** | `DICWW` |
| **Horizontal eddy viscosity** | `VICUV` |
| **Water level** | `S1` |
| **Density** | `RHO` |
| **Sediment concentrations** | `R1` |
| **Transport layer composition** | `MSED, LYRFRAC` |

**Table 3.8:** List of properties that are reset with their Delft3D-FLOW output keywords.

Resetting is done by manually overwriting values in the output dataset from which the following run reads the initial conditions. Resetting is a practical necessity to keep computational time within bounds. Other possible solutions are discussed in Chapter 9 RECOMMENDATIONS & FUTURE

WORK. The downside of resetting the transport layer is that grain size patterns are discarded.

## 3.9 SCENARIO SLOPES

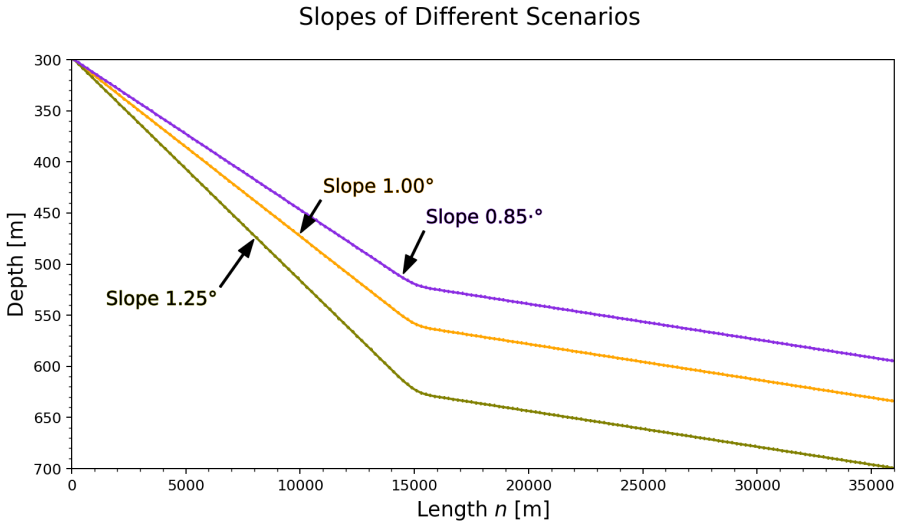


**Figure 3.8:** Depth profiles through channel of the three scenarios. Vertical exaggeration is approximately 30.

Three scenarios with different bathymetries were made. In each scenario only the slope of the channel is varied, this is illustrated in Figure 3.8. The initial idea was to center the slopes around 1.00° with step of 0.25° in negative and positive direction. A test run with a channel slope of 0.75° showed that the flow waned significantly before reaching the channel mouth. Therefore, the slope was increased to 0.85°.

The modeled slopes are comparable to those of small, sandy submarine fan systems, on the higher end of the range of slopes, as is evident from Figure 3.9 by Hamilton et al. [2017].

Each scenario comprises 50 consecutive flow event simulations. This number was based on expected deposit thickness and computational time.

## 3.10 MODEL SETUP WORKFLOW

1. The Delft3D-4 GUI is used to make all necessary input files for an initial, template model.

2. For the three scenarios, three bathymetry files — each with a different channel slope — are generated using Python scripts. The slope breaks are smoothed by fitting a Bézier curve Hermes [2017].

3. Multiple successive 'restart' models are generated based on the template model, in which start times in all relevant input files are adjusted according to their run number by use of a Python script.

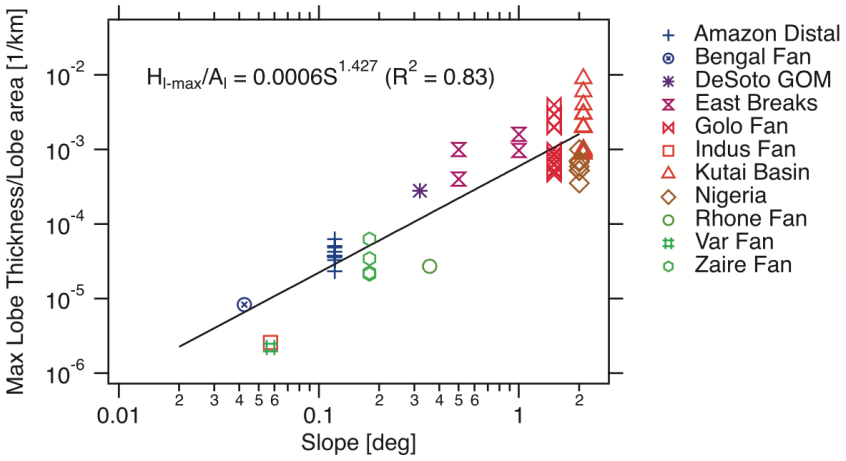


**Figure 3.9:** Plot of the maximum lobe thickness scaled by planform area against slope of several submarine fan systems. From Hamilton et al. [2017] with data from Prelat et al. [2010]

4. The simulations are run consecutively using Delft3D-FLOW Version 6.03.00.62434 with NetCDF outputin batches of five. NetCDF is a file format for self-described, hierarchical datasets [Unidata, 2019].

5. After every five runs, some properties in the output dataset are reset to their initial values (see Section 3.8.1) before they are fed to the next simulation.

For more information on the Python scripts used to prepare input files, the interested reader is refered to Appendix B.

# 4 ANALYSIS METHODS

This chapter describes how the output data from the simulations was processed.

## 4.1 ANALYSIS WORKFLOW

- Delft3D-FLOW is configured to write output in NetCDF format following the Climate and Forecast metadata conventions [CFc, 2020]. These files contains discrete values for bathymetry, the hydrodynamic conditions and sediment properties in the model at each output timestep (every 108 minutes).

- The Python libraries xarray [Hoyer et al., 2016] with netCDF4-python [Whitaker et al., 2019] are used to open and analyze the NetCDF datasets. xarray automatically decodes the values in the NetCDF objects according to CF conventions.

- The Python libraries Matplotlib [Hunter, 2007], HoloViews [Stevens et al., 2015] and PyVista [Sullivan and Kaszynski, 2019] are used to visualize the data.

All of the above-mentioned software are free and open-source, see appendix DELFT3D-FLOW & PYTHON for a more detailed description on processing Delft3D-FLOW output using Python and a link to the scripts and notebooks used to process and visualize output data.

## 4.2 BATHYMETRIC DIFFERENCE MAPS

Bathymetric difference maps show the cumulative erosion and sedimentation between two times. The bathymetric difference per run is obtained by subtracting the bathymetry at the end, from at the start of the run. This shows one flow's sedimentation and erosion patterns. The total bathymetric difference for successive simulations is obtained by subtracting the final bathymetry from that of the initial bathymetry of the very first simulation.

The threshold thickness for a grid-cell to be distinguished as a deposit is set to 0.2 cm, which is the lamina level of bed thickness. Lamina are generally defined as being less than 1 cm thick beds.

### 4.2.1 Mean Deposit Thickness

To calculate the mean deposit thickness, the arithmetic mean is taken of deposit thickness (i.e.difference in depth) between two times.

### 4.2.2 Planform Area

To determine the planform area of the deposits, grid-cells with values above a threshold are counted and multiplied by the grid-cell area.

# 5 RESULTS

The purpose of the simulations was to assess the effect of channel slope on the flow dynamics, their deposits, and if and how stacking patterns are affected in a process-based model. We report on 50 sequential simulations run of 3 scenarios with different channel slopes. First, a general description of the hydro- and morphodynamics is given of the first run in general. Then the results of a sequence of 5 runs are described. This chapter ends with a description of the evolving morphology over all 50 runs, with a section on how it is preserved in the stratigraphy.

## 5.1 FIRST RUN

The observations in this section apply to each first run of each scenario and after resets. The flows dynamics are similar between scenarios, however, exact values differ. When a property is described three values are listed behind, increasing in order channel slope (0.85°, 1.00°, 1.25°).

Right after the discharge of sediment-laden water, part of the sand fraction falls out of suspension and is deposited on the first 2 to 3 km of the channel bed. Afterwards, the discharged sediment concentrates to form a dense, stratified bottom-hugging, flow moving down the channel (Figure 5.1 & Figure 5.4).

The front of the flow is more dilute (silt conc. ∼5%, sand conc. 1% and slower ca 0.6 m/s (Figure 5.1b). Highest flow densities are reached 200 m upstream from the front (excess density up to 45–80 kg/m$^3$). Here, both sand and silt are more dispersed, with silt and sand reaching volume concentrations of 0.5% at 125 m and 65 m above the bed respectively (Figure 5.1d & Figure 5.1d). The density, sediment concentrations, and velocity decrease upstream from the front (Figure 5.1e).

A dense lower part — with highest densities directly above the bed — and an overlying, dilute plume characterize the flow's concentration profile (Figure 5.3). The dense basal layer is around 2–3 m thick, with excess density ranging from 30–55 kg/m$^3$ (Figure 5.1e). Suspended sand is concentrated in this dense basal layer, with maximum volume concentrations in the range of 20% behind the front decreasing to ∼1% upstream (Figure 5.1c). Suspended sand is less dispersed than suspended silt regardless of scenario. The concentration of suspended silt is also highest in the basal layer (60-80% behind the front) but it not restricted to a basal layer. Volume concentrations in the plume range from 10% just above the basal layer, to less than 1% higher up (Figure 5.1d).

The maximum velocity coincides with the upper boundary of the dense sub-layer (up to 2.6, 2.9, 3.4 m/s) and decreases towards the bed (Figure 5.3).

Turbulent kinetic energy is highest at 200 m upstream from front of the flow and decreases upstream (Figure 5.1a).

In a vertical profile, turbulent kinetic energy is at its maximum near the bed and decreases to 0 at the point of maximum velocity and steepest concentration gradients, at the interface of the dense basal layer (Figure 5.2).

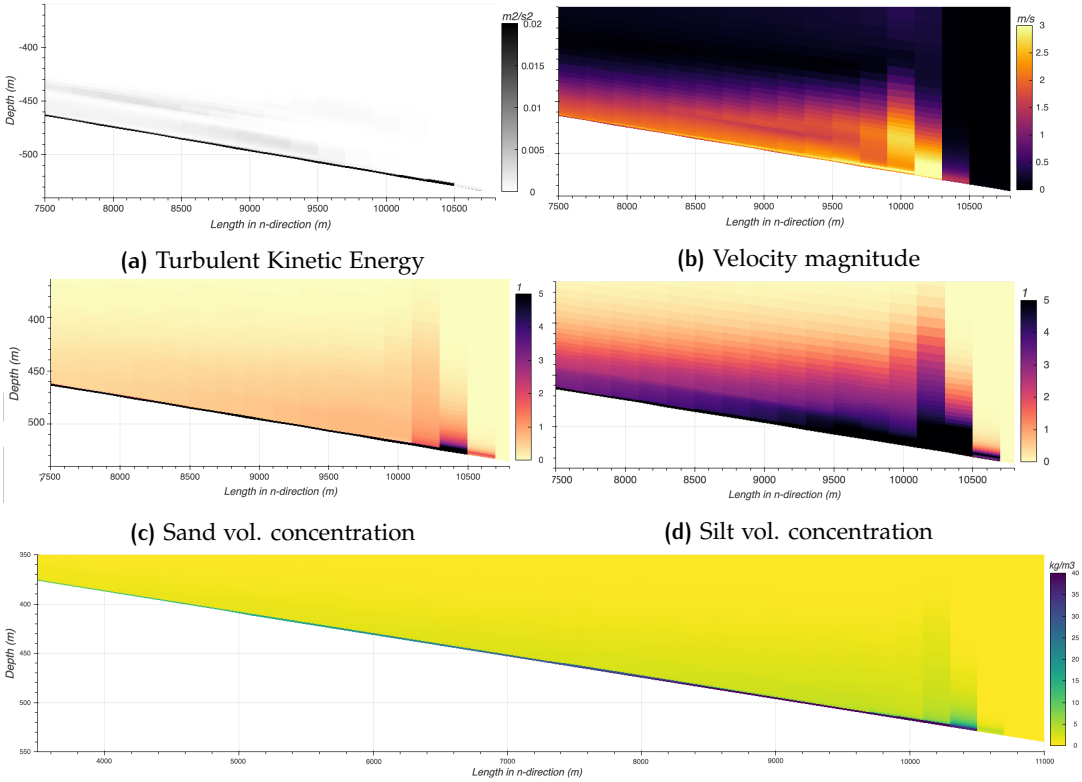


**(a)** Turbulent Kinetic Energy

**(b)** Velocity magnitude

**(c)** Sand vol. concentration

**(d)** Silt vol. concentration

**(e)** Extra wide cross-section of excess density to show horizontal extent of modeled flow

**Figure 5.1:** Vertical cross-sections along channel (X = 13 100 m) of turbulent kinetic energy, velocity, silt- and sand concentration, and excess density at 1 hour 48 min after start of first run. Vertical exaggeration of ∼50. Scenario with channel slope 1.25°

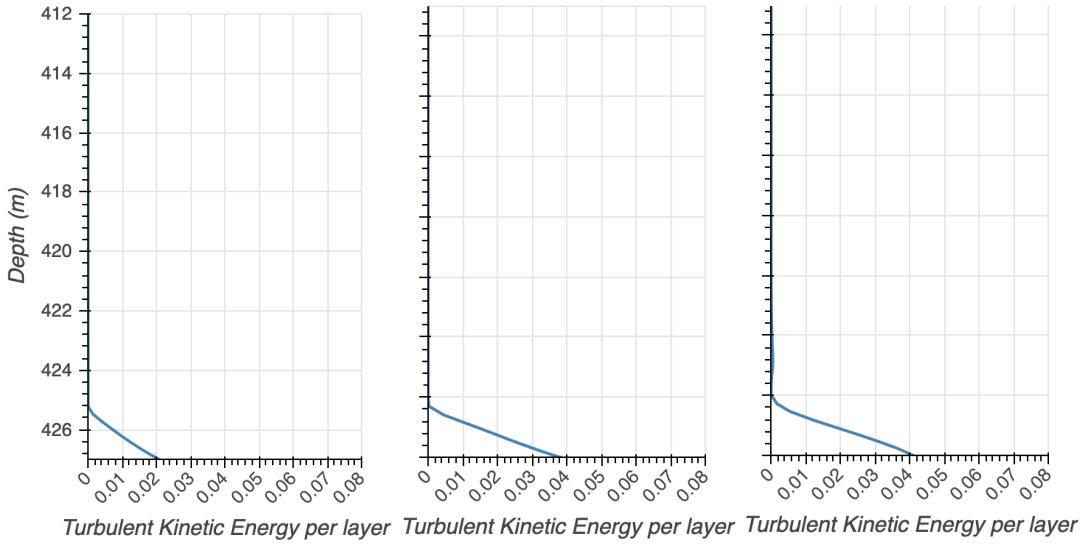


**(a)** Slope 0.85° y = 8600 m

**(b)** Slope 1.00° y = 9200 m

**(c)** Slope 1.25° y = 10 000 m

**Figure 5.2:** Profiles of turbulent kinetic energy at the front of the flow. x = 13 100 m

The following figures depict vertical profiles of density, velocity, and sediment volume concentration 200 m the front of the flow at the vertical grid cell centers. These profiles are taken in the channel (x = 13 200 m) at 1 hour 48 min after the start of the first simulation.

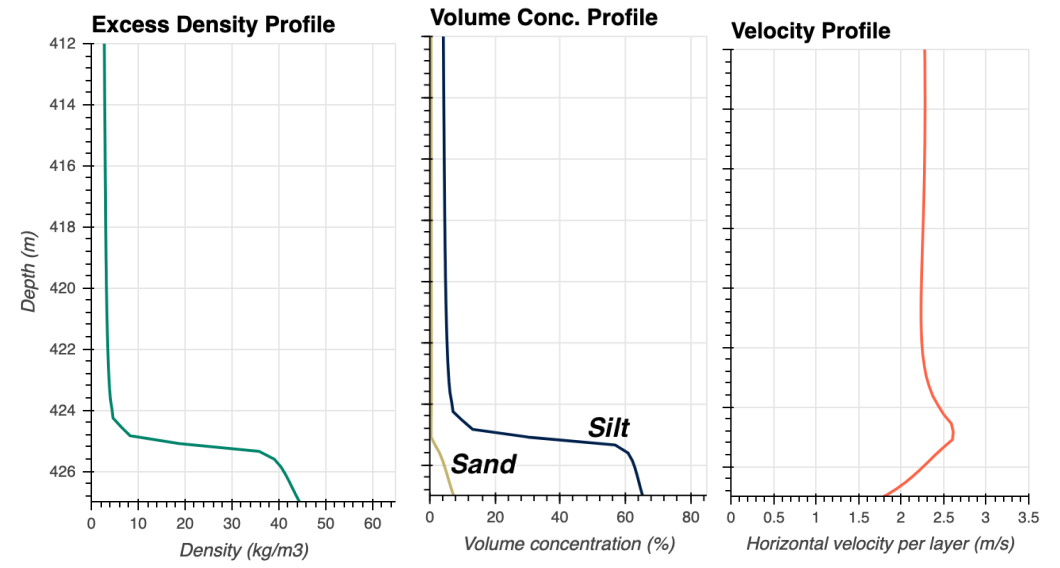


**Slope 0.85° y = 8600 m**

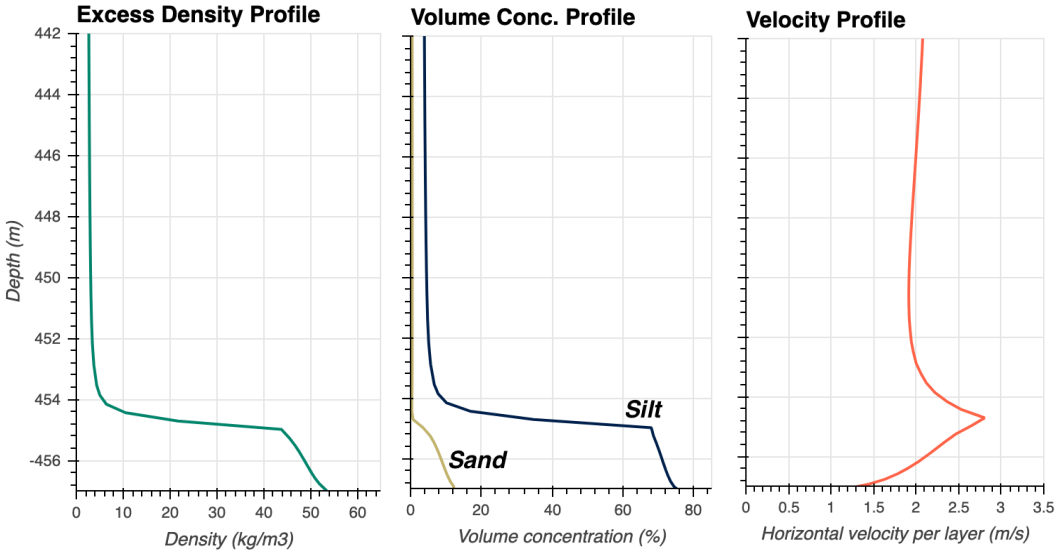


**Slope 1.00° y = 9200 m.**

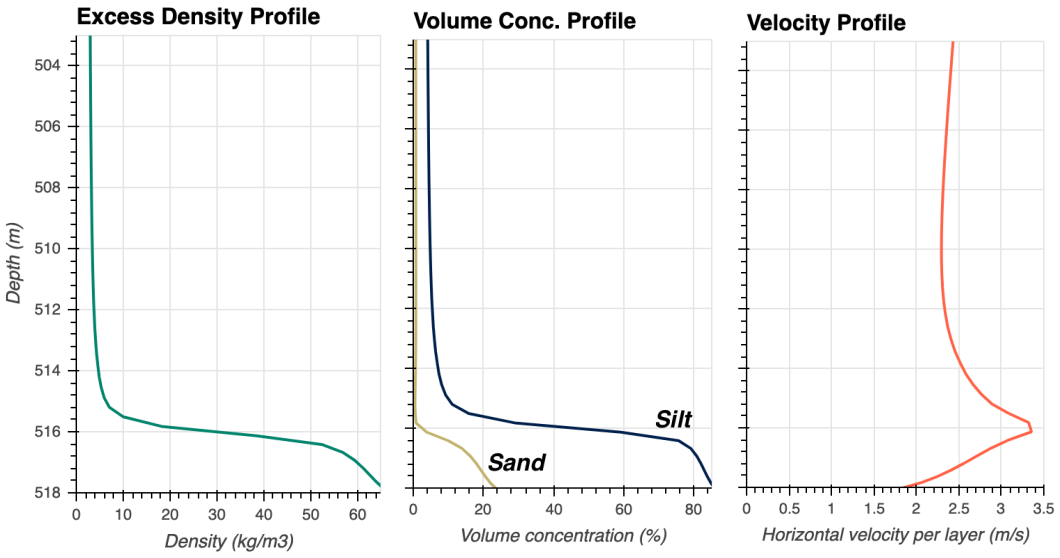


**Slope 1.25° y = 10 000 m**

**Figure 5.3:** Vertical profiles at center of vertical layers at 200 m up-dip of the flow head. 1 hour 48 minutes after start in the first simulation. X = 13 100 m)

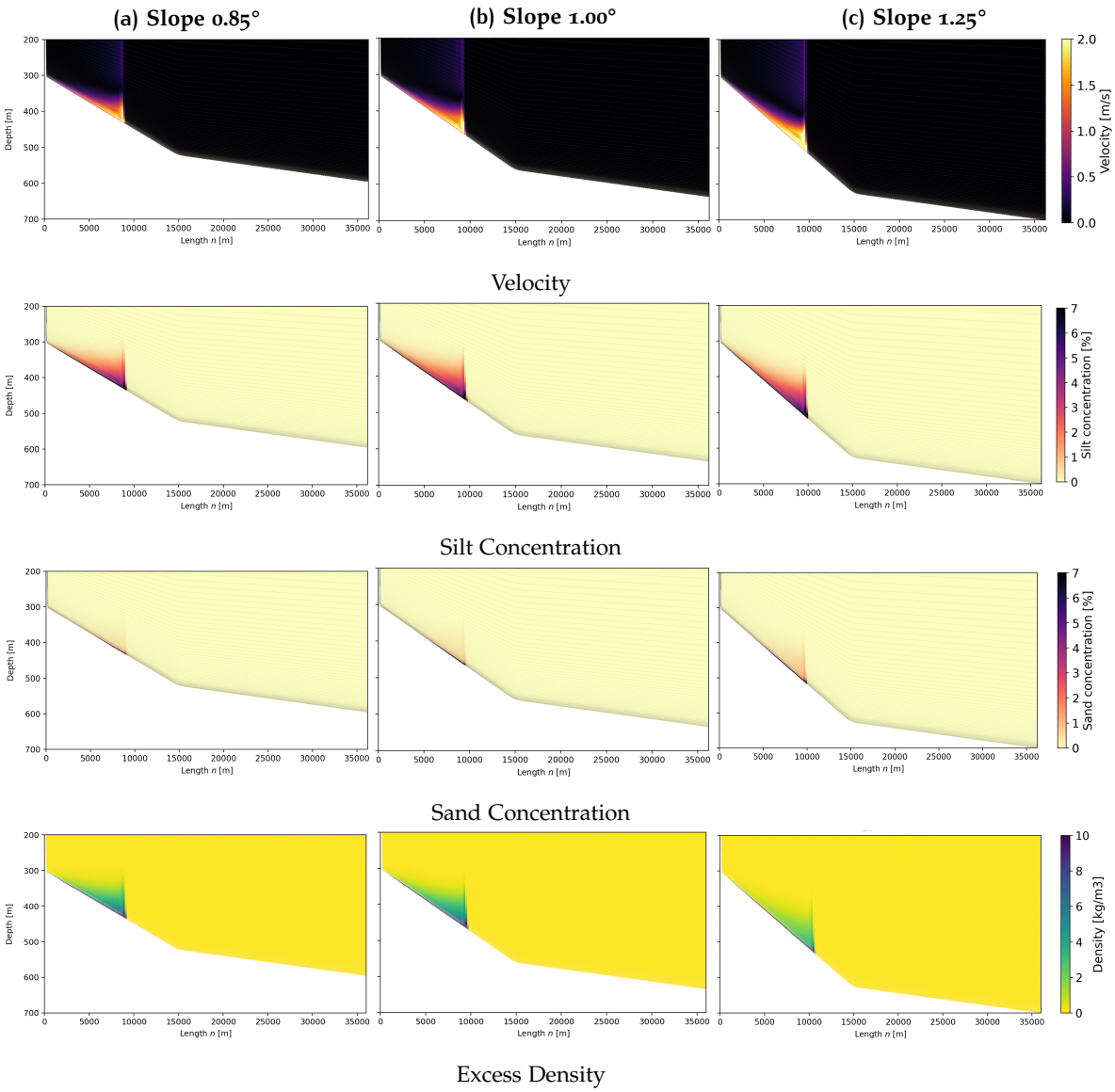


**Figure 5.4:** Plots of vertical cross-section along channel (X = 13 100 m) of density, velocity, silt- and sand concentration at 01:48:00 after start of first run. Scenarios are ordered in to columns with channel slope increasing rightward. Vertical exaggeration of ∼50. The flows in channels with higher slopes (rightward) are faster, have higher concentrations of suspended sediment and are consequently denser. Suspended sand is less dispersed than suspended silt regardless of scenario.

The density and velocity magnitude in the front both increase as the current flows down-slope in the channel. The flow erodes the channel bed and entrains silt as it flows down-slope (Figure 5.9d, Figure 5.9e, Figure 5.9f).

Only in the last ∼4 km of the channel, the flow entrains sand as well (Figure 5.9g, Figure 5.9h, Figure 5.9i). As the flow approaches the channel mouth, it decelerates over the gradually decreasing channel slope (Figure 5.6).

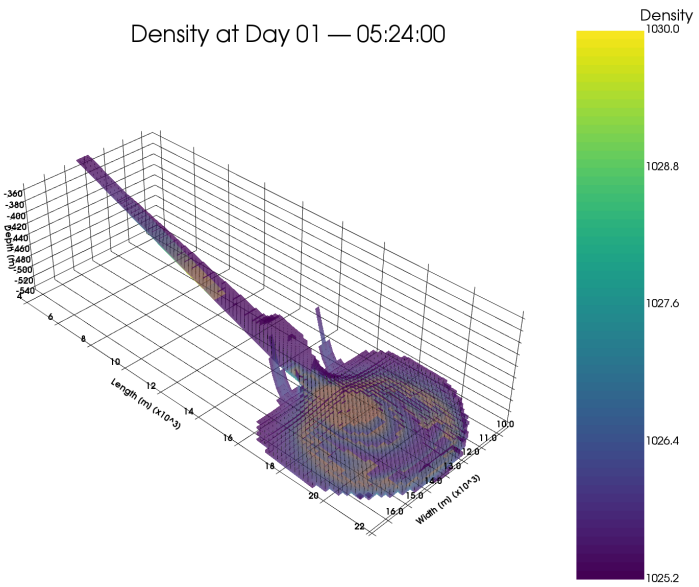


**Figure 5.5:** 3D plot of hydrodynamic grid-cells color coded by density values, constant water density values (1025 kg/m$^3$) are excluded. This depicts the expanded flow after it has exited the channel of scenario with channel slope 0.85°. Densest layers can be seen at the base of the flow, just above the bed around the channel mouth. Bathymetry surface is excluded.

When the flow exits the channel, it expands laterally and becomes more dilute Figure 5.5 depicts this in 3D, and Figure 5.7 depicts this in 2D along a vertical $\sigma$-grid layer. Bottom stresses increase to around 6 to 15 N/m$^2$ in the area down-stream of the channel mouth. Turbulent kinetic energy decreases as the flow spreads.

Over a distance of ∼4 km from the channel mouth, silt is entrained from the seabed, while sand is deposited. More silt is entrained from the bed than sand is deposited so the net result is erosion (Figure 5.9). As a result, the channel and deposited beds are separated by a coarse, net erosional zone downstream of the channel mouth of approximately 4 km long and 3 km wide.

Compared to sand particles, suspended silt particles remain suspended for longer and are transported farther out into the basin (Figure 5.8). Suspended sand does not travel farther than the area downstream of the channel mouth, and tends to deposit proximally (Figure 5.11a).

As the flow expands in the basin, bed shear stress magnitudes are higher at the front of the flow than in the center of the flow (Figure 5.9a, Figure 5.9b, Figure 5.9c), high enough to entrain silt from the bed. On the inside of the flow , silt is deposited (Figure 5.9d, Figure 5.9h, Figure 5.9f).

Finally, the flow continues spreading and gradually dissipates until it is depleted of suspended sediment around the 14-hour mark after inflow, re-

gardless of scenario. Velocities of 0.15 m/s remain until the end of the simulation and silt volume concentration remain up to ∼0.15%.

The following plots (Figure 5.6) depict the same properties at the same vertical cross-section as shown in Figure 5.4 above, only at a later time-step when the flow has entered the basin.

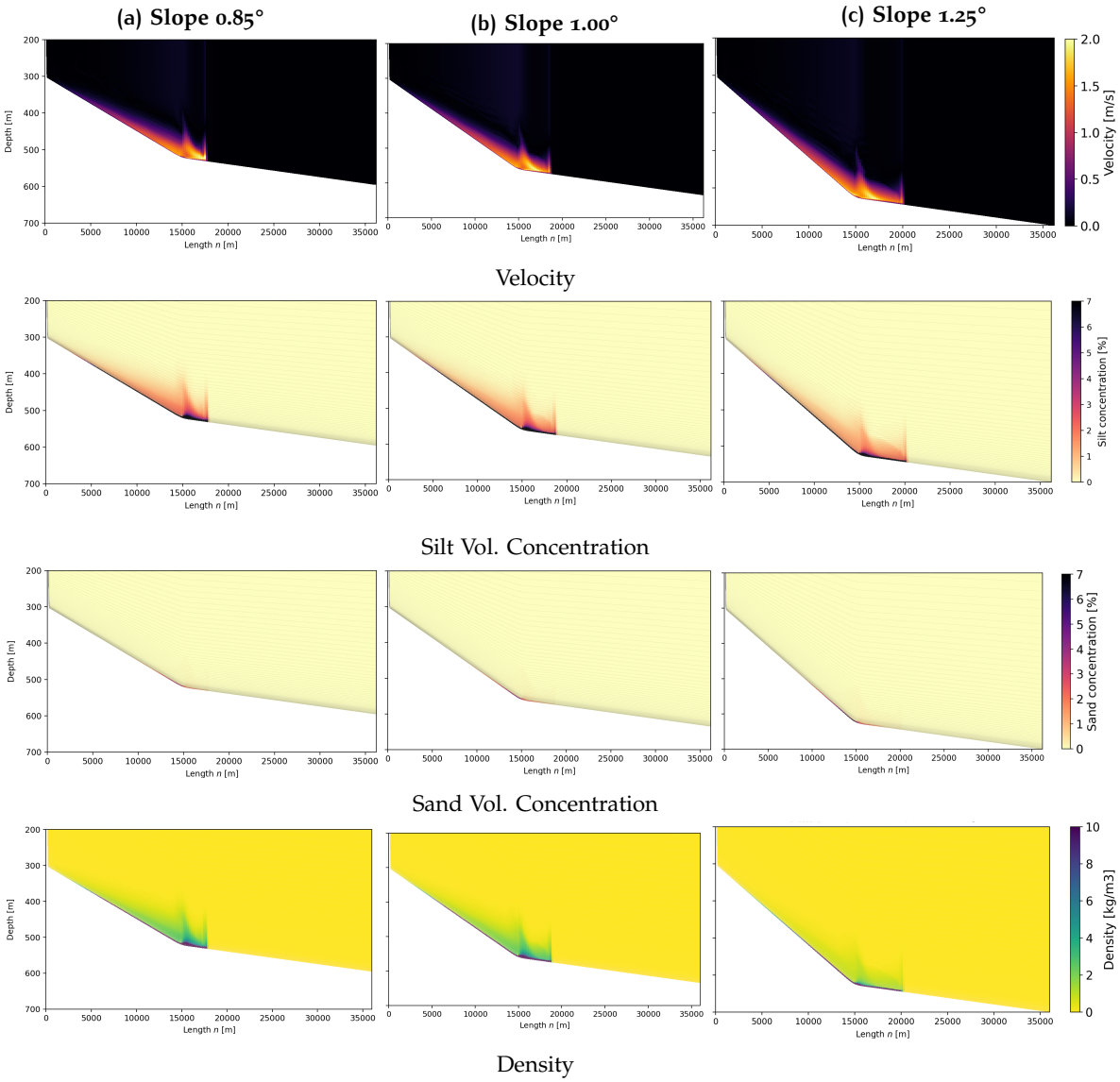


**Figure 5.6:** Cross-sections along channel of density, velocity, silt- and sand volume concentration at 3 hours 34 min after start of first run when the flow has passed over the slope break and has lost confinement. Vertical exaggeration of ∼50

At the end of the simulation, a deposit of at most 5 cm thick has formed the basin. The deposit is symmetrical and elongated in the direction of the flow. The thickest point of the deposit is situated downstream of the erosional zone, $\sim$ 5 km from the channel mouth. The deposit decreases in thickness with distance downstream and consists of $\sim$45% sand and $\sim$55% silt (Figure 5.10d, Figure 5.10e, Figure 5.10f). Sand is dominantly deposited downstream of the channel mouth in the erosional zone, whereas silt is dominantly deposited in the thick parts of the deposits and a smaller amount in the fringes of the basin.

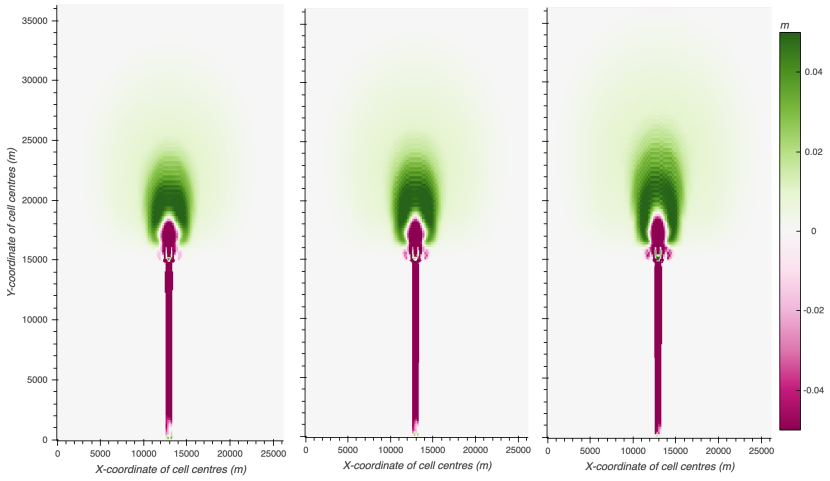


(a) Slope 0.85° (b) Slope 1.00° (c) Slope 1.25°

**Bottom Difference**

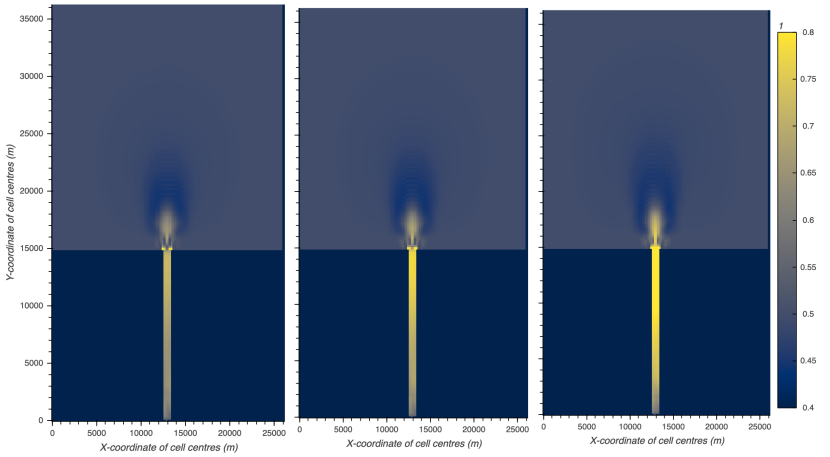


(d) Slope 0.85° (e) Slope 1.00° (f) Slope 1.25°

**Sand volume fraction in top of bed**

**Figure 5.10:** Difference in bathymetry and bed sand volume fraction showing depositional patterns at end of first run for all three scenarios.

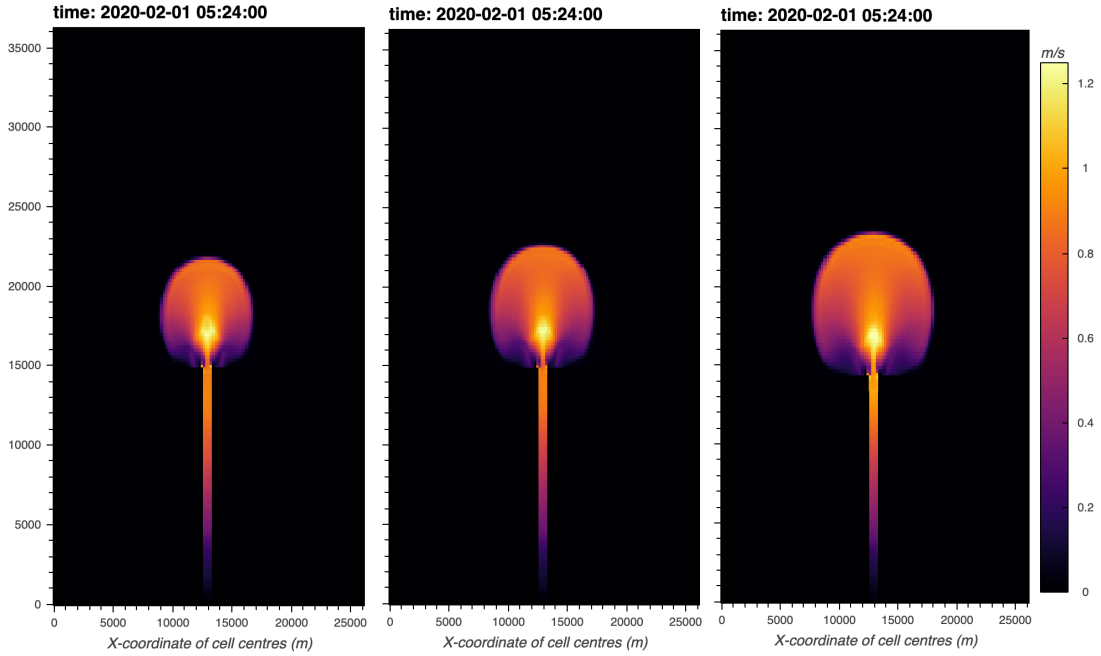


**(a)** Slope 0.85° **(b)** Slope 1.00° **(c)** Slope 1.25°

**Velocity**

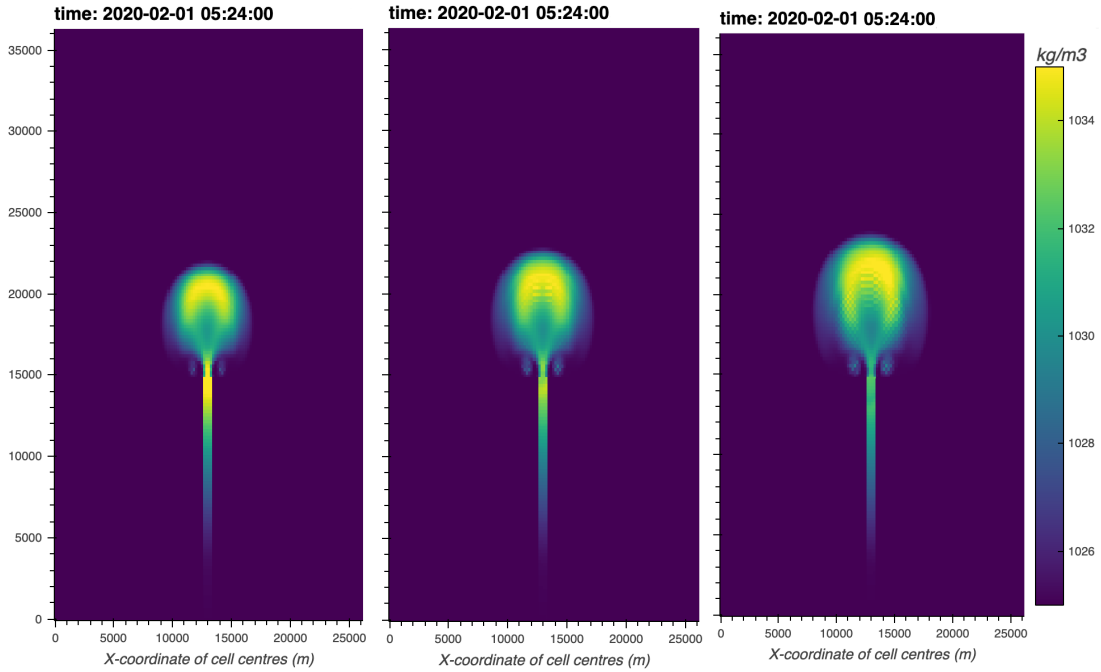


**(d)** Slope 0.85° **(e)** Slope 1.00° **(f)** Slope 1.25°

**Density**

**Figure 5.7:** Plan view densities along bottom $\sigma$-grid layer and horizontal velocities along a $\sigma$-grid layer 67, which is ~3 m above the bed at the slope break and ~4.5 m at the front of the flow. Here velocities are at their maximum. All at 5 hours 24 min after start of first run. A checkerboard pattern is visible in the cross-section of density.

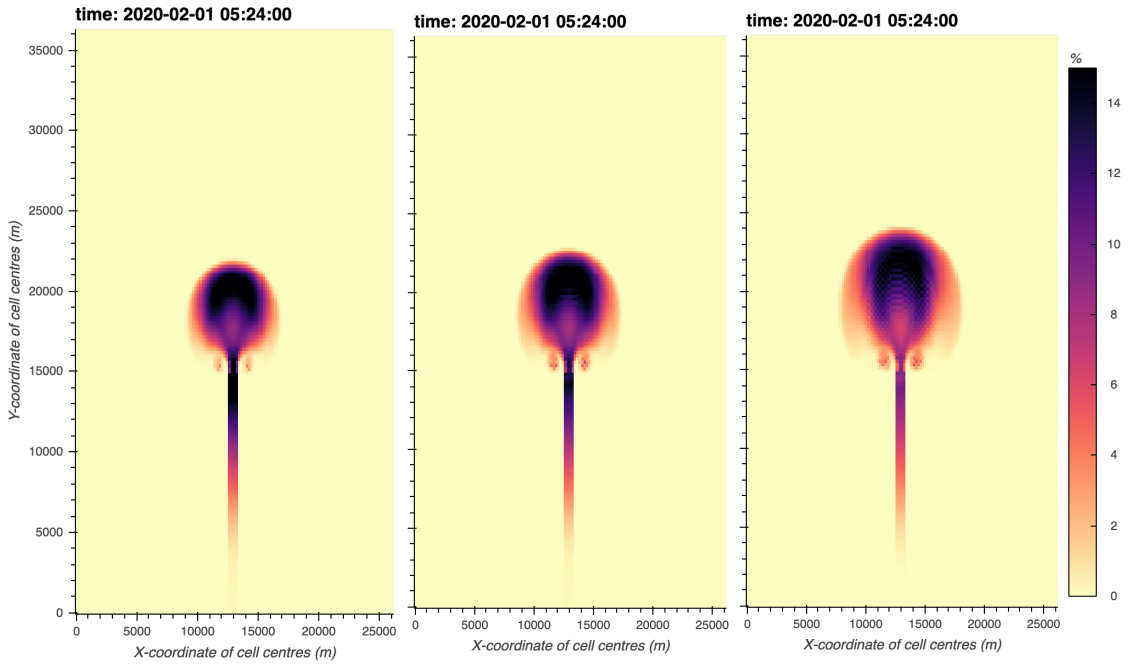


(a) Slope 0.85° (b) Slope 1.00° (c) Slope 1.25°

**Silt vol. concentration**

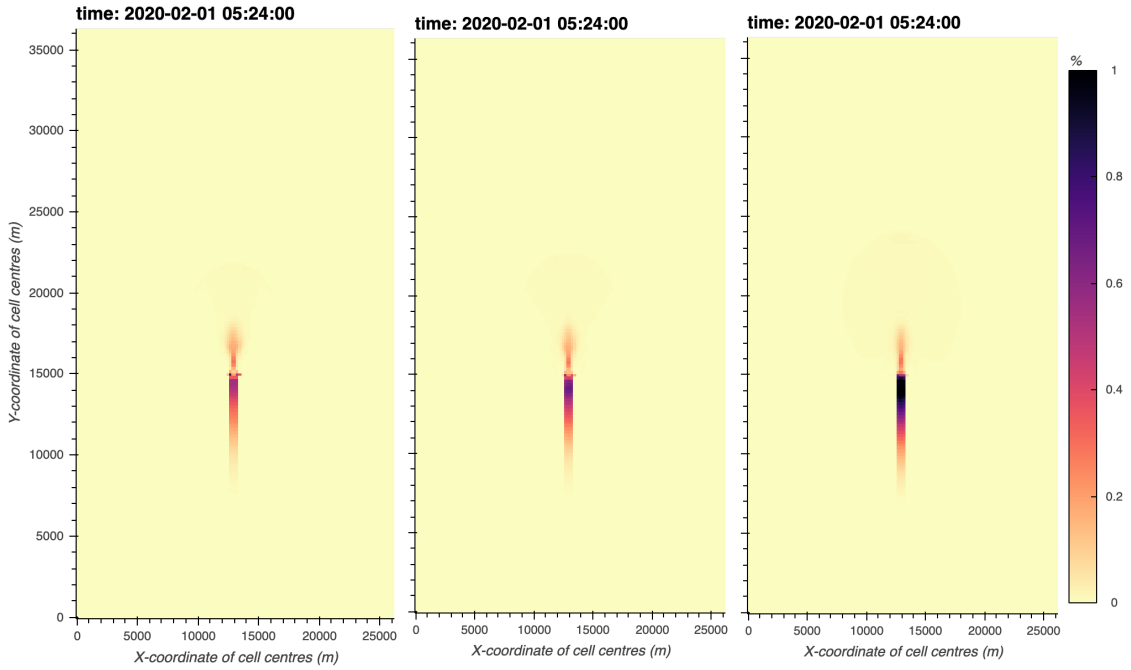


(d) Slope 0.85° (e) Slope 1.00° (f) Slope 1.25°

**Sand vol. concentration**

**Figure 5.8**: Plan view of volume concentrations along bottom $\sigma$-grid layer, showing the lateral expansion of the flow. All at 5 hours 24 min after start of first simulation. Note that color limits are different for silt (upper row, 0–15%) and sand (bottom row, 0–1%) concentrations.

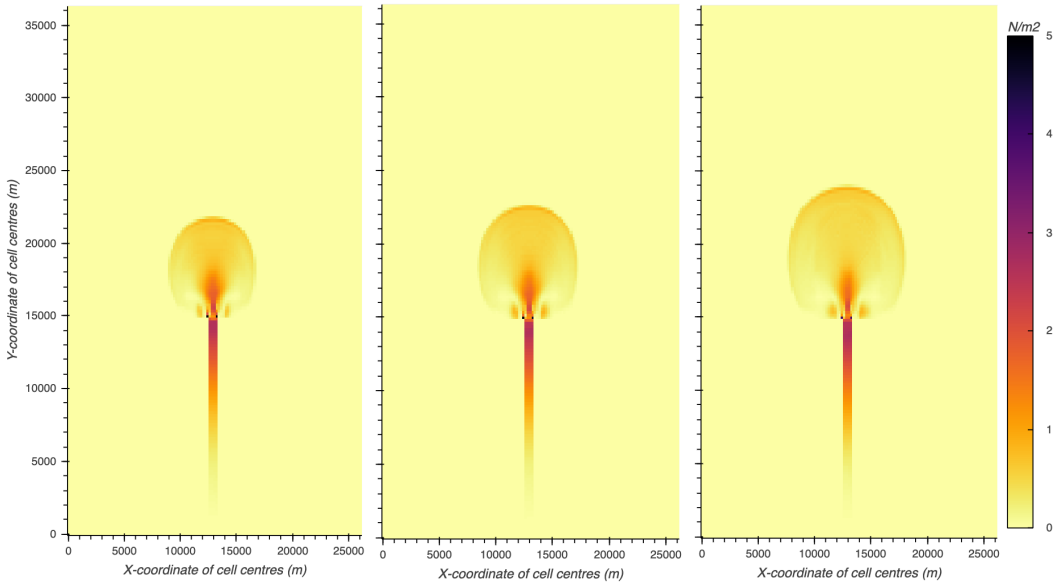


(a) Slope 0.85° (b) Slope 1.00° (c) Slope 1.25°

**Bottom stress**

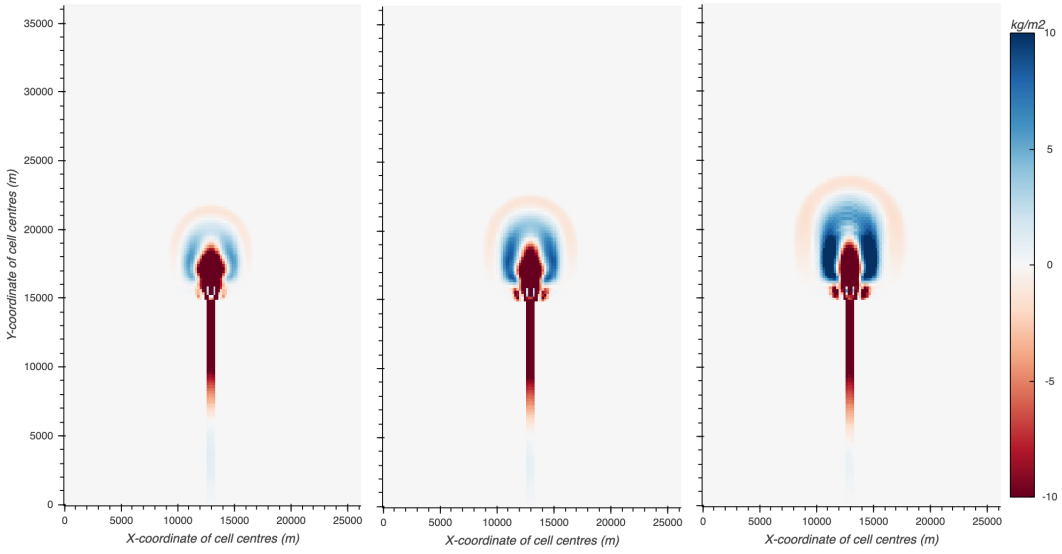


(d) Slope 0.85° (e) Slope 1.00° (f) Slope 1.25°

**Accumulated net silt flux**

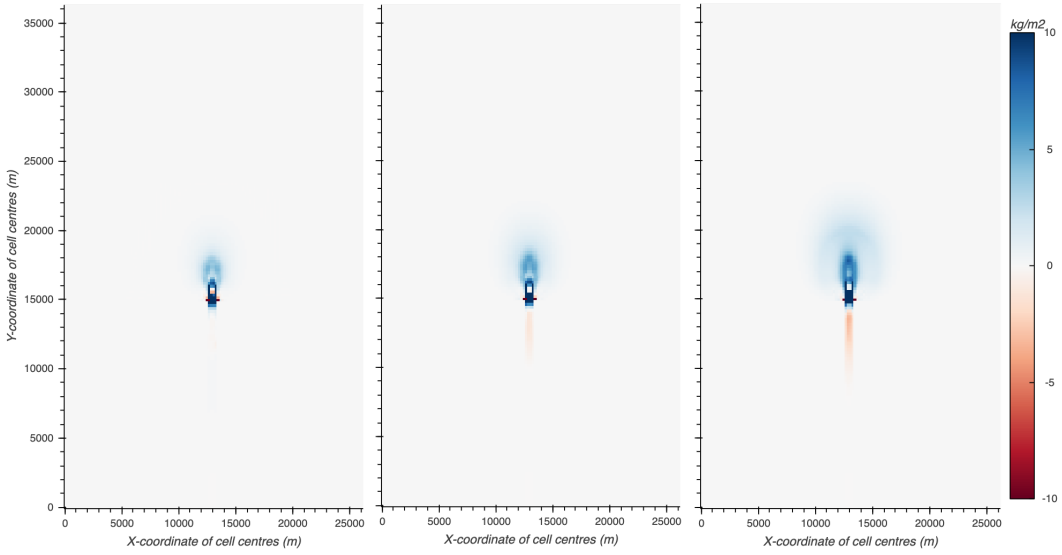


(g) Slope 0.85° (h) Slope 1.00° (i) Slope 1.25°

**Accumulated net sand flux**

**Figure 5.9:** Plan view of bed shear stress magnitude and accumulated net sedimentation fluxes. Positive fluxes (blue) imply deposition, negative fluxes (red) erosion. All at 5 hours 24 min after start of first run.

## 5.2 SEQUENCE OF 5 RUNS

This section describes how the hydro- and morphodynamic changes in a sequence of 5 runs in between *resets* (see Section 3.8.1), e.g.for runs 6 – 10, runs 20 – 25, runs 46 – 50.

Each flow follows the same sequence of moving down the channel, decelerating on the slope break and spreading and depositing in the basin. However, the following flows show decreased dispersion of sediment. Flow properties like density, velocity and sediment concentrations decrease in magnitude over a sequence of 5 runs. The bed shear stress magnitude decreases in tandem with velocity and density (Figure 5.13). The accumulated net sedimentation fluxes decrease between the first and the fifth run (Figure 5.14). In the channel and channel mouth area, the volume fraction of silt in the sea-bed decreases with each flow passage.

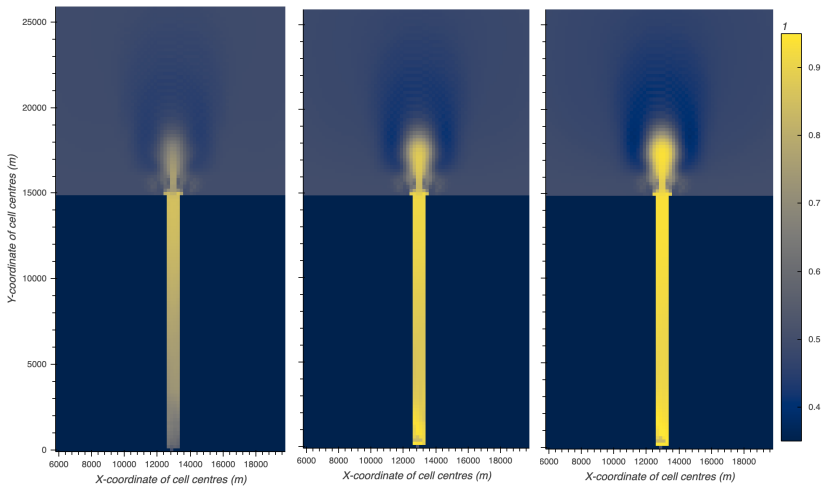


**(a)** End of run 1 **(b)** End of run 3 **(c)** End of run 5

**Figure 5.11:** Bed layer (0.5m thick) sand volume fraction in channel and channel mouth area, showing progressive coarsening over subsequent runs for scenario with 1.25° channel slope. After 5 runs, the bed composition is reset to initial composition of 50% sand, 50% silt.

The magnitude of bed shear stress decreases over a sequence of five runs, both in magnitude and in area covered, as the flow spreads more slowly.

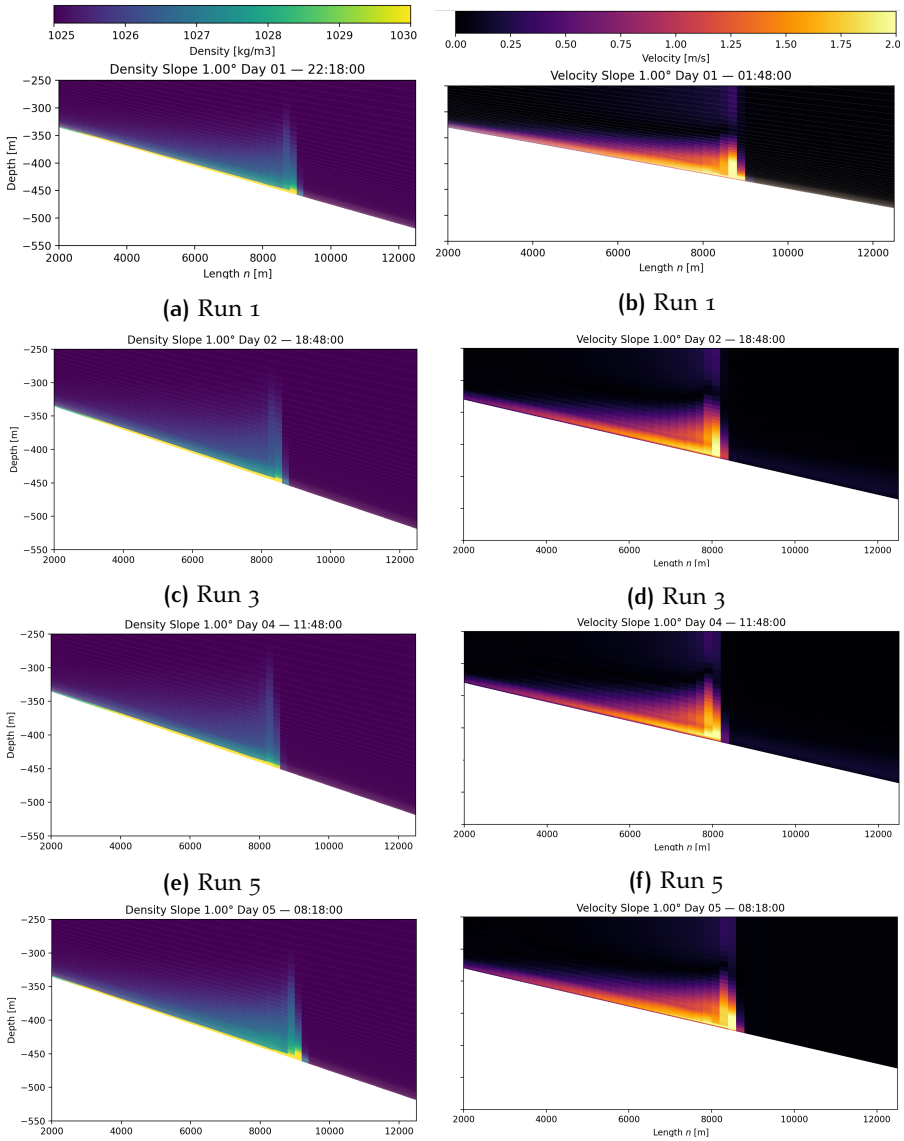


**(a)** Run 1

**(b)** Run 1

**(c)** Run 3

**(d)** Run 3

**(e)** Run 5

**(f)** Run 5

**(g)** Run 6: Reset bed composition.

**(h)** Run 6: Reset bed composition.

**Figure 5.12:** Cross-sections along channel of density (left) and velocity magnitude (right) in runs 1, 3, 5 and 6; each at the same output time (108 minutes after start). Scenario with channel slope 1.00°. The flows are progressively slower and less dense in following runs. The flow in run 6 is denser and faster again than the previous flow.

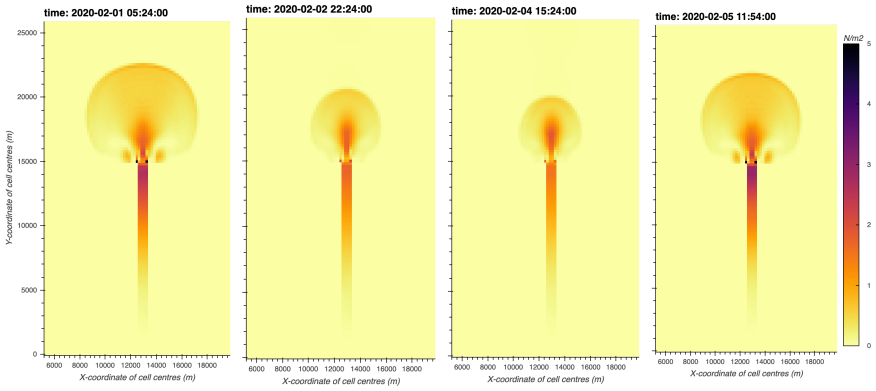


**(a)** Run 1 **(b)** Run 3 **(c)** Run 5 **(d)** Run 6

**Figure 5.13:** Plan view of bed shear stress in channel and channel mouth area at same time after start in different runs. All at 5 hours 24 min after start of simulation. The sequence shows decreasing magnitude and area of bed shear stress in successive runs, until the reset of bed layer composition after run 5 after which bed shear stress increases again.

The accumulated net sedimentation flux (kg/m$^2$) over an interval between two output times (1 hour 48 min) changes in each subsequent run (Figure 5.14). The net sedimentation fluxes are observed to decrease over subsequent runs.

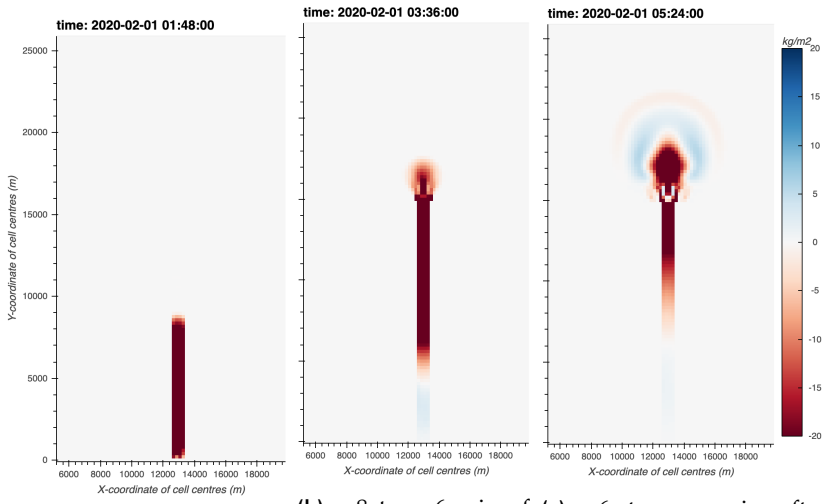


**(a)** 0 to 108 min after start **(b)** 108 to 216 min after start **(c)** 216 to 324 min after start

**Run 1**

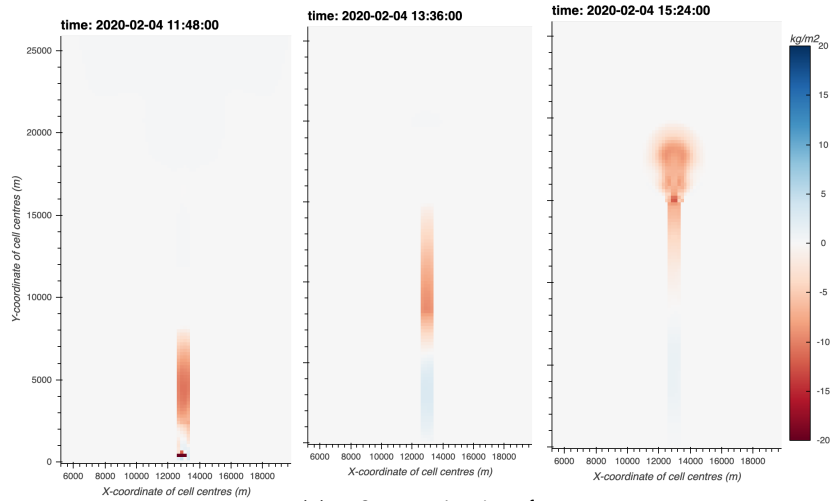


**(d)** 0 to 108 min after start **(e)** 108 to 216 min after start **(f)** 216 to 324 min after start

**Run 5**

**Figure 5.14:** Plan view of accumulated net sedimentation flux (kg/m$^2$) of silt over the period between two output times (108 min). Sequence of first three output-steps (up to 05:24) in first run (top row) and fifth run (bottom row). Scenario with channel slope 0.85°

## 5.3 ALL RUNS

Besides the effects of bed coarsening described above, each flow is modified by the deposit relief. The channel slope also changes by erosion by prior runs.

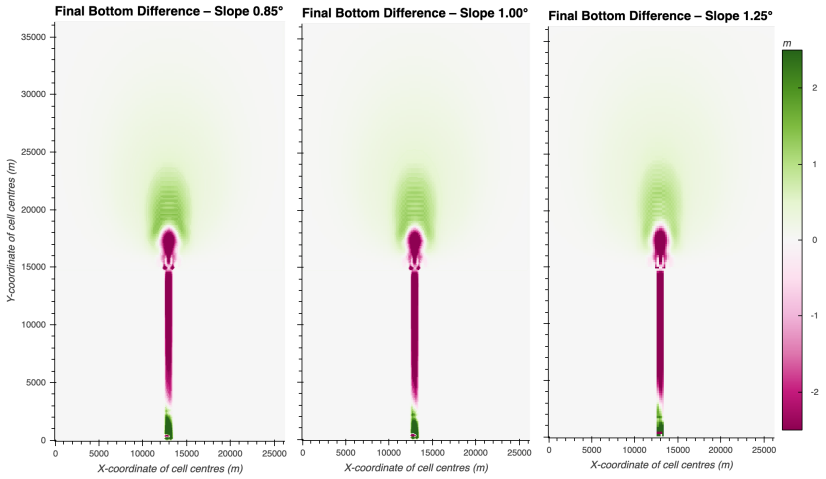


**(a)** Slope 0.85° **(b)** Slope 1.00° **(c)** Slope 1.25°

**Figure 5.15:** Plan view of accumulated sedimentation and erosion (m) at end of 50 successive runs for all three scenarios.

### 5.3.1 Stratigraphy

The final deposit in the basin dominantly consist of the silt fraction (approximately 60%) in all scenarios. Slight changes in underlayer composition in the vertical direction can be observed in deposits. Sand is common in the channel and in the area around the channel mouth, where top 50 cm of the bed is composed of $\geq$75 vol% sand (Figure 5.16). The sand volume fraction is higher ($\geq$80 vol%) in scenarios with steeper channel slope. The distal fringes consist exclusively of a thin (2—9 mm), laterally extensive layer of silt.

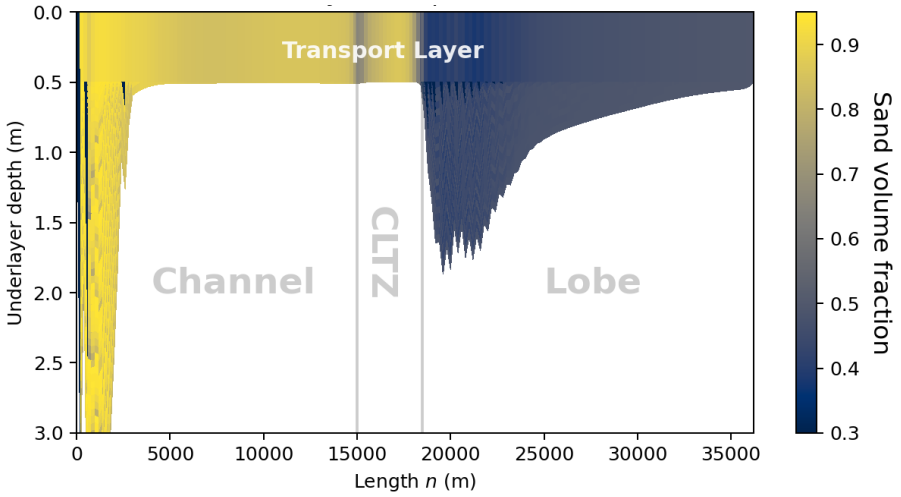


**(a)** Slope 0.85°

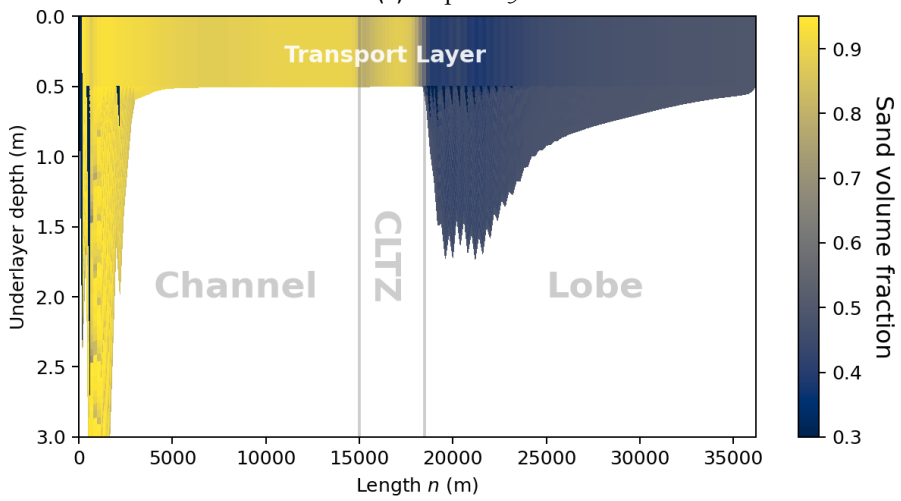


**(b)** Slope 1.00°

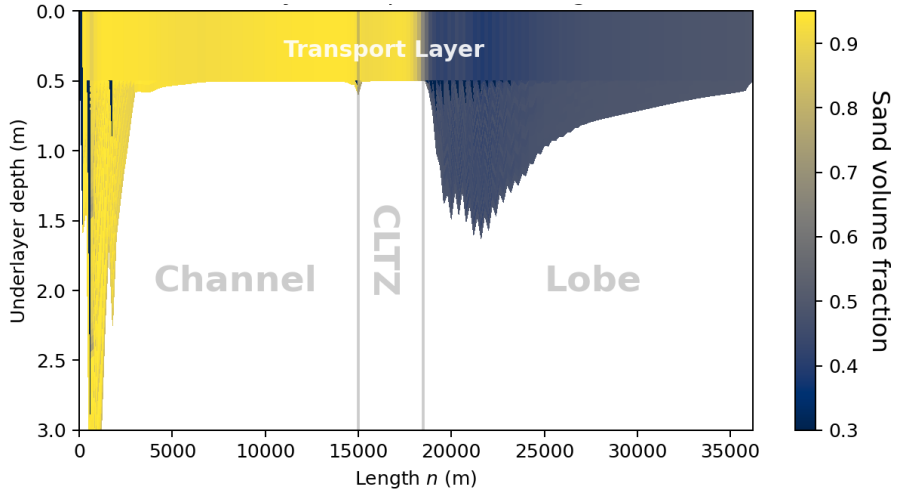


**(c)** Slope 1.25°

**Figure 5.16:** Sand volume fraction in underlayers. Lines demark interpreted zones.

# 6 INTERPRETATION

In this chapter, the results are interpreted and the differences between scenarios are compared and discussed. The effect of slope on flow dynamics and deposits is assessed. The effects of and reasons for bed coarsening are also discussed.

## 6.1 FIRST RUN

The model demonstrates that a discharged sediment-laden flow forms a turbidity current that erodes bed sediment in the channel and channel mouth. The modeled turbidity current decelerates upon a decrease in slope and loss of confinement. A loss of confinement causes the turbidity current to spread laterally and thin. Finally, the current loses its capacity to suspend sediment as velocity decreases and a deposit forms.

### 6.1.1 Flow Evolution

The flow evolution can roughly be divided into five phases.

(1) Immediately after inflow, conditions need to adjust to the discharge. The flow lacks the capacity to transport all discharged sediment, especially the coarser sand fraction. As a result, a depositional cone of mostly the coarser sediment fraction forms in the first 2—3 km of the channel (Figure 6.4 & Figure 5.15). The formation of this feature evidently allows the flow and sediment concentration to adjust to flow capacity and competence [Fernandez et al., 2014]. A similar feature is observed in scaled turbidity current laboratory experiments by Cantelli et al. [2009] and Fernandez et al. [2014].

(2) The flow stabilizes and erodes sediment in the remainder of the channel. Here, the currents vertical structure is characterized by stepped-concentration profiles (Figure 5.3). A stepped-sediment concentration profile like this is commonly observed in erosional currents in scaled laboratory experiments [Kneller and Buckee, 2000], which is in accordance with the erosional behavior observed in the channel (Figure 5.13a & Figure 5.14a).

Experiments in which vertical grain size distributions have been measured show that fine-grained material is more uniformly distributed in the vertical than the coarse material, which tends to become concentrated in the lower part of the current García [1993]; Kneller and Buckee [2000]. Our results are in agreement with such observations (e.g.Figure 5.3).

Turbulent kinetic energy is close to zero at the height of the velocity maximum. The maximum turbulent kinetic energy occurs towards the base of the current. This agrees well with published results of such profiles in turbidity currents [Meiburg and Kneller [2010] and references therein].

As the flow moves down the channel, the front of flow is slower and less dense due to mixing with ambient water. Approximately 200 m upstream

of this dilute front, velocities and densities are highest. Here, both sand and silt are more dispersed, presumably due to the mixing with water and entrainment of bed sediment that occur at the front. Turbulent kinetic energy is highest here which causes the mixing. The overlap of the high turbulence kinetic energy (Figure 5.1a) and suspended sand concentration (Figure 5.1c) indicate that sand is kept in suspension by turbulence. Farther upstream (up to 6 km) from the front, flow velocities decay rapidly and the flow dissipates.

(3) When the flow encounters the slope break and exits the channel, it's characteristics change greatly, it decelerates, spreads and becomes thinner due to loss of confinement. The bed stresses increases to level above the critical threshold for sediment motion The simultaneous increase in bed stress (Figure 5.9) explains the entrainment of silt from the bed in the proximity of the channel mouth, (Figure 5.9d, Figure 5.9e, Figure 5.9f), which forms the erosional zone that separpates the channel from the deposits in the basin that resembles a large scour in a CLTZ. The occurrence of erosional zone (scours) downstream of a submarine channel is commonly interpreted (e.g.Mutti and Normark [1987]) to be related to flows that have undergone a hydraulic jump, which mark the transformation from supercritical to subcritical flow conditions [Hofstra et al., 2015; Hamilton et al., 2015].

More recently, Pohl [2019] put forward the idea that hydraulic jumps are likely not the mechanism behind increased erosion at the CLTZ and proposed an alternative mechanism, 'flow relaxation'. Flow relaxation describes the lateral spreading and thinning of the flow upon leaving the confinement. A lateral pressure gradient develops between the dense current and the ambient fluid that drives flow spreading and lowering of the high velocity core and an increased erosion potential of the flow [Pohl, 2019].

This phase is followed by (4) a depletive, strongly depositional phase (proximal lobe) which forms the thickest deposits (at least 3 cm thick from y = 18 km to 24 km). Due to decreased velocities and lower turbulent intensities the flow can no longer keep the sand fraction — and to lesser extent, the silt fraction — suspended as the flow spreads. (Figure 5.9g, Figure 5.9h, (Figure 5.9i).

Finally phase (5) is a depletive, weakly depositional phase in which the flow continues to spread, velocities decrease from 0.5 m/s to 0.25 m/s and exclusively silt is deposited over a large area.

## 6.2 SEQUENCE OF 5 RUNS

Following flows in a sequence of five differ in that they are slower and less dense. The presumed reason is coarsening of the channel bed, this is explained in the following subsection.

### 6.2.1 Bed Coarsening & Self-Acceleration

Erosion and entrainment of sediment results in increased flow density which increases the gravitational pull on the flow. The down-stream velocity increases as the flow becomes denser, this self-reinforcing cycle is termed self-acceleration [Parker, 1982; Sequeiros et al., 2009].

In the first run in a sequence of five, there is plenty of readily erodible sediment in the channel bed, which is entrained into the flow, thereby increasing the flow density. This may lead to self-acceleration. Thus, each flow event

diminishes the amount of readily erodible sediment in the bed. So for each following flow, there is less sediment available for entrainment. This phenomenon is sometimes termed *winnowing*. The progression of coarsening bed over successive runs is illustrated in Figure 5.11 and is mostly the same for all sets of 5 runs between resets.

As a result, the sediment concentration and hence density are lower in following flows, which reduces the down-slope gravitational pull, thereby limiting the flow's acceleration. Hence, subsequent flows do not self-accelerate like flows over finer-grained beds do. The effect of channel bed coarsening on flow density and velocity in the channel is illustrated in Figure 5.12. As flow velocity and density decrease, the stresses that are exerted by the flow on the bed decrease, therefore the flow is less capable of eroding bed sediment. Lower magnitude in bed shear stresses decrease the flow's capacity to entrain bed sediment which results (again) in lower flow density. Thus, bed coarsening is a self-reinforcing cycle of decreasing flow density and velocity.

Bed coarsening explains why in profiles of net deposition and erosion per run (Figure 6.7), the profiles of a sequence of 5 runs are close together; less erosion and deposition occur after the run with fine bed due to decreased bed sediment entrainment. As mentioned before in Section 3.8.1, to counteract the coarsening of the channel bed and to prevent complete depletion of the bed, the transport-layer composition is reset to its original composition after every 5 successive runs. The effect of resetting the transport-layer on deposition and erosion is clearly visible in Figure 6.7. After resetting the bed composition, there is readily erodible sediment available again for flow to entrain, which leads to self-acceleration, which leads to more sediment being eroded and deposited. This increase in erosion and depostions results in a vertical jump in the profile.

The difference between in flow behavior between flows over coarse-grained bed with and flows over fine-grained beds suggests that bed coarsening is largely responsible for diminished flow intensity and ability to transport and erode sediment.

## 6.3 ALL RUNS

### 6.3.1 Influence of Slope

This section describes the differences in flow dynamics and morphodynamics that result from changes in channel slope.

#### *In Channel*

Steeper channel slope increases the gravitational pull on the turbidity current, which increases the down-stream flow velocity in the channel. When plotting overall maximum flow velocity over one run, maximum velocity of the turbidity current is observed to be proportional to the channel slope angle (Figure 6.1). It should be noted that the amount of sample points here are limited and the peak might appear sharper than it really is.

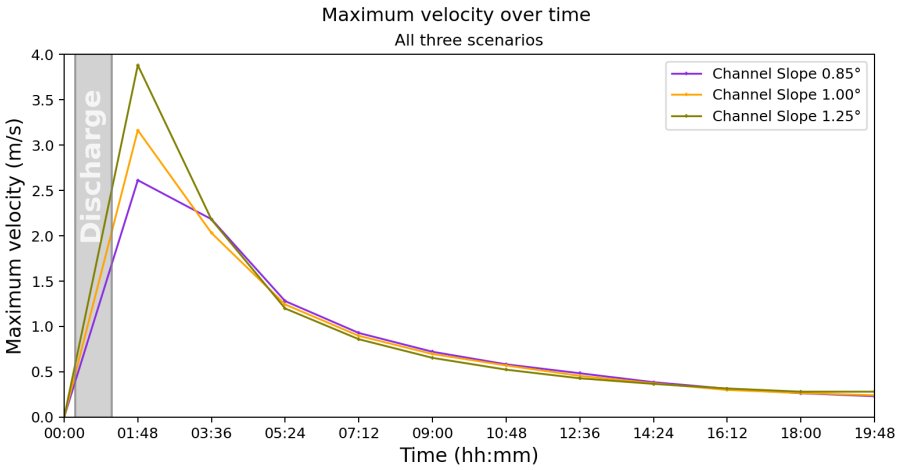


**Figure 6.1:** Maximum velocity over time of one run for three scenarios with discharge interval indicated. Maximum velocities are higher for steeper channel slopes and are reached some time after discharge has stopped.

Increased flow velocity leads to higher bed shear stress magnitude, which increases capacity to pick-up bed sediment into the front of the flow, especially fine bed sediment as it is more erodible. Faster flows can also keep more coarse sediment in suspension (turbulence likely plays a role here), higher amounts of coarse suspended sediment increase bed stress. Therefore, more sediment — especially silt — is eroded and entrained in flows over steeper slope channels, this is evident when comparing the sedimentation and erosion profiles between scenarios in Figure 6.4. Consequently, the channel bed is composed of coarser sediment in scenarios with steeper channel slopes (Figure 5.16).

Additionally, higher flow velocity increases turbulent intensities (Figure 5.2) and the capacity to keep sediment in suspension, resulting in higher overall sediment concentrations (e.g.Figure 5.4 & Figure 5.3).

### *In Basin*

Due to lower flow velocities in gentler slope scenarios, the threshold for deposition is met sooner as the flow exits the channel and decelerates. Therefore, these flows do not spread as far as those in steep slope scenarios, their deposits are are placed closer to the channel mouth, and are less spread out and more peaked (Figure 6.2). As a result, these deposits reach greater cumulative maximum deposit thicknesses than the flatter, more dispersed deposits in steep slope scenarios (Figure 6.7). Flows in steeper slope scenarios with higher velocities can keep sediment in suspension over longer distances. Due to longer run-out (e.g.Figure 5.8), the deposits accumulate farther downstream in higher slope scenarios than in gentler channel slopes (Figure 5.15, Figure 6.4).

When plotting the channel slope against the cumulative maximum deposit thickness in Figure 6.3, it can be observed that flows over gentler slopes result in deposits with higher maximum deposit thickness. Maximum deposit thickness shows a clear decrease with increasing channel slope.

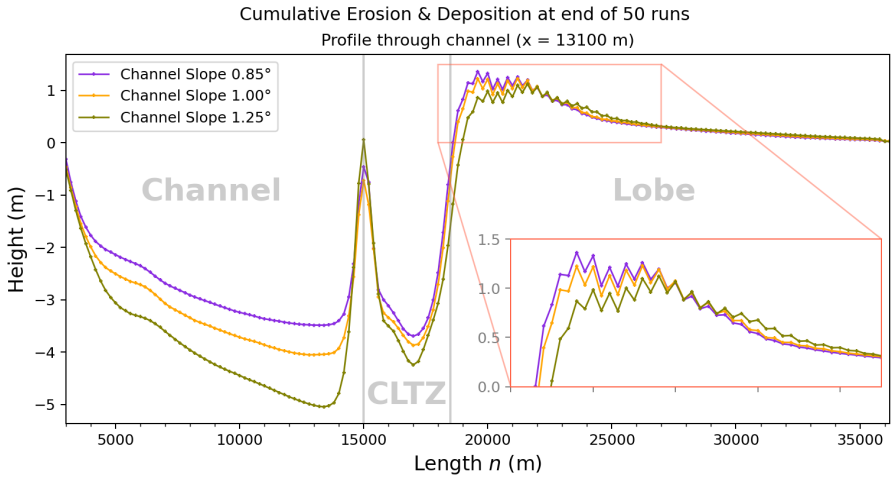


**Figure 6.2:** Erosion & sedimentation profile at end of 50 runs for all scenarios. Wiggles in lobe surface are numerical instabilities. Vertical lines demark interpreted zones which are labeled.

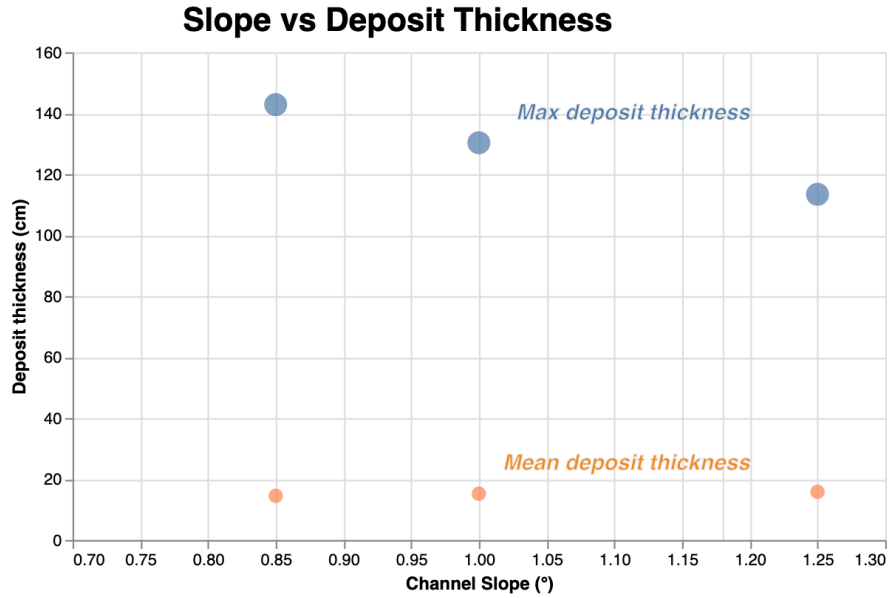


**Figure 6.3:** Channel slope vs mean & maximum of total deposit thickness

### 6.3.2 Planform Area

The exact value for planform area depends on the threshold deposit thickness that is chosen to distinguish deposits. Here, the threshold thickness is set to 0.2 cm,. For this value, total planform area of the deposits with thickness becomes independent of channel slope after 35 runs, with the deposit area of all three scenarios converging to $\sim$548 $\pm$1 km$^2$.

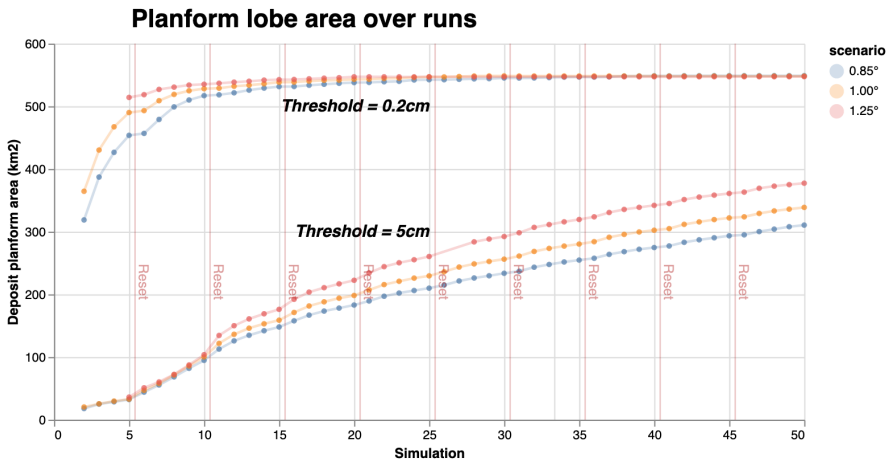


**Figure 6.5:** Planform area of deposits over simulations with threshold set to 0.2 cm (top lines), 5 cm (middle lines)

### 6.3.3 Stacking Patterns

Despite different depositional patterns between scenarios, the deposition is mostly aggradational or 'anti-compensational' throughout all 50 runs in all scenarios, no abrupt lateral shifts in deposition are observed. Hence, intensity of compensation and connectivity between lobe-elements can not be assessed. This aggradational behaviour is thought to be due to insufficient relief of the deposits to redirect the flow. The fixed position of the channel likely also strongly controls the deposit emplacement.

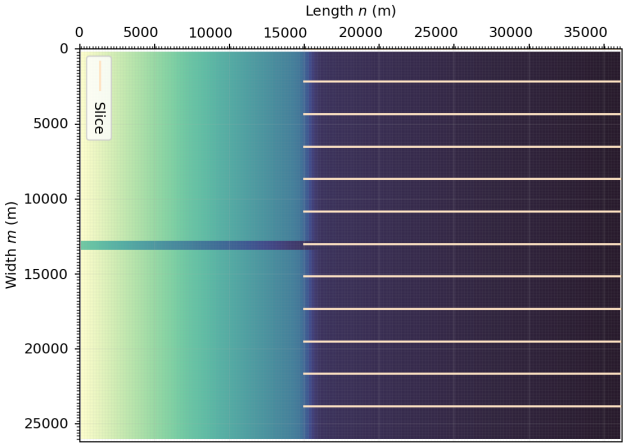


**(a)** Top-down view of locations of transects

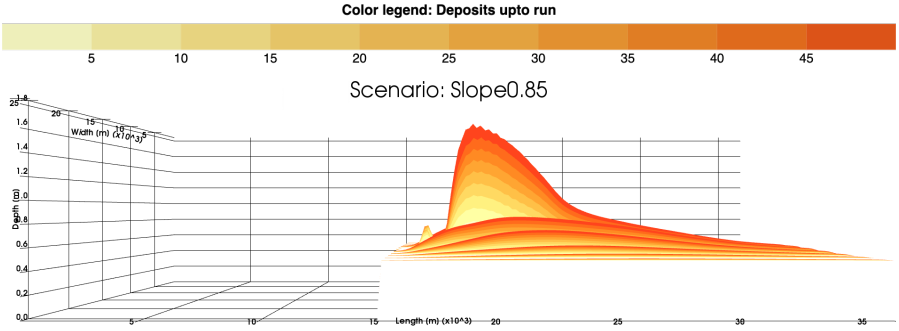


**(b)** Slope 0.85°

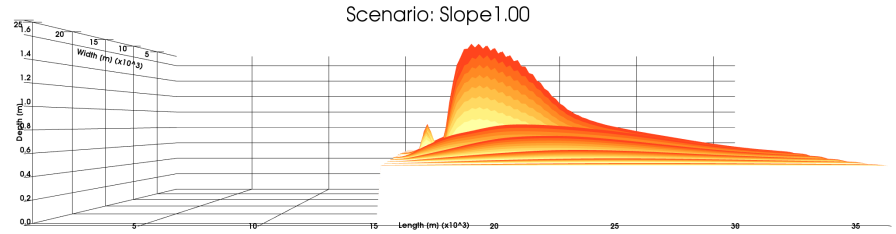


**(c)** Slope 1.00°

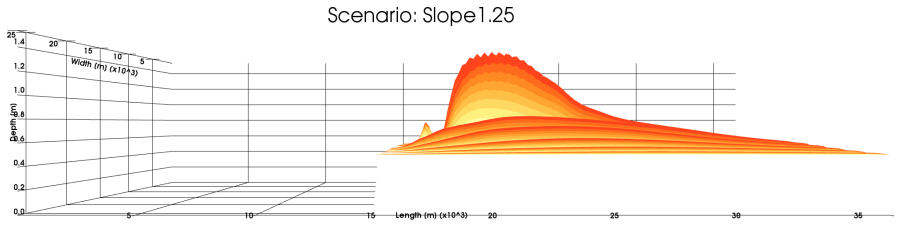


**(d)** Slope 1.25°

**Figure 6.6:** Side-views of transects of deposits in the basin part per 5 runs. Vertical exaggeration 5000. Deposits are color coded per 5 runs, with younger deposits being more saturated in color.

Because gentler slopes produce thicker deposits that emplaced are closer to the channel mouth, it is expected that these deposits will form the threshold relief to reroute flows and start stacking in compensation in fewer flow events.

### 6.3.4 Stratigraphy

The bed layer composition in gentler channel slopes are siltier ($\sim$ 70%) than in higher channel slopes ($\sim$ 90%) (Figure 5.16a & Figure 5.16c). This likely is due to lower amounts of entrainment of fine particles as the flows of steeper slopes erode more fine bed sediment as explained in Section 6.2.1.

As there are no abrupt lateral shifts in deposition, there are also no abrupt shifts in stratal patterns.

Because the bed layer is completely reset every 5 runs, a lot of information on stratigraphic composition is lost in the model. The effect of resetting is noticeable in the composition as increases in fine-grained sediment in the vertical direction. After a reset, more fine-grained sediment is deposited again.

### 6.3.5 Numerical Issues

Spurious oscillations (wiggles) are observed in cross-sections of various flow properties like density, concentrations). This manifests as a *checkerboard pattern* in cross-sections of density (Figure 5.7) which is more pronounced in steeper slope scenarios. Such oscillations are also present in the bottom depth profiles (e.g.Figure 6.4). These non-physical oscillations are indicative of numerical instabilities and are greater in scenarios with steeper slopes.

One possible explanation is that steeper slopes result in deeper total depths resulting in thicker vertical grid layers, thus, lower vertical resolution.

| **Vertical Layer** | **Slope 0.85°** | **Slope 1.00°** | **Slope 1.25°** |
|---|---|---|---|
| **75** | 0.260 | 0.279 | 0.311 |
| **77** | 0.208 | 0.223 | 0.249 |
| **78** | 0.208 | 0.223 | 0.249 |
| **79** | 0.208 | 0.223 | 0.249 |
| **80** | 0.156 | 0.167 | 0.187 |

**Table 6.1:** Vertical grid layer thickness in m of all scenarios at slope-break.

However, a comparison of vertical layer thicknesses at the slope break (Table 6.1) shows that the differences are at most a few centimeters between scenarios. These difference are most likely not the cause for the numerical instabilities.

Closer inspection reveals that numerical instabilities are greatest in the area in the basin at the time and place where rates of deposition are high (Figure 5.7e & Figure 5.7f). The numerical instabilities might be related to deposition and updates of the bed level as these areas overlap. Other possible causes are insufficiently small time-step and horizontal grid-cell size.

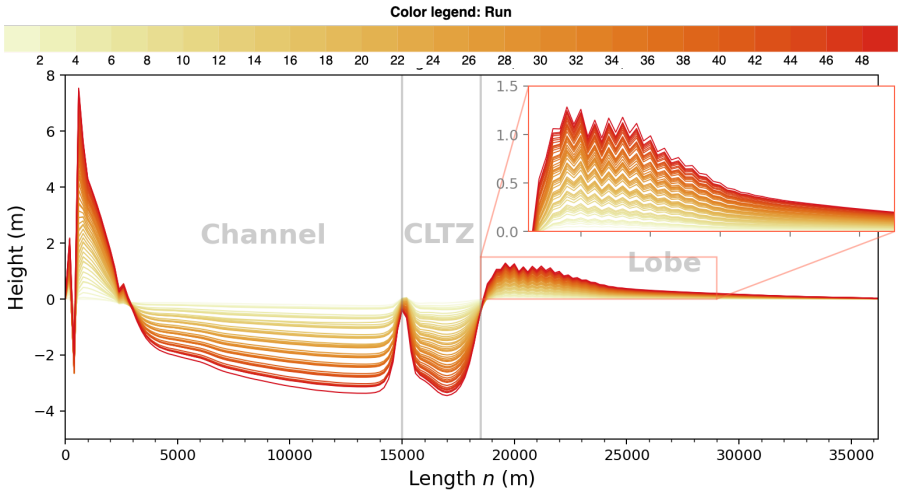


**(a)** Slope 0.85°

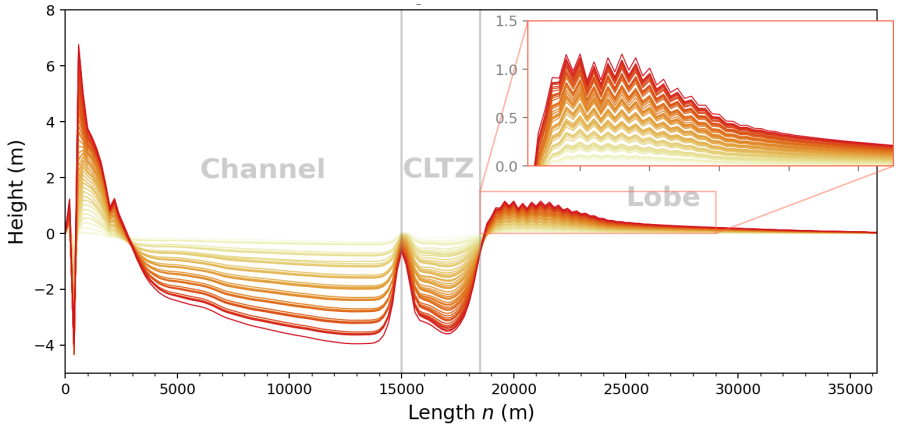


**(b)** Slope 1.00°

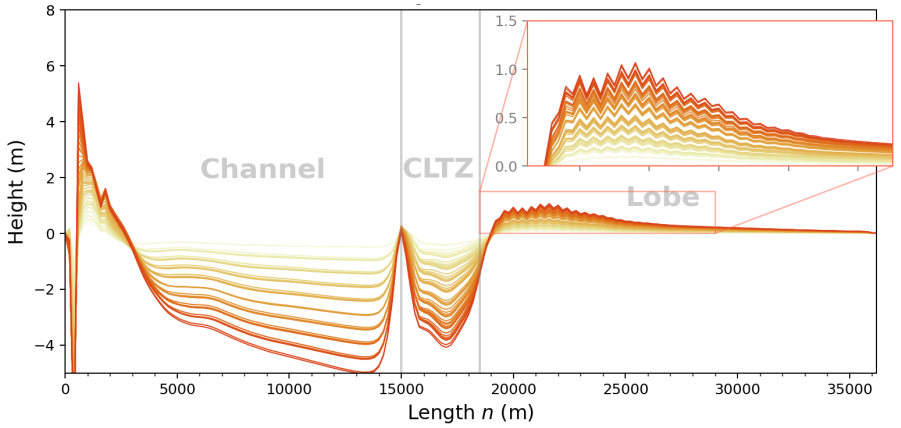


**(c)** Slope 1.25°

**Figure 6.4:** Profiles through channel (X = 13 100) of accumulated sedimentation and erosion of all 50 successive runs. Each line corresponds to sedimentation/erosion profile of one run. Saturation of line-color increases with run number (i.e.younger runs are more saturated in color. These figures demonstrate that

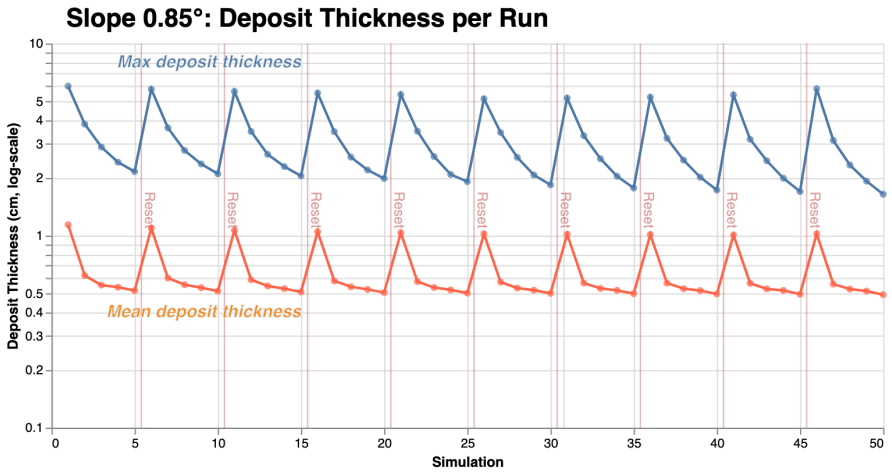


(a) Slope 0.85°

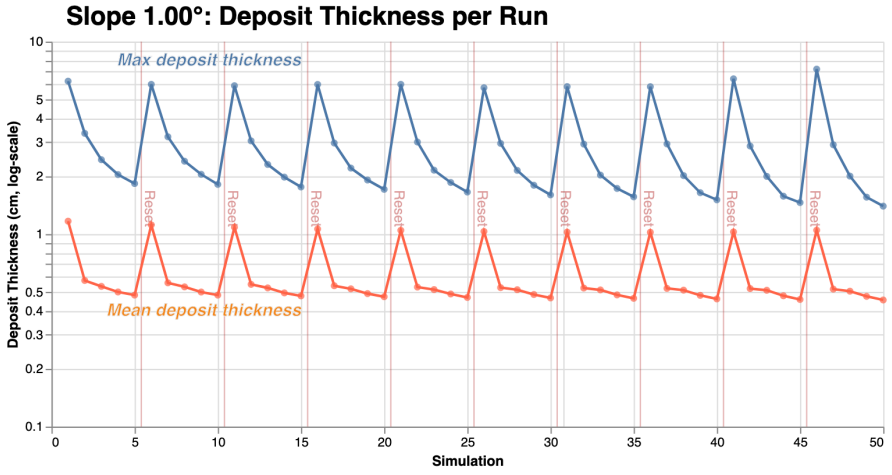


(b) Slope 1.00°

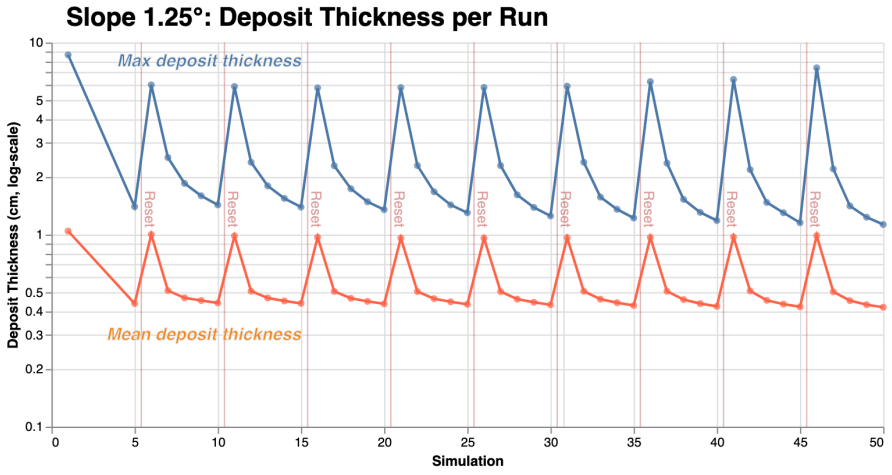


(c) Slope 1.25°

**Figure 6.7:** Mean and maximum deposit thickness in the basin per run.

# 7 DISCUSSION

Here, we discuss the realism of the model and compare it to literature and other models, both numerical and experimental, as well as the suitability of Delft3D-FLOW for geological modelling.

## 7.1 REALISM AND LIMITATIONS OF THE MODEL

The model is a simplified representation of reality based on several assumptions, certainly real submarine fan deposits are more complex. Here we discuss differences in and processes that drive the development of the lobe and are not included in the model.

### 7.1.1 Bed Thickness

The most prominent limitation is that total deposit thickness was insufficient to induce lateral shifts in deposition (compensational stacking). To simulate rich patterns of morphodynamic evolution — such that the focus of flow migrates repeatedly across the fan surface and forms multiple lobe-elements — more deposit relief is needed.

A 'brute-force' approach of simply repeating the current simulation more times is not recommended. This approach is inefficient in terms of computer time and storage. A more efficient approach would be to increase the deposited bed thickness per run, so the deposit relief forces a new preferential flow path in fewer runs. Several ways to achieve this are suggested in Section 9.1 RECOMMENDATIONS & FUTURE WORK.

To model compensational stacking of lobe elements, a reasonable target for flow event bed thickness is 50 cm, which is the average bed thickness measured by Prélat et al. [2009] in submarine fan lobe outcrops of the Karoo Basin, South Africa, perhaps the most-studied submarine fan outcrops. In these outcrops, lobe-elements are typically 1 to 3 m in thickness and comprise 1 to 6 beds [Prelat et al., 2010]. This gives a limited indication of the amount of flow events needed to make a lobe-element. For a detailed review on range of volumes, morphologies, and dimensions of submarine lobes, the interested reader is referred to Prelat et al. [2010].

### 7.1.2 Coarsening

Our results suggest that coarsening of channel bed by has a significant effect on turbidity current behavior (see Section 6.2.1). In real systems, turbidity currents do not immediately follow each other as they do in our model. Background sedimentation by hemipelagic fallout in between flow event replenishes the amount of fine particles in the bed. Additionally, compaction and consolidation of the bed affects dry bulk density, porosity and bed erodibility [Parsons et al., 2007]. Neither of these processes are included in this

model. It is also uncertain to what extent bed coarsening effects turbidity currents in real systems, although the effects are most likely not as consequential as in our model

Resetting the bed composition is a crude approach that discards valueable information on bed composition. Better approached are suggested in Section 9.1.3 in RECOMMENDATIONS & FUTURE WORK.

### 7.1.3 Constant Conditions

The assumption that flow's initial conditions are constant is useful to isolate controls and model purely autogenic behavior. In reality, flows characterized by different volume, concentration and velocity are responsible for lobe formation [Prelat et al., 2010]. Prelat and Hodgson [2013] advance the idea that a less organized bed thickness pattern in a lobe could result from more variable character of incoming flows, or a disorganized stacking of lobe elements. Deptuck et al. [2008] suggests that increased frequency of particularly vigorous flows may trigger more frequent lobe-switching and increase the architectural complexity of some composite lobes.

### 7.1.4 Grain-size distributions

Only two sediment fractions are included in the discharged sediment. Talling et al. [2013] suggests that the most important information for characterising a turbidity current is the vertical profile of sediment concentration and grain size. This is because sediment concentration and grain size — especially the cohesive finer-mud component — strongly influence flow density, flow rheology, particular support processes and mixing or entrainment rates.

The importance of multiple grain sizes is emphasized in developing realistic flow models, as they occur in most natural flows and strongly influence model results [Talling et al., 2015]. While this suggestion was originally written with laboratory experiments in mind, it is equally valid for numerical models.

## 7.2 COMPARISON TO OTHER MODELS

### 7.2.1 To lab experiments

The results of numerical model reported on here comply with that of lab experiments; a turbidity current flowing down a channel and leaving confinement spreads laterally, decelerates, and deposits sediment in a lobate body (e.g.Mulder and Alexander [2001]; Pohl [2019]; Hamilton et al. [2015]; Cantelli et al. [2009]; Fernandez et al. [2014]. What is often not replicated in laboratory experiments is formation of an erosional zone downstream of the channel mouth.

Scaled laboratory experiments performed by Pohl [2019] showed that the depositional patterns in a slope-break system are controlled by the steepness of the channel- and basin slope. In their scale experiments, steepness of the upper slope controls the initiation point of sediment deposition, while the lower slope controls thickness of the deposits [Pohl, 2019]. The floor used in the experiments was non-erodible, so it is uncertain how comparable the results are.

### 7.2.2 To Measured Flows

The distinction in the vertical structure of a thick, dilute upper layer and a much denser, thin, fast ( 1.7 m/s) and highly turbulent basal layer was also observed by Sumner and Paull [2014] in an ocean turbidity current observed with remotely operated vehicle.

Paull et al. [2018] observed a flow in the Monterey Canyon using ADCP moorings. The flow consisted fast and dense near-bed layers, which they attributed to remobilization of the seafloor, overlain by dilute plumes that outrun the dense layer, similar to the flow modeled here.

## 7.3 GEOLOGICAL TIMESCALE

### 7.3.1 Turbidity Current Volumes & Recurrence

Turbidity currents occur in a range of event volumes and recurrence rates. Jobe et al. [2018] applied a simple mass-balance approach to four well-characterized Quaternary submarine-fan deposits to calculate the volumes of sediment deposited by individual turbidity currents and the recurrence of those events. They concluded that the ranges of event volume and recurrence can be classified into three overlapping categories, corresponding to subsystems of the submarine sediment routing systems. The categories are i) submarine canyon/channel, ii) submarine fan, iii) and abyssal plain.

Small flows are generated in submarine canyons very frequently, but many of these flows dissipate prior to reaching the submarine fan. Measured turbidity currents in submarine canyons have small volumes (less than $10 \times 10^5$ m3) and short recurrence intervals (hours to years) [Jobe et al., 2018]. Fans are constructed by flows large enough to bypass and sculpt canyons, but small enough to die out before reaching the abyssal plain [Jobe et al., 2018].

Very large (greater than $10 \times 10^8$ $m^3$) and infrequent flows (recurrence of $10 \times 10^2$ to $10 \times 10^6$ years) deposit sediment onto the abyssal plain. Turbidites deposited on abyssal plains have very large event volumes and long recurrence intervals. Thus, fan-building flows build occupy an intermediate position in terms of event volume and recurrence [Jobe et al., 2018].

It is also important to note that event volume and recurrence are not single values, but rather distributions, and it is likely that these distributions are truncated as flows move from canyon to basin plain [Allin et al., 2017; Jobe et al., 2018].

While the methods of Jobe et al. [2018] rely on assumptions that oversimplify the complexity and uniqueness of submarine-fan systems, they provide a general framework for estimating event volume and recurrence for systems with limited data [Jobe et al., 2018]. It also uncertain to what extent these relations apply to deposits by submarine fan-systems from geological periods other than the Quarternary.

### 7.3.2 Geological Time-frame of Model

Knowledge of timing and recurrence of turbidity current is crucial in building realistic, integrative models of submarine fan deposits. Whats missing for experimental simulations such as these is a equivalent range of time. The lifespan of a submarine fan system is system-specific and depends on

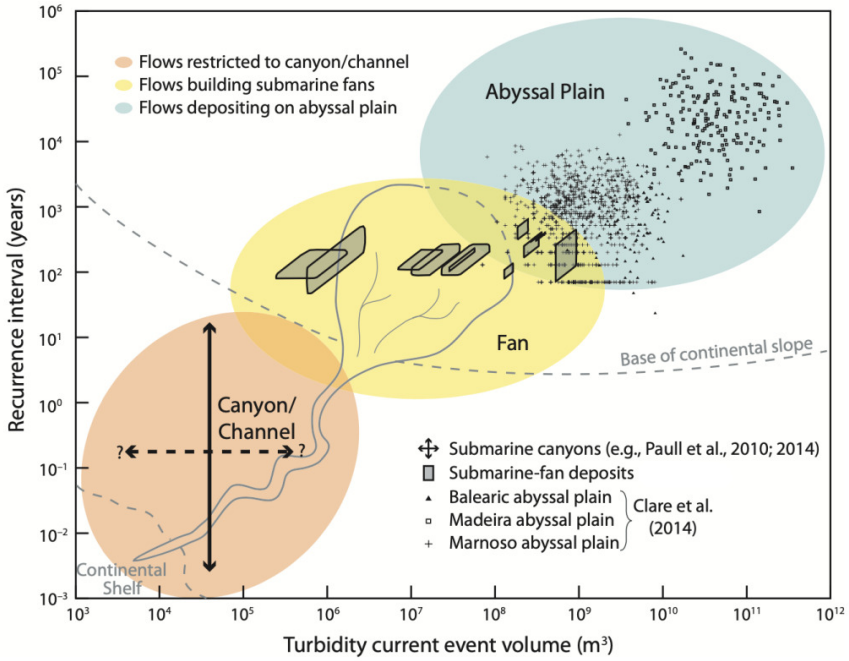


**Figure 7.1:** Simplified parameter space for event volume and recurrence of turbidity currents across the submarine sediment routing system interval. The plot is overlain with a simplified submarine sediment routing system for visualization purposes. By Jobe et al. [2018].

the tectonic and climatic framework and the source area (hinterland). Necessarily, no such information exist for experiments like in the one in this thesis.

Using Jobe's framework, we can attempt to make a — admittedly very rough — estimate for the models time-span.The total discharged sediment volume for the modeled flow events is $3.159 \times 10^5$ m$^3$. It should be noted that in-flowing sediment volume does not correspond one-to-one with sediment volume deposited in the basin due to entrainment due to entrainment and transport of bed sediment. This volume is on the lower end of the range for fan-building turbidity currents volume of the parameter space (Jobe et al. [2018] see Figure 7.1). A very rough estimate for the recurrence rate for the modeled event volume is $10 \times 10^2$ years. A very rough estimate for the modeled total time of deposition, following this parameter space, is then $50 \times 10^2 = 5000$ years. The margin of error of this estimate is very high, as there is no other information to constrain it.

### 7.3.3 Interim Background Sedimentation & Coarsening

The estimate for time provides a way to estimate interim hemipelagic *background* sedimentation. A rate of background sedimentation per time can be multiplied by the estimated total time to obtain an estimate of the volume of hemipelagic sediment accumulated in between flow events.

## 7.4 SUITABILITY OF DELFT3D-FLOW

Delft3D-FLOW4 is originally geared to building coastal and river models. While the computational kernel of Delft3D-FLOW is very powerful and purpose-agnostic, and capable of modelling turbidity currents, it is evident that geological modelling is a tangential use for which Delft3D-FLOW was not designed. The problems can be summarized as: 1) hard to define input 2) impractical visualization options and 3) very large output datasets. For these reasons, Delft3D-FLOW suffers from poor usability. The following subsections specify some of the problems in the modelling process.

### 7.4.1 Defining input

The existing graphical user interface (GUI) for Delft3D-FLOW4 input suffices for defining input of a single model. However, in the following ways it is lacking for geological modelling

- The GUI does not not support more advanced options such as defining underlayers or netCDF output.
- It is ill-suited for generating multiple, successive models quickly. Times need to be adjusted manually for each successive run, which makes it a tedious task. If longer timescales are to be modelled, generating successive models would take an inordinate amount of time
- Constructing bathymetry with the GUI is painstaking process that takes a long time does not scale for generating a large ensemble of different bathymetries.
- Currently, turbidity current parameters like flow concentration and inflow height require multiple intermediate calculations to define as input in a 3D boundary conditions. This makes defining boundary conditions, like 3D discharge profiles, unnecessarily hard and opaque. The conversion makes boundary condition files inscrutable; there's no straightforwards way to retrieve entered parameters from them.
- The visualization options for input in the GUI are fairly limited. For instance, the vertical grid and 3D-discharge boundary profiles can not be visualized.

Editing the collection of input files manually with a text editor is a minefield: the file formats are arcane, single parameters are often defined in multiple files and need to match between multiple files (e.g.times, boundary condition names). Cryptic keyword names and character length restrictions for values make it even more difficult.

Multiple scenarios requires many copies of marginally different input files. File names are often identical between different scenarios because renaming them requires editing multiple files which is a lot of work. Great care must be taken to ensure that the files don not get mixed up, which almost invariably happens with many identically-named files.

All these factors make defining input both time-consuming and error-prone.

### 7.4.2 Viewing Output

Viewing and making sense of Delft3D-FLOW4 output is about as hard as defining its input. Deltares' has developed QuickPlot for this purpose. QuickPlot is an easy-to-use MATLAB suite to visualise and animate numerical results produced by the Delft3D modules in 2D in MATLAB. Despite QuickPlot being free open-source, MATLAB itself is closed-source and requires a licensing fee. QuickPlot is also unable to simultaneously load and combine multiple large datasets for processing and plotting. Lastly, QuickPlot is built on an older version of MATLAB (Release 2013b) [Deltares, 2019] which is incompatible with modern, 64-bit only systems (e.g.Windows 10, Mac OS 10.15 Catalina) and makes use of functions that have been deprecated in newer MATLAB versions. Therefore, like the GUI, it is not cross-platform and lacks portability.

### 7.4.3 Large Output Datasets

Total Delft3D-FLOW output file size depends on model dimensions, selected output quantities, number of processes taken into account, and the number of time-steps written to file [Deltares, 2019]. The last factor is the most important control on file size; when writing many time-steps to file (high-resolution output), a single simulation produces a large (tens of GB's) output file. Modelling stratigraphic evolution by turbidity currents requires many successive simulations to be run. Which produces large datasets that are too large to effectively download and analyze locally.

In our simulations, output intervals and saved quantities had to be reduced greatly to practically process the datasets. Ideally, output of many parameters would be written at a high temporal resolution, so processes can be analysed and visualized in small time-steps.

#### *Retrieving Output Files*

For rewriting output files, large files need to be moved to and from the server. In our case, file-transfer can take up to 45 minutes (on a slow day) halting the workflow. Moreover, not all data in a dataset is needed at once, only a few output properties at specific times are needed when analyzing. This set-up is not scalable to larger datasets.

# 8 CONCLUSIONS

The principal aim of this master thesis was to assess the effect of channel slope on turbidity currents and terminal-lobe deposits in a process-based numerical model. We report on three scenarios of 50 runs each that model the emplacement of turbidity current deposits

- Delft3D-FLOW is able to fairly realistically simulate the hydrodynamic structure of a turbidity current and appears capable of modelling turbidity current dynamics and resulting deposit.
- Here, we have demonstrated the capability of Delft3D-FLOW to model many successive turbidity currents flowing over a self-formed, evolving morphology. These experiments provide hydrodynamic, morphodynamic and stratigraphic insight into the evolution of multiple turbidite beds under only autogenic influences.
- The model demonstrates that a sediment-laden discharge flowing down a channel will form a turbidity current that erodes bed sediment here. The modeled turbidity current decelerates upon a decrease in slope. The flow spreads laterally and thins upon loss of confinement. Finally, the flow loses its capacity to suspend sediment as velocity decreases forming a thin, laterally extensive deposit.
- Turbidity current dynamics are observed to be sensitive to changing bed composition. Coarsening of the bed in successive simulations leads to progressively diminishing capacity of the turbidity current to erode and transport sediment, which in turn leads to decreased deposit thickness in the basin per flow event. To better model stratigraphic evolution, the issue of coarsening bed and associated decrease in flow intensity needs be addressed in future research.
- In this process-based model, channel slope controls turbidity current velocity in the channel, which increases the flow's capacity to entrain and transport sediment, leading to more erosion there. This also results in coarser bed composition in the channel for steeper slopes.
- Channel (upper) slope controls the geometry and maximum thickness of deposits in the basin. Gentler channel slopes make thicker deposits that are less spread out.
- The relief of deposits produced in 50 runs was insufficient to induce lateral or compensational stacking, only vertical stacking is observed. Therefore, the effect of channel slope on lobe-switching and related stacking patterns cannot be assessed. Either more runs are needed or the model needs to be modified to produce thicker deposits per run.
- Numerical modelling is a useful tool for researching controls on turbidity current dynamics and deposits. These results can aid in constructing more accurate and detailed models of turbidites.

- More and better tooling around Delft3D-FLOW tailored to geological modelling is needed, especially for generating ensembles of models and processing very large datasets.

# 9 RECOMMENDATIONS & FUTURE WORK

Having discussed how the set-up and results of the numerical model, the final chapter of this thesis addresses ways of improving it and suggests directions for future research, along with ideas for improvements to the Delft3D-FLOW geological modelling workflow.

The recommendations can roughly be divided into the following themes 1) improvements to to increase bed thickness per flow event; 2) more experiments on autogenic controls and on longer timescales; 3) introduction of allogenic signals; 4) validation by comparing numerical results to ancient- and moderns systems and 5) better tooling for geological simulations in Delft3D-FLOW.

## 9.1 IMPROVEMENTS TO CURRENT MODEL

### 9.1.1 Thicker Beds

The following paragraphs give several methods to to increase the flow event bed thickness per run, which would enable modeling of multiple lobe-elements and observe compensational stacking.

*Better Calibration of Flow*

Future models need better calibration of the inflow boundary condition (sediment mass concentration and discharge) to attain a well-adapted flow, this will conceivably prevent most of the coarser sediment fraction from being deposited shortly after inflow. More coarse sediment is expected to remain in suspension for a longer time and distance and will likely be deposited in the lobe, presumably leading to thicker deposits.

The spin-up interval until morphological changes take place (see Section 3.6.2) should be increased to prevent sediment discharge and morphological changes from overlapping, as is the case for the last three minutes of discharge in our model. The `UpdInf` keyword can be toggled in the morphology input file to prevent bed levels at inflow boundaries from being updated.

*Larger Discharged Sediment Volume*

The current model's discharge sediment volume is on the lower end for turbidity currents reaching the submarine fan (see Figure 7.1). Discharging a larger, fan-building event sediment volume is expected to lead to thicker deposits per run.

The total inflowing sediment volume can be increased by 1) longer inflow duration 2) higher discharge rate 3) higher sediment concentration or 4) wider or higher inflow dimensions, i.e.a boundary condition spanning more vertical and horizontal grid cells.

#### *MORFAC*

As morphological developments take place on a time scale several times longer than typical flow changes [Deltares, 2019], modelling morphological developments require long simulation times. One technique to reduce simulation time is to use a morphological acceleration factor (MORFAC), an acceleration factor for bed-level change.

The effect of the morphological factor is different for bed and suspended load. At each time step bedload is picked-up from the bed and deposited on the bed: only the transports are increased by the morphological factor used for the time step considered. However, in case of suspended load there is a time-delay between the time of erosion and the time of deposition. The erosion and deposition fluxes are increased by the morphological factor, but the suspended concentrations are not as that would influence the density effects. Use of a MORFAC was briefly attempted in during trial simulations, but quickly abandoned due to erroneous results. The most likely reason was a failure to multiply the thickness of the bed (transport) layer by the MORFAC too. Further work could look into applying a MORFAC with appropriately sized underlayers.

### 9.1.2 Measures of Stacking

If thicker deposits are achieved, autogenic lobe-element-switching dynamics can be modelled in fewer runs, which opens the door to assessing inter-element connectivity. A quantitative measure of static connectivity is required to constrain fluid-flow simulations [Funk et al., 2012]. The following measures can be used to assess element connectivity.

#### *Compensation Index*

Straub et al. [2009] developed the compensation index, a metric that quantifies the degree of compensation in sedimentary deposits by comparing observed stacking patterns to simple, uncorrelated stacking. This method uses the rate of decay of spatial variability in sedimentation between picked depositional horizons with increasing vertical stratigraphic scale. This approach allows identification of specific time and space scales relevant to stratigraphic architecture Straub et al. [2009]; Wang et al. [2011] and is especially useful for long-term ($> 10 \times 10^3$ yr discussed later in Section 9.1.5) perspective of stacking patterns.

#### *Overlap Index*

The overlap index (OI) is a parameter used to describe the degree to which the succeeding depositional element overlaps with the underlying one [Liu et al., 2018]. It is represented by $OI = A_0/A_1$, where $A0$ is the overlap area and A1 is the area of the older depositional element. Overlap index is good a measure to indicate when and to what extent a bed first starts stacking laterally.

### 9.1.3 Other Improvements for Current Model

#### *Resetting Residual Hydrodynamics*

A considerable volume of silt particles remains suspended in the water column. Extending the simulation time to let all the fine particles settle would

be an inefficient fix. Settling of fine particles is a slow process which would likely demand a lot of simulation time. Additionally, near bed layer are still in motion at the end of a simulation. In our simulations, residual conditions (velocities, density, concentrations, eddy viscosity & diffusivity) are all reset to equilibrium conditions after every 5 runs (Section 3.8.1). A better approach would be to reset all hydrodynamic properties after every run. To retain the suspended silt in the model, the future modeller could read the output data to sum the suspended sediment concentration per grid column and manually add it to the underlying bed layer grid cell, artifically 'settling' it instantaneously.

Ideally, all of these edits in between runs would be performed on the server where the simulations are run, to avoid the time-consuming transfer of files. This idea is developed further in Section 9.6.3.

*Coarsening of Bed*

As described in Figure 3.8.1 and the INTERPRETATION chapter, the coarsening of the channel bed diminishes subsequent flow's capacity.

The first and simplest option is to only reset the bed layer composition only in the channel and leave the basin's bed layer untouched.

Another options to counter-balance coarsening is to add fine particles to the transport layer manually as follows

1. Read values of transport layer composition of output
2. Calculate or estimate the volume of fine particles that accumulates in between flow events (see discussion on turbidity current recurrence in Section 7.3.3). If assigning a time-frame is too ambiguous, a simple percentage can be used, for example add 20% finer particles.
3. Add this volume to transport layer composition
4. Overwrite transport layer with these new values and write to NetCDF file

Another possibility to limit coarsening of the bed is to simulate accelerated hemi-pelagic background sedimentation by adding a discharge boundary condition spanning the whole domain. This can be performed during a run sandwiched in between flow event simulations.

*Grid Refinement*

The grid ultimately determines the accuracy of the model results. Future work could use a horizontal grid adapted to the areas of interest, for example a non-uniformly-spaced grid with higher resolution in the channel, the CLTZ, and the lobe itself, and lower resolution towards the distant boundaries. Refinement of the horizontal grid is expected to resolve the minor numerical instabilities (wiggles) seen in the surface of the lobe deposits (Figure 6.4).

The vertical resolution can be increased in the bottom layers, this also might alleviate the numerical issues and results in more detailed near-bed flow dynamics too.

*More Slope Combinations*

To reinforce the relation between channel slope, deposit thickness and stacking patterns, more variations channel- and basin slope can be run. The

smoothing curve appled the slope determines the abruptness of the slope-break which may affect the deceleraration of the flow.

#### *More Sediments Fractions*

More sediment fractions should be included to better approximate a continuous distribution of grain sizes to closer resemble real flows. Addition of more grain size classes will enable approximation of petrophysical properties like permeability and porosity of the output deposits for use in reservoir analogues (see Section 9.7).

### 9.1.4 Sensitivity Analysis

Since each scenario takes around 10 days of continuous computation in a high-performance computing cluster, additional runs for a sensitivity analysis were not practical.

#### *Entrainment*

By setting the `NeglectEntrainment` keyword to `true` in the morphology input file (.mor), entrainment of suspended sediment in the mass balance is neglected [Deltares, 2019]. The volume of entrained bed sediment can then be assessed by comparing it to an identical simulation with said keyword set to `false`. The sensitivity of the flow dynamics to entrainment can be assessed similarly.

#### *Sediment Parameters*

Behaviour of sediments depends on the input parameters. Parameters describing erosion and sedimentation are important thresholds for the geomorphology. For example, strongly cohesive settings may generate more relief than more mobile landscapes [Hajek and Straub, 2017]. Future research could evaluate the sensitivity of this model to these parameters. The following parameters can be altered slightly: 1) erosion parameter 2) erosive and depositional critical bed shear stresses for the cohesive fraction, to investigate their impact on the flow and on deposits to understand the effects of variable cohesion.

### 9.1.5 Autogenic Dynamics over Longer Timescales

To characterise purely autogenic lobe-switching patterns, the future modeller could extend the simulated time to model elements higher order elements — multiple stacked lobe-elements forming a lobe and research the exact mechanisms behind flow switching.

This would require the addition of hemipelagic sedimentation as described above to separate the architectural elements.

#### *Compaction*

Nienhuis et al. [2018] included 'pseudo-compaction' in the results of a Delft3D-FLOW model of fluvial crevasse splays. They achieved this by calculating the amount of soil compaction on the results with a consolidation rate that depends on the effective vertical stress, soil compressibility, and time outside of Delft3D-FLOW [Nienhuis et al., 2018]. A similar approach can be

applied to our results to account for evolving evolving properties of the bed by compaction.

## 9.2 STUDY OTHER AUTOGENIC CONTROLS

Besides slopes, other controls on autogenic behavior like stacking patterns can be investigated in Delft3D-FLOW. The effect of input variables like sediment parameters or flow parameters such as discharge, sediment concentration are controls that can be varied.

*Confinement*

Confinement has a strong effect on the lobes geometry. When lobes are more constrained by local topographic highs, they are areally restricted and stack vertically (aggradational stacking) [Prelat et al., 2010]. The ratio of the area of deposition vs. maximum thickness is on average 30 times larger for lobes deposited in unconfined settings than for those deposited in more confined areas [Prelat et al., 2010]. Highly confined setting likely suppress the autocyclic signal due to decreased accommodation space [Liu et al., 2018]. Future research could investigate how and to what extent autogenic stacking patterns are affected by confinement, for example in ponded minibasins, which are three-dimensionally closed topographic lows (doubly-plunging synclines) on continental slopes [Prather, 2003].

### 9.2.1 Stochastic Input Parameters

To better mimic an actual lobe, temporal changes in flow properties ought to be included in the model. To research the effect of flow variability over many flow events on deposit architecture, values for discharge volume and sediment composition parameters could be obtained by sampling from stochastic distributions.

## 9.3 MODELLING OTHER SUBMARINE ELEMENTS

### 9.3.1 Submarine Channel & Levees

Channels represent the dominant form observed in natural submarine fan fans [Parsons et al., 2007]. Like lobes, submarine channels and levee deposits can also form attractive reservoir elements. Research has shown that rivers and submarine channels share many similar morphologic elements and processes, such as levees, meandering planforms, point bars, and scroll bars [Konsoer et al., 2013]. Channel-levee elements also exhibit typical stacking patterns due to repeated avulsions [McHargue et al., 2011] and can — like lobes — be divided into hierarchical classification.

Delft3D-FLOW has formulations for some flow processes in the fluvial, surface equivalents (e.g.helical flows in channel bends) [Deltares, 2019]. Channel avulsion also controls where lobes are deposited. Instead of focusing only on lobes, the focus can shift to modelling how turbidity currents sculpt submarine channel and levees using Delft3D-FLOW.

## 9.4 INTRODUCE ALLOGENIC FORCINGS

In the future, submarine fan stratigraphy could be modelled in Delft3D-FLOW over longer timescales (10 – 100 k years). For realism, this would require the introduction of an allogenic signal to couple the Delft3D-FLOW model to the encompassing source-to-sink system. Measured allogenic signals can be mimicked by varying upstream boundary conditions. For example, by periodically varying the volume of sediment transported by the flows, cyclic sea-level- or climate-driven variations in sediment supply can be mimicked [Groenenberg et al., 2010]. The same idea can be applied to variations in sediment composition and recurrence intervals, which determine the amount interim hemipelagic sediment and draping of lobe-elements with mudstone sheets [Parsons et al., 2007].

## 9.5 VALIDATION & CALIBRATION AGAINST ENVIRONMENTAL DATA

Experimental and numerical models of turbidites are limited by the lack of testing against environmental data, due to the large scale nature of natural turbidity currents and the inherent difficulties in comparing model output with turbidite deposits for which the initial conditions are largely or wholly unknown [Kneller and Buckee, 2000]. Comparing environmental data to the model can shed light on the limitations and strengths of the model. However, outcrop analogues and modern data are generally limited to 2D with poor expression of the 3D.

### 9.5.1 Modern Submarine Fan Systems

Further work could aim to investigate flow–deposit interactions and resulting stacking pattern of lobes and lobe elements at field-scale using input parameter constraints from quantitative field studies of modern systems [Groenenberg et al., 2010; Kneller and Buckee, 2000]. However, field-scale applications of numerical models require guesswork of the initial conditions, as the magnitude and unpredictability of the events make it extremely difficult to gather the required input data [El-Gawad et al., 2014].

Accuracy of the model can be improved the by calibrating and validating against bed topography data of present-day submarine fan system (sensu El-Gawad et al. [2014]). The advent of seismic and sonar technology has been revealing the seabed morphology with increasing details [El-Gawad et al., 2014]. Publicly available bathymetric data (from NOAA, emodnet, Gebco, Bureau of Ocean Management) can be used as as input topography by converting these to Delft3D-FLOW depth files if the bathymetric data resolution resolution is sufficient (similar functionality is already implemented by Breyiannis et al. [2016] in pyPoseidon). Measured turbidity current properties like concentrations, flow height derived from measurement instruments can constrain initial flow conditions. The results can be validated — and if necessary, recalibrated — with samples from corings, ultra-high resolution seismic-reflection profiling that show bed thicknesses and/or grain size trends.

*Past Systems*

A comparable idea is to rely on outcrop-derived data of past systems to provide ground-truth detail to constrain the model. Similar to Groenenberg et al. [2010], a simulation of a lobe-element constrained by outcrop-, core- and various logging data can be performed. The main question here is to what degree are flows are represented by their deposits. The outcrop dataset needs to be of exceptional quality and size to constrain the input parameters for the model (e.g. grain-size range, bed dimensions, flow volumes, bathymetry) [Groenenberg et al., 2010]. Paleo-bathymetry of ancient systems can be extracted from an interpreted seismic surface. The simulation results can be compared and validated and the input parameters tuned accordingly if the results are off.

In this vein, Vacek [2018] applied Delft3D-FLOW to make a geological model of a ancient Gilbert-type delta constrained by field data to within 17% similarity of grain size.

## 9.6 IMPROVEMENTS TO MODELLING TOOLS

As stated in the above sections, there are numerous possibilities for future research for Delft3D-FLOW in geological modelling. These would necessitate operational improvements to the modelling process — better, more intuitive tooling around Delft3D-FLOW. This section offers possible solutions to the operational issues described in Section 7.4 Suitability of Delft3D-FLOW.

### 9.6.1 Declarative Wrapper for Input

To construct experimental setups, one needs to be able construct different setup iteratively and be able to change input quickly. The ability to directly declare input — such as bathymetry and flow parameters – programmatically instead of manually would cut down model development time greatly, permitting faster iterative improvement of scenarios by shortening the feedback loop.

We suggest a *declarative wrapper* or *framework* adapted for geological modelling; a piece of software between the modeller and Delft3D-FLOW that enables entry in *human terms* and hides implementation details such as unit conversions, file formatting and writing. *Declarative* is paradigm from borrowed from computer science, to paraphrase a saying about declarative programming for modelling: "Declarative modelling is the act of making Delft3D-FLOW models that conform to the thought pattern of the modeller rather than the operational pattern of the modelling software". For example for 3D boundary conditions, *declarative* entails that the modeller can directly provide a high-level specification of what the flow should include in terms of duration, inflow height, concentration, total sediment volume and composition, rather than having to convert the parameters in terms of discharge and mass concentration per grid layer. A declarative wrapper can provide expressiveness for certain tasks that a is harder to achieve with GUI, for example for generation of many experimental models in which parameters vary slightly per scenario (e.g.slope, discharge, sediment composition), or for input that derive values from distributions rather than fixed values, as suggested in Section 9.2.1. Some examples of such wrappers for Delft3D-FLOW and similar modelling software are mentioned in Appendix B.

See DELFT3D-FLOW & PYTHON Appendix B for a description of a small, nascent Python package designed to help reading and constructing of Delft3D-FLOW input and visualizing its input and output. Further work could make it more usable and more declarative.

### 9.6.2 3D-visualization

Geology and fluid flow are both inherently 3D phenomena; the ability to visualize input and output in 3D is key to glean insights during the modelling and analysis steps. A small start was made to plot models in 3D with PyVista [Sullivan and Kaszynski, 2019], a Python interface to the Visualizition ToolKit (VTK), a powerful software system for manipulating and visualising scientific data in 3D. VTK is capable of displaying time-varying properties, filtering and slicing volumetric data and exporting to web (see also PyVista in appendix Appendix B). ParaView is a front-end application for the VTK platform that provides interactive data analysis and visualization options for 3D data. ParaView was developed to analyze large datasets using distributed memory computing resources. Like VTK, ParaView is both open-source and multi-platform.

ParaView and VTK are used extensively in CFD and climate modelling, so they can be applied to process Delft3D-FLOW data. Further work could attempt to process Delft3D-FLOW output for use in the VTK/ParaView suite for analysis and visualization.

### 9.6.3 Large Output Datasets

With multiple runs and multiple scenarios, the total dataset reaches filesizes that are inconvenient to process on regular PCs. The total filesize of the dataset produced for this thesis approaches 100 GB even after compression and with limited output times. Ideally, output is saved in high temporal resolution, without concern for filesize constraints. If system dynamics and stratigraphy are to be modelled over longer timescales — as proposed in Section 9.4 — the amount of data will be unmanageable for storage and processing for practical purposes with a regular PC.

Hence, there is a need for efficient storage, retrieval and processing of simulation output data, especially if simulations will be performed for longer timescales. Fortunately, this problems is not unique to geological modelling, storing very large (100's of GB to TB range) multi-dimensional, gridded datasets is an issue in other geo-

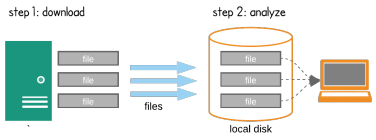


**(a)** (Current solution) File-based approach: all dataset files are stored and all post-processing is done on a PC


**(b)** Database approach (openDAP): Files are stored in database and only requested data are transferred

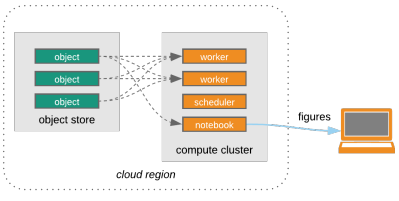


**(c)** Cloud-based approach (zarr): Files are stored in cloud data-store and intensive post-processing operations are offloaded to cloud workers

**Figure 9.1:** Diagram of approaches to data-access for large scientific datasets. From Abernathey [2020]

sciences — such as meteorology, remote sensing and oceanography — too.

Hence, solutions for remote storage of scientific datasets have existed for a long time (e.g.openDAP) (Figure 9.1b) and newer, more efficient solutions have been developed in recent years. Zarr is one such new development, a promising new data format specification originating from the geoscience community (the Pangeo project). Zarr has cloud-native capabilities that can handle parallel combining, reading and writing of very large (TB's) datasets (Figure 9.1c). Zarr allows performant extraction of data by anyone without relying on data services like OPeNDAP [Signell and Pothina, 2019]. Either of these solution can be used to make a remote-access data-store for simulation results.

An integrated modelling suite on on a (cloud-)server with connection to data-store with ample storage space would solve many problems of the modelling process at once. This approach is illustrated in Figure 9.1c. This would provide the following benefits

- Intermediate processing, such as resetting hydrodynamic conditions, could (should!) be automated to be done after every run. Multi-run simulations can then run automatically without intermissions.
- Solves the storage issue and time-consuming back-and-forth transfer of large files.
- Computationally intensive post-processing can be offloaded to the server, so that only the necessary results (e.g.processed data, figures) are transferred to the modeller. For example, demanding calculations or 3D rendering can be performed server-side.
- Enables effective sharing of data with collaborators and interested stakeholders.
- Can scale with demand

## 9.7 TOWARDS RESERVOIR MODELS

Once it is possible to adequately simulate submarine fan elements over longer spatial- and time-scales with a realistic grain size range, integration of the geologic information like grain-size trends and geometries produced by these simulations can be used to inform submarine fan reservoir models. In turn, these reservoir models form the basis for porous media flow simulations and may result in better models of reservoir response.

### 9.7.1 Delt3D-GeoTool

Further work could integrate such models into Delft3D-GeoTool. Delft3D-GeoTool is a user-friendly wrapper around the Delft3D-FLOW core for making fluvio-deltaic reservoir analogue models, with ability to export to industry-standard modelling software like Petrel™ and JewelSuite™ [Storms et al., 2016].

# BIBLIOGRAPHY


(cited March 2020). Netcdf climate and forecast metadata conventions version 1.9.

Abernathey, R. (2020). Data access modes in science.

Allen, J. R. L. (1971). Mixing at turbidity current heads, and its geological implications. *Journal of Sedimentary Research*, 41(1):97–113.

Allen, P. A. (2017). *Sediment Routing Systems: The Fate of Sediment from Source to Sink*. Cambridge University Press.

Allin, J. R., Hunt, J. E., Clare, M. A., and Talling, P. J. (2017). Eustatic sea-level controls on the flushing of a shelf-incising submarine canyon. *GSA Bulletin*, 130(1-2):222–237.

Azpiroz, M. (2018). *Understanding the dynamics of submarine density flows through direct observations from modern systems*. PhD thesis, University of Southampton.

Azpiroz Zabala, M., Storms, J. E. A., van der Vegt, H., Walstra, D.-J., Obradors-Latre, A., Pontén, A., and Jagers, B. (2020). Turbidity current signature on consecutive turbidity current analysis through numerical simulations of multiple consecutive submarine flows. *EGU General Assembly Abstracts*, 2020.

Breyiannis, G., Petroliagkis, T., and Annunziato, A. (2016). Exploring delft3d as an operational tool coastal risk exploratory project. In *JRC Technical Reports*.

Burgess, P. M., Masiero, I., Toby, S. C., and Duller, R. A. (2019). A Big Fan of Signals? Exploring Autogenic and Allogenic Process and Product In a Numerical Stratigraphic Forward Model of Submarine-Fan Development. *Journal of Sedimentary Research*, 89(1):1–12.

Caminha, G. (2019). The cfl condition and how to choose your timestep size.

Cantelli, A., Pirmez, C., Fenandez, R., and Parker, G. (2009). Morphodynamic and stratigraphic evolution of self-channelized subaqueous fans emplaced by turbidity currents and dilute mudflows (invited). *AGU Fall Meeting Abstracts*.

Commandeur, A. (2015). Turbidity currents in reservoirs. Master's thesis, Delft University of Technology, Faculty of Civil Engineering and Geosciences.

Dask Development Team (2016). *Dask: Library for dynamic task scheduling*.

Deltares (2019). *Delft3D-FLOW User Manual*.

Deptuck, M., Piper, D., Bruno, S., and Gervais, A. (2008). Dimensions and architecture of late pleistocene submarine lobes off the northern margin of east corsica. *Sedimentology*, 55.

Deptuck, M. and Sylvester, Z. (2017). *Submarine Fans and Their Channels, Levees, and Lobes*, pages 273–299.

El-Gawad, S., Pirmez, C., Cantelli, A., Minisini, D., Sylvester, Z., and Imran, J. (2014). 3-d numerical simulation of turbidity currents in submarine canyons off the niger delta. *Marine Geology*, s 326–328:55–66.

Fernandez, R., Cantelli, A., Pirmez, C., Sequeiros, O., and Parker, G. (2014). Growth patterns of subaqueous depositional channel lobe systems developed over a basement with a downdip break in slope: Laboratory experiments. *Journal of Sedimentary Research*, 84.

Funk, J., Slatt, R., and Pyles, D. (2012). Quantification of static connectivity between deep-water channels and stratigraphically adjacent architectural elements using outcrop analogs. *AAPG Bulletin*, 96:277–300.

García, M. H. (1993). Hydraulic jumps in sediment driven bottom currents. *Journal of Hydraulic Engineering*, 119(10):1094–1117.

Geleynse, N., Storms, J. E., Walstra, D.-J. R., Jagers, H. A., Wang, Z. B., and Stive, M. J. (2011). Controls on river delta formation; insights from numerical modelling. *Earth and Planetary Science Letters*, 302(1):217 – 226.

Gerritsen, H., Goede, E., Platzek, F., Kester, J., Genseberger, M., and Uittenbogaard, R. (2008). Validation document delft3d-flow.

Groenenberg, R. (2007). *Process-based modelling of turbidity-current hydrodynamics and sedimentation*. PhD thesis, Delft University of Technology.

Groenenberg, R., Sloff, K., and Weltje, G. (2009). A high-resolution 2-dh numerical scheme for process-based modeling of 3-d turbidite fan stratigraphy. *Computers & Geosciences*, 35:1686–1700.

Groenenberg, R. M., Hodgson, D. M., Prelat, A., Luthi, S. M., and Flint, S. S. (2010). Flow–Deposit Interaction in Submarine Lobes: Insights from Outcrop Observations and Realizations of a Process-Based Numerical Model. *Journal of Sedimentary Research*, 80(3):252–267.

Hajek, E. and Straub, K. (2017). Autogenic sedimentation in clastic stratigraphy. *Annual Review of Earth and Planetary Sciences*, 45.

Hamilton, P., Gaillot, G., Strom, K., Fedele, J., and Hoyal, D. (2017). Linking hydraulic properties in supercritical submarine distributary channels to depositional-lobe geometry. *Journal of Sedimentary Research*, 87:935–950.

Hamilton, P., Strom, K., and Hoyal, D. (2015). Hydraulic and sediment transport properties of autogenic avulsion cycles on submarine fans with supercritical distributaries. *Journal of Geophysical Research: Earth Surface*, 120.

Hawie, N., Covault, J., Dunlap, D., and Sylvester, Z. (2018). Slope-fan depositional architecture from high-resolution forward stratigraphic models. *Marine and Petroleum Geology*, 91:576–585.

Hawie, N., Covault, J., and Sylvester, Z. (2019). Grain-size and discharge controls on submarine-fan depositional patterns from forward stratigraphic models. *Frontiers in Earth Science*, 7:334.

Hermes, D. (2017). Helper for bezier curves, triangles, and higher order objects. *The Journal of Open Source Software*, 2(16):267.

Hiscott, R., Hall, F., and Pirmez, C. (1997). Turbidity-current overspill from the amazon channel: Texture of the silt/sand load, paleoflow from anisotropy of magnetic susceptibility, and implications for flow processes. *Proceedings of the Ocean Drilling Program, Scientific Results*, 155.

Hofstra, M., Hodgson, D., Peakall, J., and Flint, S. (2015). Giant scour-fills in ancient channel-lobe transition zones: Formative processes and depositional architecture. *Sedimentary Geology*, 329:98 – 114.

Hoyer, S., Fitzgerald, C., Hamman, J., et al. (2016). *xarray: v0.15.0*.

Hunter, J. D. (2007). Matplotlib: A 2d graphics environment. *Computing in Science & Engineering*, 9(3):90–95.

Jagers, B. (2012). Sediment mixtures and bed stratigraphy.

Jobe, Z. R., Howes, N., Romans, B. W., and Covault, J. A. (2018). Volume and recurrence of submarine-fan-building turbidity currents. *The Depositional Record*, 4(2):160–176.

Jobe, Z. R., Sylvester, Z., Howes, N., Pirmez, C., Parker, A., Cantelli, A., Smith, R., Wolinsky, M. A., O'Byrne, C., Slowey, N., and Prather, B. (2017). High-resolution, millennial-scale patterns of bed compensation on a sand-rich intraslope submarine fan, western Niger Delta slope. *GSA Bulletin*, 129(1-2):23–37.

Kneller, B. and Buckee, C. (2000). The structure and fluid mechanics of turbidity currents: a review of some recent studies and their geological implications. *Sedimentology*, 47(s1):62–94.

Konsoer, K., Zinger, J., and Parker, G. (2013). Bankfull hydraulic geometry of submarine channels created by turbidity currents: Relations between bankfull channel characteristics and formative flow discharge. *Journal of Geophysical Research: Earth Surface*, 118(1):216–228.

Kuenen, P. H. and Migliorini, C. I. (1950). Turbidity Currents as a Cause of Graded Bedding. *Journal of Geology*, 58(2):91–127.

Kumar, V. (2011). *Bed Roughness*, pages 94–94. Springer Netherlands, Dordrecht.

Liu, Q., Kneller, B., Fallgatter, C., and Valdez Buso, V. (2018). Quantitative comparisons of depositional architectures of unconfined and confined turbidite sheet systems. *Sedimentary Geology*, 376.

Lomas, S. and Joseph, P. (2004). Confined turbidite systems. *Geological Society, London, Special Publications*, 222:1–7.

Lopez-Cabrera, J. and Manzocchi, T. (2017). Quantifying compensational stacking in deep water deposits. an example from the lettergesh fm., ireland.

Major, J. J. (2003). *Hindered settling*, pages 358–360. Springer Netherlands, Dordrecht.

McHargue, T., Pyrcz, M., Sullivan, M., Clark, J., Fildani, A., Romans, B., Covault, J., Levy, M., Posamentier, H., and Drinkwater, N. (2011). Architecture of turbidite channel systems on the continental slope: Patterns and predictions. *Marine and Petroleum Geology*, 28:728–743.

Meiburg, E. and Kneller, B. (2010). Turbidity currents and their deposits. *Annual Review of Fluid Mechanics*, 42.

Mulder, T. and Alexander, J. (2001). Abrupt change in slope causes variation in the deposit thickness of concentrated particle-driven density currents. *Marine Geology*, 175(1):221 – 235.

Mutti, E. and Normark, W. R. (1987). Comparing examples of modern and ancient turbidite systems: problems and concepts.

Mutti, E. and Sonnino, M. (1981). Compensation cycles: A diagnostic feature of turbidite sandstone lobes. *International Association of Sedimentologist 2nd European Regional Meeting*, 5:120–123.

Nienhuis, J., Törnqvist, T., and Esposito, C. (2018). Crevasse splays versus avulsions: A recipe for land building with levee breaches. *Geophysical Research Letters*, 45(9):4058–4067.

NOAA (2018). What is a turbidity current?

Normark, W. R. and Damuth, J. E. (1997). Sedimentary facies and associated depositional elements of the amazon fan.

Ooms, J. (2017). 2dv numerical simulations of turbidites in ponded basins: Insights from depositional patterns. Master's thesis, Utrecht University, Faculty of Geosciences.

Ortiz, J. and Klompmaker, A. (2015). Turbidity currents: Comparing theory and observation in the lab. *Oceanography*, 28:220–227.

pandas development team, T. (2020). pandas-dev/pandas: Pandas.

Parker, G. (1982). Conditions for the ignition of catastrophically erosive turbidity currents. *Marine Geology*, 46(3):307 – 327.

Parker, G., Fukushima, Y., and Pantin, H. M. (1986). Self-accelerating turbidity currents. *Journal of Fluid Mechanics*, 171:145–181.

Parsons, J., Friedrichs, C., Traykovski, P., Mohrig, D., Imran, J., Syvitski, J., Parker, G., Puig, P., Buttles, J., and García, M. (2007). The mechanics of marine sediment gravity flows. *International Association of Sedimentologists*, 37:275 – 337.

Parsons, J., Schweller, W., Stelting, C., Southard, J., Lyons, W., and Grotzinger, J. (2002). A preliminary experimental study of turbidite fan deposits: Reply. *SEPM (Society for Sedimentary Geology*, 72:619–628.

Paull, C. K., Talling, P. J., Maier, K. L., Parsons, D., Xu, J., Caress, D. W., Gwiazda, R., Lundsten, E. M., Anderson, K., Barry, J. P., Chaffey, M., O'Reilly, T., Rosenberger, K. J., Gales, J. A., Kieft, B., McGann, M., Simmons, S. M., McCann, M., Sumner, E. J., Clare, M. A., and Cartigny, M. J. (2018). Powerful turbidity currents driven by dense basal layers. *Nature Communications*, 9(1):4114.

Piper, D. and Normark, W. (2001). Sandy fans—from amazon to hueneme and beyond. *AAPG Bulletin*, 85:1407–1438.

Piper, D. J. and Normark, W. R. (2009). Processes That Initiate Turbidity Currents and Their Influence on Turbidites: A Marine Geology Perspective. *Journal of Sedimentary Research*, 79(6):347–362.

Pohl, F. (2019). *Turbidity currents and their deposits in abrupt morphological transition zones*. PhD thesis.

Prather, B. E. (2003). Controls on reservoir distribution, architecture and stratigraphic trapping in slope settings. *Marine and Petroleum Geology*, 20(6):529 – 545. Turbidites: Models and Problems.

Prelat, A., Covault, J., Hodgson, D., Fildani, A., and Flint, S. (2010). Intrinsic controls on the range of volumes, morphologies, and dimensions of submarine lobes. *Sedimentary Geology*, 232:66–76.

Prelat, A. and Hodgson, D. (2013). The full range of turbidite bed thickness patterns in submarine lobes: Controls and implications. *Journal of the Geological Society*, 170:209–214.

Prélat, A., Hodgson, D. M., and FLINT, S. S. (2009). Evolution, architecture and hierarchy of distributary deep-water deposits: a high-resolution outcrop investigation from the permian karoo basin, south africa. *Sedimentology*, 56(7):2132–2154.

Pyrcz, M., Octavian, C., and Deutsch, C. (2005). Stochastic surface-based modeling of turbidite lobes. *Aapg Bulletin - AAPG BULL*, 89:177–191.

Richardson, J. and Zaki, W. (1954). The sedimentation of a suspension of uniform spheres under conditions of viscous flow. *Chemical Engineering Science*, 3(2):65 – 73.

Sequeiros, O. (2012). Estimating turbidity current conditions from channel morphology: A froude number approach. *Journal of Geophysical Research (Oceans)*, 117:4003–.

Sequeiros, O., Naruse, H., Endo, N., García, M., and Parker, G. (2009). Experimental study on self-accelerating turbidity currents. *Journal of Geophysical Research*, 114.

Signell, R. and Pothina, D. (2019). Analysis and visualization of coastal ocean model data in the cloud. *Journal of Marine Science and Engineering*, 110:7.

Slatt, R. M. (2013). *Stratigraphic Reservoir Characterisation for Petroleum Geologists, Geophysicists, and Engineers*, volume 61. Elsevier, Amsterdam, The Netherlands, 2 edition.

Stevens, J.-L., Rudiger, P., and Bednar, J. (2015). Holoviews: Building complex visualizations easily for reproducible science.

Stevenson, C. J., Jackson, C. A.-L., Hodgson, D. M., Hubbard, S. M., and Eggenhuisen, J. T. (2015). Deep-Water Sediment Bypass. *Journal of Sedimentary Research*, 85(9):1058–1081.

Storms, J., Walstra, D., Li, L., van der Vegt, H., Howes, N., de Boer, W., van Putten, H., and Forzoni, A. (2016). Towards an open-source web-based delft3d geotool. In *Proceedings of the 2nd Conference on Forward Modelling of Sedimentary Systems*, pages 1–6. EAGE.

Straub, K., Paola, C., Mohrig, D., Wolinsky, M., And, and George, T. (2009). Compensational stacking of channelized sedimentary deposits. *Journal of Sedimentary Research*, 79:673–688.

Straub, K. and Pyles, D. (2012). Quantifying the hierarchical organization of compensation in submarine fans using surface statistics. *Journal of Sedimentary Research*, 82:889–898.

Straub, K. M. (2019). Morphodynamics and stratigraphic architecture of shelf-edge deltas subject to constant vs. dynamic environmental forcings: A laboratory study. *Frontiers in Earth Science*, 7:121.

Sullivan, C. B. and Kaszynski, A. (2019). PyVista: 3d plotting and mesh analysis through a streamlined interface for the visualization toolkit (VTK). *Journal of Open Source Software*, 4(37):1450.

Sumner, E. J. and Paull, C. K. (2014). Swept away by a turbidity current in mendocino submarine canyon, california. *Geophysical Research Letters*, 41(21):7611–7618.

Sylvester, Z. (2013). Exploring grain settling with python.

Talling, P., Allin, J., Armitage, D., Arnott, R., Cartigny, M., Clare, M., Felletti, F., Covault, J., Girardclos, S., Hansen, E., Hill, P., Hiscott, R., Hogg, A., Clarke, J., Jobe, Z., Malgesini, G., Mozzato, A., Naruse, H., Parkinson, S., and Xu, J. (2015). Key future directions for research on turbidity currents and their deposits. *Journal of Sedimentary Research*, 85(2):153–169.

Talling, P., Paull, C., and Piper, D. (2013). How are subaqueous sediment density flows triggered, what is their internal structure and how does it evolve? direct observations from monitoring of active flows. *Earth-Science Reviews*, 125:244–287.

Unidata (2019). Netcdf 4.7.2.

Vacek, M. (2018). Utilizing process-based models to better incorporate heterogeneities within reservoir modelling. Master's thesis, Delft University of Technology, Faculty of Civil Engineering and Geosciences.

van der Vegt, H., Storms, J., Walstra, D.-J., and Howes, N. (2016). Can bed load transport drive varying depositional behaviour in river delta environments? *Sedimentary Geology*, 345:19–23.

van Rijn, L. (2007). Unified view of sediment transport by currents and waves.ii: Suspended transport. *Journal of Hydraulic Engineering*, 133:244–287.

Wang, Y., Straub, K., and Hajek, E. (2011). Scale-dependent compensational stacking: An estimate of autogenic time scales in channelized sedimentary deposits. *Geology*, 39:811–814.

Weimer, P. and Slatt, R. (2007). Introduction to the petroleum geology of deep-water settings. *AAPG Student Geololgy*, 57:149–227.

Whitaker, J., Khrulev, C., Huard, D., Paulik, C., Hoyer, S., Filipe, Pastewka, L., Mohr, A., Marquardt, C., Couwenberg, B., Taves, M., Whitaker, J., Cuntz, M., Bohnet, M., Brett, M., Hetland, R., Korenčiak, M., barronh, Onu, K., Helmus, J. J., Hamman, J., Barna, A., fredrik 1, Koziol, B., Kluyver, T., May, R., Smrekar, J., Barker, C., Gohlke, C., and Kinoshita, B. P. (2019). Unidata/netcdf4-python: Version 1.5.3 release.

# A FAILED ATTEMPTS TO INCREASE DEPOSIT THICKNESS

## A.1 HIGHER CONCENTRATION

Total sediment volume concentration of 4.5% with discharges 2200 and 3000 $m^3/s$ could not sustain the sediment load, too much of the sand fraction much drops out near the discharge boundary condition.

## A.2 MORFAC

Applying a morphological acceleration factor was tried, but was shown to produce erratic deposits. The rate of erosion is limited by the thickness of the transport layer. If a MORFAC is applied, the thicknesses of the stratigraphic layers needs to be multiplied by the same factor, which was not done in the test simulation.

## A.3 GREATER SEDIMENT DISCHARGES

Either increased discharges duration ($>$ 1 hour) or higher discharge rates ($>$ 5500 $m^3/s$) caused the flow to reach and reflect against the boundaries of the model.

A discharge of 15 000 $m^3/s$ was attempted, the model dimensions were too small and the flow reflected against the side boundaries.

## A.4 SMALLER TIME-STEP

Time-steps of 0.30 min and 0.45 min was shown to produce more numerical instabilities in the deposits. A smaller time-step of 0.1 min showed little difference between the selected time-step of 0.3 min.

# B DELFT3D-FLOW & PYTHON

PyDelft3D-FLOW is an offshoot of this thesis, it's a small Python package that were developed to help with 1) reading and writing of several input files of a Delft3D4-FLOW model, 2) auto-generating multiple successive runs, 3) (interactive) plotting of the Delft3D-FLOW output (NetCDF format only) as and 4) overwriting values in NetCDF output.

## B.1 BUT WHY?

I think scientific software should strive for a high degree of openness, interoperability, readability and robustness. In my opinion, MATLAB does not check all of the boxes, also read the section Improvements to Modelling Tools in RECOMMENDATIONS & FUTURE WORK. Python is completely free, open-source and multi-platform. This stack can be run any platform that supports Python, meaning it can easily be ported from a desktop to cloud environment, or a High-Performance Cluster (HPC) to handle petabyte-scale datasets. Python offer many choices for graphics package and there are increasingly impressive options for (geo)scientific libaries. Python has more sane dependency management that doesn't require you to place tangle of files and nested folders in a folder like MATLAB does. Thus, PyDelft3D-FLOW is an alternative to Deltares' QuickPlot and OpenEarthTools.

Lastly, Python is also a more readable language and labeled arrays — as implemented by xarray & Dask — are much more intuitive and less error-prone in manipulating large amounts of data. Interactive visualizations like HoloViews/hvPlot enable immediate, automatic visualization of data.

## B.2 PACKAGES/DEPENDENCIES

This section gives an overview of the packages that are used in pyDelft3D-FLOW.

### B.2.1 xarray & Dask

The core functionality is provided by xarray. Delft3D-FLOW writes output in the NetCDF3 64-bit format with metadata following the Climate & Forecast Conventions. xarray is Python package for opening and analysing multidimensional gridded data sets. xarray is particularly tailored to working with self-describing NetCDF files and has native support for CF convention metadata [Signell and Pothina, 2019], like that written by Delft3D-FLOW. xarray introduces labels in the form of dimensions, coordinates and attributes on top of raw multidimensional arrays, which allows for a more intuitive, more concise, and less error-prone developer experience [Hoyer et al., 2016].

xarray integrates tightly with Dask under the hood to facilitate out-of-memory and parallel computations on large datasets that do not fit into memory. Dask arrays allow handling very large array operations using many small arrays known as *chunks* [Dask Development Team, 2016; Signell and Pothina, 2019]. This enables many successive simulations to be combined and opened as one dataset. xarray also includes basic built-in visualization options with matplotlib [Hunter, 2007]. xarray is used extensively in other geosciences such as climatology and oceanography, but sadly not much (yet?) in geology and geological modeling.

### B.2.2 HoloViews/hvPlot

HoloViews is a a Python library that enables visual exploration of multi-dimensional parameter spaces using auto-generated widgets that read the datasets metadata [Stevens et al., 2015]. Thanks to built-in Dask and Datashader integration HoloViews scales easily to millions of datapoints. hvPlot is a convenience wrapper around xarray for plotting data with HoloViews for more advanced, interactive visualizations.

#### *Datashader*

Datashader renders 2D visualizations of large data into rasters, allowing accurate, dynamic representation of datasets that would otherwise be too intensive to display [Stevens et al., 2015].

### B.2.3 PyVista

PyVista PyVista is a pure Python library wrapping the VTK library's Python bindings for a streamlined and intuitive toolset for 3D Visualization and mesh analysis/processing. PyVista can be used across platforms, has extensive documentation and is open-source with a permissive MIT Licence. Structures created in PyVista are immediately interoperable with any VTK-based software [Sullivan and Kaszynski, 2019].

## B.3 SCRIPTS IN PYDELFT3D-FLOW

This section gives a brief description of each script in PyDelft3D-FLOW. pyDelft3D-FLOW is intended to be used in a notebook environment like JupyterLab or nteract. The code is meant to be reusable and is mostly commented. The exact functionality and documentation are subject to change. For the latest and more extensive documentation refer to the code repository and the latest source code, see the GitHub repository.

### B.3.1 3D visualization

`plotPyVista.py` is a script that processes Delft3D-FLOW NetCDF output and uses PyVista to make a structured grid for 3D visualization. A structured grid assumes that points are input in a certain order, which determines the connectivity between cells.

*2D Visualization*

processNetCDF.py is a script that processes a Delft3D-FLOW netCDF file for plotting with HoloViews. If an enclosure is applied, Delft3D-FLOW write blanks for unused grid cells to file and the grid must be 'repaired' for plotting. At present repairing the grid is only supported for uniform rectilinear grids, although HoloViews supports any type of rectilinear grid.

## B.4 SCRIPTS FOR READING & WRITING INPUT FILES

These make use of modified and updated version of Deltares' Python OpenEarthTools, which are released under the GNU General Public License v2. Code from PyDelft (MIT license) and Delft3D-Toolbox (MIT license) is also used.

### B.4.1 Quick Description

*mdf.py*

All information for a flow simulation is stored in a Master Definition Flow file (MDF-file) [Deltares, 2019]. `mdf.py` contains a Python class to read this file into a Python dictionary structure and a function for the converse, writing a dictionary to an .mdf file. All comment lines and keyword formatting are not preserved when writing a dictionary to an .mdf file.

*dep.py*

Read and write NumPy mesh grids from/to Delft3D-FLOW bathymetry (`.dep`) files.

*grid.py*

Read and write NumPy mesh grids from/to (`.grd`) files.

*enc.py*

Read, construct and write enclosure (.enc) files.

*SedMor.py*

Read sediment (.sed) and morphology (.mor) files into a Python dictionary structure and vice-versa write them to file.

*TimeSeries.py*

Write and write time-series files such as the boundary condition (.bcc & .bct) and discharge (.dis) files.

Slope-Break Bathymetry With `SlopeBreak.py`, depth and grid files for a slope-break bathymetry can declaratively be constructed. The function takes the channel and basin dimensions, and slope angles of the upper and lower parts as arguments and the script generates the grid and depth and writes them to file.

*Multi-flow Script*

`multipleruns.py` is a script that generates successive restart models. It reads a template model folder, duplicates it for subsequent runs and automatically updates times in all necessary files of a model (.bcc, .bct and .sed, and .mdf).

### B.4.2 3D-profile Discharge Boundary Conditions

Generates records for boundary condition files for 3D-profile type boundary condition by specifying a concentration, number of grid-cells and discharge while considering the vertical grid.

## B.5 ROOM FOR IMPROVEMENT

There a lot of room for improvement to these scripts. A few ideas are listed here

- More robust, consistent and Pythonic code base with better error handling. Several separate functions can be grouped into classes.
- Reading and displaying of more Delft3D-FLOW input files, e.g.underlayers in morphology file, boundary conditions files, sediment files.
- Make use of pandas for time-series values. pandas is an open source data analysis and manipulation tool, built on top of Python pandas development team [2020].
- Tighter integration with xarray for analysing output. There are already several xarray extensions for geosciences, see Xarray related projects for inspiration. A comparable extension of the xarray data model could be made for use with Delft3D-FLOW. Perhaps simlab, a general-purpose tool to easily build custom computational models can be used for this.
- A function for defining, visualizing and writing $\sigma$-grid layer percentages to the `.mdf` files conveniently and calculating the maximum layer thickness with the model's depth.
- Support for unit-aware arrays with pint to define, operate and manipulate physical quantities. Pint is already integrated in xarray, this would be very useful in calculating sediment volumes of in-flow boundary conditions for example.
- Out-of-core (lazy) operations for summing vector components like velocity and bottom stress.
- More extensive documentation with examples
- A PVGeo Delft3D-FLOW NetCDF reader for viewing output in ParaView.
- Better support for plotting non-uniform grids with enclosures in HoloViews by making use masks.

- Closer adherence to the SGRID conventions for the staggered grid. NOAA's Gridded package has implemented a SGRID parser that perhaps can be adapted for use with xarray.
- Efficiently plotting vector fields (quiver plots) without loading the all required data into memory at once.
- Combining and storing multiple simulation datasets using zarr.
- Support for NEFIS — a proprietery file format by Deltares — files. There are Python bindings Nefis2netcdf and nefis-python but both packages have been unmaintained for several years and require a compilation of system-specific binaries, which is difficult. (Something similar.
- Integrate the Delft3D-FLOW file reading/writing and bathymetry conversion functionality from pyPoseidon, an open-source storm surge framework a released under the EUPL v1.2 license.

### B.5.1 Grand Visions for a Complete Open-Source Python Delft3D-FLOW Geological Modelling Package

A long-shot goal is be to make a complete Python package that facilitates working with Delft3D-FLOW geological models, as iMOD-Python (developed by Deltares no less) is to iMOD in aquifer modelling.

pyPoseidon by Breyiannis et al. [2016] is a declarative framework around Delft3D-FLOW for storm-surge modelling. Both iMOD and pyPoseidon use the same dependencies that are listed above in Packages/Dependencies and can serve as an example.

## B.6 LICENSE

All scripts developed for this thesis are free and open source can be found on GitHub under the BSD 3-Clause Revised License. A few reduced and compressed datasets with example notebooks are included in this repository.

# C DATA AVAILABILITY

- The complete source code of the processing and visualisation of simulation output and many attempts at various analyses that did not even make the report is hosted on GitHub as a code repository as an open-source package, under an BSD Clause 3 Licence.
- The Delft3D-FLOW model files are available in said GitHub repository as well.
- Some of the functionality has been split in to a separate Python package, pyDelf3D-FLOW, which is available in another GitHub repository. See also appendix DELFT3D-FLOW & PYTHON.
- The datasets generated for this study are not available online due prohibitively large file sizes. The datasets are available on request to the corresponding author.

## COLOPHON

This document was typeset using LaTeX. The document layout was generated using the `arsclassica` package by Lorenzo Pantieri, which is an adaption of the original `classicthesis` package from André Miede.

The figures and diagrams were mostly drawn using HoloViews, PyVista, matplotlib, Vega-lite and d3.js.